# Dynamics and Correlations

# in Quantum Many-Body Systems


Michele Fava

Merton College

University of Oxford

A thesis submitted for the degree of

*Doctor of Philosophy*

Trinity 2022

To Maria Claudia and my parents

# Acknowledgements

First of all, I would like to thank my DPhil supervisor: Prof. Sid Parameswaran. Throughout these four years I have greatly benefited from many discussions with him (both about physics and food): many of the research directions reported in this thesis stem from insights of his.

I would also like to thank other people that have been like extra supervisors to me over the years: Prof. Fabian Essler, Prof. Romain Vasseur, and Prof. Sarang Gopalakrishnan. I think I learned a lot from them and from seeing their various approaches to physical problems.

I am also extremely grateful to all the other people I have had the opportunity to collaborate with on various projects: Prof. Radu Coldea, Brayden Ware, Sounak Biswas, Abhishodh Prakash, Max McGinley, Prof. Shivaji Sondhi, and Prof. Markus Heyl. Among my collaborators, a special thank is due to Angelo Russomanno and Prof. Rosario Fazio, who somehow have not gotten tired yet of having to deal with me.

I sincerely thank my examiners, Prof. Steve Simon and Prof. Benjamin Doyon, for their careful reading of this thesis, their feedback and suggestions to improve it, and for the enjoyable viva they conducted.

A huge thank you goes to all the other amazing colleagues and friends I have had throughout the years, with whom I had many stimulating physics discussion, as well as having shared many of the ups and downs of the DPhil: Yves Kwan, Joe Huxford, Minghao Li, Patrick Wilhelm, Sthitadhi Roy, Nick Bultinck, Glenn Wagner, Sam Garratt, Aleksandra Ziolkowska, Filippo Revello and Pietro Ferrero, as well as many others.

Finally, I would like to thank my wife, Maria Claudia, who has always been there for me throughout the years, even when I was getting paranoid about some signs in some calculation and needed a second pair of eyes.

# Abstract

This thesis is a collection of three exact results on correlation and response functions in integrable systems.

In the first part we study transport (two-point functions) in the 1D Hubbard model. First, we analyze the limit of large on-site repulsion and characterize spin transport as a function of temperature. Then, we consider the case where the model displays non-abelian symmetries, e.g., spin $SU(2)$, and argue that in this case transport is anomalous with dynamical scaling exponent $z = 3/2$ and follows KPZ scaling.

In the next two parts we focus instead on (perturbative) nonlinear response functions, which can be expressed as $n$-point correlators with $n > 2$. Given the lack of a systematic understanding of the information which can be extracted from these, we compute them in integrable 1D systems. We therefore focus on two distinct scenarios. In the first scenario, we consider a finite temperature system perturbed by some inhomogeneous field coupling to local charges — thus the perturbations can only accelerate quasiparticles, but not create/annihilate them. In this context, we develop a diagrammatic framework based on generalized hydrodynamics that allows a systematic calculation of nonlinear response functions. We show that, in the hydrodynamic limit, nonlinear response functions qualitatively distinguish between non-interacting and interacting systems. In the second scenario, we instead consider a zero temperature system whose ground state coincides with the quasiparticle vacuum. In this simpler setting we consider more general perturbations that can also create and annihilate quasiparticles. Focusing on the Ising chain as a paradigmatic model we show that the long-time limit of four-point functions (third-order response) grows linearly in time. We interpret these divergences in terms of semiclassical processes where quasiparticles propagate ballistically and scatter when their trajectories intersect.

# Contents

# Acronyms

**GGE** Generalized Gibbs Ensemble.

**GHD** Generalized Hydrodynamics.

**KPZ** Kardar-Parisi-Zhang.

**QP** Quasiparticle.

**TBA** Thermodynamic Bethe Ansatz.

# Chapter 1

# Introduction

The study of many-body systems is arguably one of the most interesting topics in physics. As nicely summarized by P. W. Anderson in "More is Different" [1] systems with many degrees of freedom can exhibit complex and surprising emergent phenomena even in cases where the microscopic laws governing each separate entity are simple and well-understood. Many-body physics is one of the simplest settings in which the emergence of new phenomena can be investigated. In particular, in the context of condensed matter, many emergent phenomena have been understood and discovered during the last century, such as spontaneous symmetry breaking, emergent symmetries, and topological phases, just to cite a few. In this setting dynamical correlation and response functions give physicists an invaluable tool to understand and characterize emergent phenomena.

From a theoretical point of view, the dynamics of many-body systems is extremely difficult to study for arbitrary far-from-equilibrium initial conditions. Dynamical correlation and response functions on top of an equilibrium state offer one of the simplest setting to study dynamics: with the deviation from equilibrium being perturbatively weak. In spite of the fact that dynamical correlation functions probe near-equilibrium dynamics, their phenomenology can be very rich. One striking example is the possibility to observe emergent Kardar-Parisi-Zhang universality (see e.g. Ref. [8]) in two-point correlation of quantum spin chains [26].

From a more practical point of view, response functions are arguably the main way experimental physicists can extract information from condensed-matter systems —the quintessential platform of many-body physics. It then becomes important to develop a theoretical understanding of correlation and response functions, in order to better understand and interpret experimental data.

In the rest of the introduction we recapitulate some basic definition and results in response theory and, finally, describe the structure of the thesis.

## 1.1 Response theory

We consider a quantum system, prepared in some equilibrium state described by the density matrix $\hat{\rho}_0$ at time $t = -\infty$. In isolation, the system evolution is described by the time-independent Hamiltonian $\hat{H}_0$. To experimentally probe the system we imagine coupling it to some external field, which effectively perturbs its Hamiltonian in the following time-dependent way:

$$\hat{H}(t) = \hat{H}_0 + \phi(t)\hat{A}. \tag{1.1}$$

Here $\phi(t)$ is a classical function that controls the strength of the perturbation and $\hat{A}$ is the operator to which the perturbation is coupling, which, for simplicity, we assume to not change with time. Since the system is initially prepared in equilibrium $\phi(t) \to 0$ as $t \to -\infty$.

Finally, at some time $t$, we try to assess the effect of the perturbation on the system by measuring the expectation value of some operator. For simplicity, we assume here that the operator being measured is $\hat{A}$, i.e. the same operator the perturbation couples to. Its expectation value can be computed as

$$\langle \hat{A}(t) \rangle = \mathrm{Tr}\left( \hat{U}^\dagger(t)\hat{\rho}_0\hat{U}(t)\hat{A}(t) \right) \tag{1.2}$$

where $\hat{A}(t)$ denotes the time-evolved operator in the interaction picture $\hat{A}(t) = e^{i\hat{H}_0 t}\hat{A}e^{-i\hat{H}_0 t}$ and

$$\hat{U}(t) = \overleftarrow{\exp}\left( -i \int_{-\infty}^{t} dt'\, \phi(t')\hat{A}(t') \right) \tag{1.3}$$

is the time-evolution operator in the interaction picture. Here the arrow denotes the direction of the time-ordering (earlier times on the right). If $\phi$ is sufficiently weak, one could expect that the deviation of $\langle \hat{A}(t) \rangle$ from its equilibrium value of $\langle \hat{A} \rangle_0 = \mathrm{Tr}(\hat{\rho}_0\hat{A})$ can be well-approximated by Taylor-expanding Eq. (1.2) in $\phi$ up to some finite low order.

### 1.1.1 Linear response

In many experimentally relevant cases, ranging from transport to optical spectroscopy, the linear order in $\phi$ is sufficient to quantitatively understand experimental data. In this case we can truncate the expansion at first order

$$\langle \hat{A}(t) \rangle - \langle \hat{A} \rangle_0 = \int_{-\infty}^{+\infty} dt' \, \phi(t') \chi^{(1)}(t', t) + O(\phi^2) \tag{1.4}$$

with

$$\chi^{(1)}(t', t) = \frac{\delta \langle \hat{A}(t) \rangle}{\delta \phi(t')} = i \Theta_H(t - t') \left\langle \left[ \hat{A}(t'), \hat{A}(t) \right] \right\rangle \tag{1.5}$$

denoting the linear response function. Here $\Theta_H$ denotes Heaviside-$\Theta$ function, which enforces the causality of the response (i.e. the system is affected by the perturbation only after the perturbation has acted on it). Note that since the expectation value are taken on top of the time-independent state $\hat{\rho}_0$, the linear response function $\chi^{(1)}(t', t)$ only depend on the time difference $t - t'$, viz. $\chi^{(1)}(t', t) = \chi^{(1)}(t - t')$

Linear response functions on top of a thermal state have a natural interpretation given by the fluctuation-dissipation theorem. This relates the Fourier transform of $\chi^{(1)}$

$$\chi^{(1)}(\omega) = \int_0^{+\infty} dt \chi^{(1)}(t) e^{i\omega t} \tag{1.6}$$

to the Fourier transform of the two-point connected correlation function $C_2$

$$C_2(\omega) = \int dt \langle \hat{A}(t) \hat{A} \rangle_C e^{i\omega t}. \tag{1.7}$$

By inserting a spectral representation between the two $\hat{A}$ operators (see e.g. Ref. [78]), one can readily obtain the fluctuation-dissipation theorem

$$\Im \chi^{(1)}(\omega) = -\frac{1}{2} \left( 1 - e^{-\beta\omega} \right) C_2(\omega). \tag{1.8}$$

From a conceptual point of view, the theorem gives a natural theoretical interpretation to linear-response functions in terms of the intrinsic fluctuations of the system's degrees of freedom. An equivalent way of deriving the fluctuation-dissipation theorem is through the Kubo-Martin-Schwinger relation. [1]

[1] The latter method allows for generalizations of the fluctuation-dissipation theorem for more general (i.e. non thermal) states, like the Generalized Gibbs Ensemble (GGE) states in integrable systems [49].

Finally, note that there are experimental setups, like inelastic neutron scattering, that, although not directly related to the setting of response theory, can be shown to effectively measure two-point functions. Therefore, conceptually, results of such experiments can again be treated within the same framework of linear response.

### 1.1.2 Nonlinear response

Going beyond the linear expansion in the previous section, we can define nonlinear response functions as

$$\begin{aligned}\langle \hat{A}(t)\rangle = \langle \hat{A}\rangle_0 &+ \int_{-\infty}^{+\infty} dt'\, \phi(t')\chi^{(1)}(t',t) \\ &+ \int_{-\infty}^{+\infty} dt' \int_{-\infty}^{+\infty} dt''\, \phi(t')\phi(t'')\chi^{(2)}(t'',t',t) \\ &+ \int_{-\infty}^{+\infty} dt' \int_{-\infty}^{+\infty} dt'' \int_{-\infty}^{+\infty} dt'''\, \phi(t')\phi(t'')\phi(t''')\chi^{(3)}(t''',t'',t',t) \\ &+ O(\phi^4)\end{aligned} \tag{1.9}$$

with

$$\chi^{(2)}(t'',t',t) = \frac{\delta^2\langle \hat{A}(t)\rangle}{\delta\phi(t'')\delta\phi(t')} = i^2\Theta_H(t-t')\Theta_H(t'-t'')\left\langle\left[\hat{A}(t''),\left[\hat{A}(t'),\hat{A}(t)\right]\right]\right\rangle \tag{1.10}$$

$$\begin{aligned}\chi^{(3)}(t''',t'',t',t) &= \frac{\delta^3\langle \hat{A}(t)\rangle}{\delta\phi(t''')\delta\phi(t'')\delta\phi(t')} \\ &= i^3\Theta_H(t-t')\Theta_H(t'-t'')\Theta_H(t''-t''')\left\langle\left[\hat{A}(t'''),\left[\hat{A}(t''),\left[\hat{A}(t'),\hat{A}(t)\right]\right]\right]\right\rangle .\end{aligned} \tag{1.11}$$

Similarly, one could continue the expansion and compute response functions at any order in the perturbation. However, we expect that, the higher the order of a response function, the harder it would be to compute it in a given system. Furthermore, one might also imagine that extracting higher-order response functions is more challenging experimentally, as it will require either generating stronger perturbations without leaving the regime where $\phi$ can be treated perturbatively, or alternatively very high-precision measurements of the final expectation value $\langle \hat{A}(t)\rangle$. In this thesis we will therefore limit ourselves to study response functions of order three or less.

A first observation is that, by expanding out all the nested commutators, the $n$-th order response function is a linear combination of $(n+1)$-point correlators. It

should be noted that the order of the operator in the correlators is ordered on the Keldysh contour, i.e. from the right to the left time flows forward from $-\infty$ to the measurement time $t$ and then back from $t$ to $-\infty$. It is also interesting to note that, while there are generalizations of the fluctuation-dissipation theorem to nonlinear response functions [38, 188, 90], unlike in the linear case, they do not directly relate nonlinear response functions of order $n > 1$ to time-ordered correlators.

**Why nonlinear response?** After having defined nonlinear response functions we comment on why their study could be useful from a practical perspective. In fact, as mentioned above linear response already gives quantitatively accurate description of most common experimental setups, whereas nonlinear response function would give only subleading corrections. Therefore, the study of nonlinear response might seem unmotivated from an experimental perspective. The argument for why this is not the case is composed of two parts.

First of all, there are experimental setups which allow for measurements of nonlinear response functions. One example is the technique of Two-Dimensional Coherent Spectroscopy (often abbreviated as 2DCS). This technique was originally devised for the study of molecules and few-body systems [148], and in more recent years it has been successfully applied to condensed-matter systems [138, 122, 104, 192, 136, 140, 33], enabling the measurement of third-order response functions.

Given that there are experimental techniques that allow the measurement of nonlinear response in many-body systems, a natural question is: in which contexts do we expect nonlinear response to be useful experimentally? One example where nonlinear response might provide some advantage over linear response is in experimental studies of systems with topological excitations, i.e. excitations that cannot be created individually by means of a local operator. In this case linear response functions indicate the presence of a continuum in the spectrum, but have trouble differentiating between different physical mechanism that might give rise to the continuum. This issue is not merely a theoretical problem, but an actual obstacle in the experimental search for exotic phases, e.g. quantum spin-liquids. In these cases, it was proposed [187] that 2D Coherent Spectroscopy could help differentiate between distinct scenarios.

More generally, it would be desirable to identify contexts in which nonlinear response could help overcome some limitation of linear response. However, nonlinear-response functions (and more broadly multi-point correlators) of many-body systems remain a poorly understood topic (even at zero temperature, where two-point and

linear-response functions are very well understood). In fact, despite a flurry of recent works [3, 4, 47, 50, 149, 175, 187, 157, 158, 151, 131, 150, 108, 37, 110, 94, 160, 174, 118, 146, 123, 129, 57, 190, 189, 183, 182, 181, 145], the theoretical toolbox for addressing nonlinear response in generic interacting quantum many-body systems is primitive, with few exact or controlled results beyond free theories and those that reduce to ensembles of two-level systems. In this context obtaining exact results in integrable model could hopefully help us improve our understanding of nonlinear response functions in general.

## 1.2 Structure of this thesis

The rest of this thesis will be structured as follows. In Chapter 2 we review some concepts related to integrability, in particular, the framework of Thermodynamic Bethe Ansatz and Generalized Hydrodynamics, which will be the main techniques used in the two successive chapters.

Chapter 3 contains a study of transport (linear-response) in the Hubbard model. The study is separated in two parts, respectively related to ballistic spin transport in the strong-interaction regime, and to anomalous spin and charge transport in the presence of non-abelian symmetries. This chapter is based on the work [62].

The next chapters are dedicated to nonlinear response functions. In Chapter 4 we introduce a diagrammatic formalism based on Generalized Hydrodynamics to compute nonlinear response functions associated to transport —i.e. the perturbation can accelerate previously-existent quasiparticles, but not create or annihilate them. We then use the formalism to compute nonlinear response functions in the Lieb-Liniger model and the XXZ chain. This chapter is based on the work [61].

In Chapter 5 we turn our attention to perturbations that can not only accelerate quasiparticles, but also create and annihilate them. We simplify the problem by considering a simple model: the transverse-field Ising model. Here we will show, through a form-factor expansion, that momentum-resolved third-order response functions associated to the order parameter diverge at long times in the paramagnetic phase. The results reported in this chapter are based on ongoing work in collaboration with Fabian Essler, Siddharth Parameswaran, Sarang Gopalakrishnan, and Romain Vasseur.

Finally, we summarize our results and speculate on future directions in Chapter 6.

# Chapter 2

# Integrable systems and generalized hydrodynamics

Integrable quantum systems are special systems for which the exact eigenstates of the Hamiltonian can be known exactly. This, at least in principle, allows for an exact computation of various static and dynamical properties. In this introductory chapter we explain some of the main techniques that will be used throughout the thesis. The ultimate goal is to introduce the framework of Generalized Hydrodynamics (GHD), which plays a central role in Chapters 3 and 4. In Sec. 2.1 we will describe how the finite-size spectrum of integrable systems can be computed through coordinate Bethe ansatz. In Sec. 2.2 we will review the key elements of Thermodynamic Bethe Ansatz (TBA), which allows us to extract certain thermodynamic properties of the system. Finally, in Sec. 2.3, we will describe the framework of GHD, which, leveraging on TBA techniques, gives us an effective description of the long-time and large-lengthscale dynamics.

There are many great pedagogical books and materials on these topics, and in preparing this chapter we relied on the followings. The Coordinate Bethe Ansatz and TBA sections are based on Refs. [179, 120, 59, 68] and the supplementary materials of Refs. [98, 96]. The GHD section is largely inspired by Ref. [48].

## 2.1 Coordinate Bethe Ansatz

For the purpose of introducing coordinate Bethe ansatz we will focus on arguably the simplest interacting integrable quantum model: the Lieb-Liniger model [133, 132]. The model describes a gas of bosons moving in one dimension and interacting through

a contact potential. Thus, in units where the mass $m = \hbar^2/2$, the Hamiltonian can be written as

$$\hat{H}_N = -\sum_{j=1}^{N} \frac{\partial^2}{\partial x_j^2} + 2c \sum_{i<j} \delta(x_i - x_j) \tag{2.1}$$

for some parameter $c$ encoding the strength of the interactions. In the above equation the index $j$ runs over the $N$ particles, whose coordinates are given by $x_j$.

**One-particle sector** We start by considering the simplest case where $N = 1$ and the Hamiltonian reduces to $H_1 = -\partial_{x_1}^2$. A basis of eigenstates is then simply given by plane-wave solutions $\psi_k(x) \equiv \langle x|k\rangle = e^{ikx}$, whose energy is $e(k) = k^2$.

**Two-particle sector** Next, we consider the case $N = 2$, where the Hamiltonian is given by $\hat{H}_2 = -\partial_{x_1}^2 - \partial_{x_2}^2 + 2c\delta(x_1 - x_2)$. The most general eigenstate will be of the form

$$\psi(x_1, x_2) = f(x_1, x_2)\theta(x_2 - x_1) + g(x_1, x_2)\theta(x_1 - x_2). \tag{2.2}$$

Given that the particles are bosons, we should impose that $\psi(x_1, x_2) = \psi(x_2, x_1)$, which implies that $g(x_1, x_2) = f(x_2, x_1)$. To proceed we focus on the region where $x_1 < x_2$ and require that the state $|\psi\rangle$ locally satisfies the Schrödinger equation. We can thus choose $f$ to be of the form

$$f(x_1, x_2) = A_{12} e^{i(k_1 x_1 + k_2 x_2)} + A_{21} e^{i(k_2 x_1 + k_1 x_2)} \tag{2.3}$$

for some $k_1$ and $k_2$ and some coefficient $A_{12}$ and $A_{21}$. Note that $k_1$ and $k_2$ uniquely determine the energy of the state $E = e(k_1) + e(k_2)$ with $e$ denoting the one-particle energy. Finally, imposing that $\psi(x_1, x_2)$ is a solution of the Schrödinger equation in the neighbourhood of $x_1 = x_2$ provides us with the condition

$$\frac{A_{12}}{A_{21}} = -e^{-i\varphi(k_1 - k_2)}, \qquad \varphi(k) \equiv 2 \arctan \frac{k}{c} \tag{2.4}$$

thus fixing the state up to an overall phase.

Therefore, we have found a family of eigenstates $|\psi_{k_1,k_2}\rangle$ parameterized by the two momenta $k_1$ and $k_2$. Furthermore, one can show that the following properties hold. (i) The set of wavefunctions $|\psi_{k_1,k_2}\rangle$ form a complete orthogonal basis. (ii) The wavefunctions vanish when $k_1 = k_2$, viz. $|\psi_{k,k}\rangle = 0$, indicating that the QP that we are using to diagonalize the model are fermionic in nature.

**$N$-particle sector** A crucial feature of Bethe-ansatz-integrable systems is that the two-particle solution can be lifted to the $N$-particle sector. Heuristically this happens because in these systems three-body (or more) scattering processes always factorize into the product of two-body scattering processes. [1]

When these conditions are met, as in the Lieb-Liniger model, $N$-particle eigenstates can be parameterized by a set of $N$ momenta $\boldsymbol{k} \equiv (k_1, \ldots, k_N)$. In the sector where $x_1 < x_2 < \cdots < x_N$ the wavefunction can be written as

$$\psi_{\boldsymbol{k}}(x_1, \ldots, x_N) = \sum_{\sigma \in S_N} A_\sigma(\boldsymbol{k}) \exp(i \sum_j k_{\sigma_j} x_j) \tag{2.5}$$

and the symmetry under exchange of two coordinates then fixes the wavefunction for an arbitrary set of coordinates $\boldsymbol{x}$. In the above equation $\sigma$ runs over $S_N$: the set of permutation of $N$ elements. Imposing that $\psi_{\boldsymbol{k}}$ satisfies the Schrödinger equation at all $\boldsymbol{x}$, the coefficient $A_\sigma(\boldsymbol{k})$ can be fixed up to an overall phase. For the Lieb-Liniger model, one can explicitly show (see e.g. [119, 179]) that if $\sigma'$ and $\sigma$ are related by the transposition of two elements $m, n$ with $m < n$, viz. $\sigma' = (m\, n)\sigma$, then $A_{\sigma'}$ is related to $A_\sigma$ by

$$\frac{A_{\sigma'}}{A_\sigma} = -e^{-i\varphi(k_{\sigma(m)} - k_{\sigma(n)})} \tag{2.6}$$

Finally, it can be proved that the set of eigenstates just constructed forms a complete orthogonal set and vanish whenever two momenta coincide, in analogy to what happens in the 2-particle sector [119].

**Finite-size spectrum** One of the easiest applications of coordinate Bethe ansatz is the computation of finite-size spectra. This problem, which normally would be exponentially hard in $N$, will be reduced to a system of $N$ algebraic (nonlinear) equations, known as the Bethe equations. The simplest boundary conditions are periodic ones. For this purpose we consider the system on a ring of finite length $L$ and impose that all physical states should satisfy $\psi_{\boldsymbol{k}}(x_1, \ldots, x_j, \ldots, x_N) = \psi_{\boldsymbol{k}}(x_1, \ldots, x_j + L, \ldots, x_N)\ \forall j$. The condition above constrains the set of possible $\boldsymbol{k}$ to a discrete set satisfying

$$e^{ik_j L} = (-1)^{N-1} \prod_{j' \neq j} e^{-i\varphi(k_j - k_{j'})} \qquad \forall j. \tag{2.7}$$

[1] Another nontrivial requirement is that the outcome of a series of two-particle scattering processes does not depend on the order in which they took place, as formally expressed by the Yang-Baxter equations (see e.g. the discussion in Ref. [179]).

This condition can be most conveniently rewritten by taking the logarithm of both sides to obtain

$$k_j L = 2\pi I_j - \sum_{j' \neq j} \varphi(k_j - k_{j'}) \tag{2.8}$$

for some set of either integer (if $N$ is odd) or half-integer (if $N$ is even) $I_j$. With some more work, it can be shown that the set of $I_j$ identifies one and only one solution of the Bethe equations above [119].

**Other models** Other models (e.g. the Heisenberg model) can be solved in a similar fashion. The starting point is to consider a simple reference eigenstate, which will be regarded as the Quasiparticle (QP) vacuum (for example the state with all spins down in the Heisenberg model). Other eigenstates are then constructed by introducing a number of QP excitations (possibly of different species) on top of the vacuum. Ultimately, a complete basis of eigenstates $|k_1, k_2, \ldots, k_N\rangle_{a_1,a_2,\ldots,a_N}$ can be similarly organized in terms of number $N$ of QPs, their species $(a_1, a_2, \ldots, a_N)$, and their momenta $(k_1, k_2, \ldots, k_N)$. The energy $E$ of each eigenstate will be again given by the sum of energy of each single QP, viz.

$$\hat{H}\,|k_1, k_2, \ldots, k_N\rangle_{a_1,a_2,\ldots,a_N} = \sum_{j=1}^{N} e_{a_j}(k_j)\,|k_1, k_2, \ldots, k_N\rangle_{a_1,a_2,\ldots,a_N}\,, \tag{2.9}$$

where $e_a(k)$ is the energy dispersion for a QP of species $a$ and will be determined by the details of model. Furthermore, such eigenstates will be compatible with periodic boundary conditions on a system of size $L$ if the momenta satisfy the Bethe equations

$$k_j L = 2\pi I_j - \sum_{j' \neq j} \varphi_{a_j,a_{j'}}(k_j, k_{j'}) \tag{2.10}$$

for some integers (or half-integers, if $n$ is even) $(I_1, I_2, \ldots, I_N)$. Again, the scattering phase shifts $\varphi_{a,b}$, describing the phase shift in a scattering between two QPs of species $a$ and $b$, can be obtained from the microscopic model in question.

Note that, in general, $\varphi_{a,b}(k_1, k_2)$ cannot be expressed as a function of momentum difference $k_1 - k_2$, unlike the case of the Lieb-Liniger model. It is then convenient to reparametrize momenta in terms of another variable $\theta$, usually referred to as rapidity, such that the scattering phase shift only depends on rapidity differences $\varphi_{a,b}(k_a(\theta_1), k_b(\theta_2)) \equiv \varphi_{a,b}(\theta_1 - \theta_2)$. In terms of rapidities the Bethe equations take

the form

$$k_{a_j}(\theta_j)L = 2\pi I_j - \sum_{j' \neq j} \varphi_{a_j,a_{j'}}(\theta_j - \theta_{j'}). \tag{2.11}$$

Finally, we briefly mention the delicate issue of complex solutions of the Bethe equations and the string hypothesis. Unlike in the repulsive ($c > 0$) Lieb-Liniger model, the Bethe equations in most integrable systems will admit complex solutions. Their presence would make the treatment of the Bethe equations much more complicated — for example all the standard TBA technology that we will outline in the next section heavily relies on the fact that rapidities are real. Fortunately, in the thermodynamic limit, almost all of the complex solutions can be interpreted within the "string hypothesis" [177, 178].

The string hypothesis states that a solution of the Bethe equation $(\theta_1, \ldots, \theta_N)$ can be organized into subsets (strings), such that the rapidities within the same string have the same real part (up to corrections that vanish in the $L \to \infty$ limit). Heuristically, strings can be associated with stable bound states of elementary QPs and can be treated as a new QP species. This intuition can be formalized at the level of the Bethe equation. Here one can show that (see e.g. [179] for many examples), for the purpose of computing the spectrum, strings can be treated on equal footing with the "elementary" QP species upon identification of their rapidity with the real part of the rapidities composing the string. In summary, we can effectively work in a situation where we are interested only in real solution of the Bethe equations (2.11) by extending the set of QP species to include bound states (strings). We will see in the next section that this assumption allows great simplifications when dealing with thermodynamic properties.

## 2.2 Thermodynamic Bethe Ansatz

As we saw in the previous subsection, the finite-size spectrum of an integrable systems can be described by a conceptually simple algebraic equation. This should be contrasted with the form of the eigenstates, that is quite involved already in simple model (see e.g. Eq. (2.5) for the Lieb-Liniger model). It is then natural to try to develop frameworks that extract as much information as possible from the spectrum alone, without using explicitly the form of the eigenstates. Along this line, we now proceed to discuss Thermodynamic Bethe Ansatz (TBA), which allows us to characterize macroscopic properties of a system by leveraging the Bethe equation (2.11)

alone. Most of the techniques we are going to present were first introduce in Ref. [193] for the Lieb-Liniger model.

**QP density, Bethe roots and their density** As mentioned, we now focus on the thermodynamic limit, i.e. the limit where both the length of the system $L$ and the number of QPs $N$ tend to infinity, while the ratio $N/L$ is kept fixed. In this context, describing an eigenstate through the rapidities of all its QPs is cumbersome. Instead, a more useful quantity that we can define for a given eigenstate is the density of QPs as a function of rapidity

$$\rho_a(\theta) \simeq \frac{1}{L}\frac{(\#\text{ of QPs of species } a \text{ in } [\theta, \theta + d\theta])}{d\theta}. \tag{2.12}$$

The underlying idea is that for many concrete purposes, as we will see shortly, eigenstates with the same QP density behave similarly and are practically indistinguishable. For example, expectation values of extensive operators can be computed from $\boldsymbol{\rho}$ alone, up to non-extensive corrections. E.g., the energy density of a given eigenstate is given by

$$\frac{E}{L} = \sum_a \int d\theta\, \rho_a(\theta) e_a(\theta) + O(1/L) \tag{2.13}$$

Another useful concept in the thermodynamic limit is that of Bethe root. Once we fix an Hamiltonian eigenstate, characterized by a set of rapidity-species pairs $\{(\theta_j, a_j)\}$, a Bethe root is a pair of rapidity-species $(\theta_R, a_R)$, s.t.

$$k_{a_R}(\theta_R)L - \sum_{j=1}^{N} \varphi_{a_R,a_j}(\theta_R - \theta_j) \in 2\pi\mathbb{Z}. \tag{2.14}$$

Note that we can always choose $\varphi$ in such a way that $\varphi_{a,a}(0) = 0$. By adopting this convention all pairs $(\theta_j, a_j)$ which define the eigenstate are Bethe roots. Furthermore, for every Bethe root that does not coincide with $(\theta_j, a_j)$ for some $j$, we can construct a new eigenstate defined by the set of rapidities $\{(\theta'_j, a_j)\}_{j=1,\dots,N} \cup \{(\theta_R, a_R)\}$ with $\theta'_j - \theta_j = O(1/L)$. In other words, given a Bethe root that is not already occupied by a QP, we can insert a QP in place of the Bethe root, and, up to a displacement of the other rapidities of $O(1/L)$, obtain a new eigenstate.

These observations prompt us to think of Bethe roots as the set of allowed rapidities of which $N$ (the set of $(\theta_j, a_j)$) are actually occupied by QPs. It is then natural to define a density of Bethe roots (also often referred to as density of states or total

density) as

$$\rho_a^t(\theta) \simeq \frac{1}{L}\frac{(\#\text{ of roots of species } a \text{ in } [\theta, \theta + d\theta])}{d\theta}. \tag{2.15}$$

In a similar spirit one can define holes as Bethe roots that do not correspond to QPs and their density $\bar{\rho}_a(\theta) = \rho_a^t(\theta) - \rho_a(\theta)$ and finally the filling factor

$$n_a(\theta) = \frac{\rho_a(\theta)}{\rho^t(\theta)}. \tag{2.16}$$

As we will always work with fermionic QPs throughout this thesis, $n_a(\theta)$ is constrained to be in the interval $[0, 1]$.

**Counting function** From the definition of Bethe roots, it is clear that $\boldsymbol{\rho^t}$ cannot be an arbitrary function, but is fixed by the rapidities of the QPs. In the thermodynamic limit this relation can be made more precise and $\boldsymbol{\rho^t}$ can be uniquely determined from $\boldsymbol{\rho}$, or alternatively from $\boldsymbol{n}$.

To show this, it is useful to introduce the counting function

$$y_a(\theta) = k_a(\theta) + \frac{1}{L}\sum_{j=1}^{N} \varphi_{a,a_j}(\theta - \theta_j). \tag{2.17}$$

We immediately observe that, by definition of Bethe root (2.14), if $(\tilde{\theta}_1, a)$ is a Bethe root, then the next Bethe root of the same species $(\tilde{\theta}_2, a)$ satisfies $|y_a(\tilde{\theta}_1) - y_a(\tilde{\theta}_2)| = \frac{2\pi}{L}$. Furthermore, in all the models that we will consider, for each $a$, $y_a(\theta)$ will be a monotonic function of $\theta$. More specifically, we will have $\sigma_a := \operatorname{sign} y_a'(\theta) = \operatorname{sign} k_a'(\theta)$. Here we introduce the commonly used convention where primes denote derivatives w.r.t. the rapidity variable.

The monotonicity of $y$ and its relation with Bethe roots allows us to link $y$ to the root density via

$$\rho^t(\theta) = \frac{1}{2\pi}|y_a'(\theta)| = \frac{1}{2\pi}\sigma_a y_a'(\theta). \tag{2.18}$$

The usefulness of the above relation stems from the fact that $y_a'(\theta)$ can be easily expressed as an integral over rapidity in the thermodynamic limit. Defining the scattering kernel as $K_{a,b}(\theta) = \varphi'(\theta)/(2\pi)$, then

$$y_a'(\theta) = k_a'(\theta) + 2\pi \sum_b \int d\theta'\, K_{a,b}(\theta - \theta')\rho_b(\theta'). \tag{2.19}$$

Combining this with the previous equation, we obtain a fundamental relation between

the density of roots and the density of QPs

$$\sigma_a \rho_a^t(\theta) = \frac{k_a'(\theta)}{2\pi} + \sum_b \int d\theta'\, K_{a,b}(\theta - \theta')\rho_b(\theta') \tag{2.20}$$

$$= \frac{k_a'(\theta)}{2\pi} + \sum_b \int d\theta'\, K_{a,b}(\theta - \theta')n_b(\theta')\rho_b^t(\theta'). \tag{2.21}$$

Note that, as a consequence, the filling factor $\boldsymbol{n}$ fully specifies the particle density $\boldsymbol{\rho}$, which can, in fact, be practically computed by inverting the linear equation above and solving for $\boldsymbol{\rho^t}$.

Since expressions like the one above will often appear in any calculation involving TBA, it is convenient to introduce the product $\star$ such that an expression of the form $\sum_b \int d\theta'\, H_{a,b}(\theta, \theta') f_b(\theta')$ can be written more compactly as $[H_{a,b} \star f_b](\theta)$. E.g., Eq. (2.20) can be rewritten as

$$\sigma_a \rho_a^t(\theta) = \frac{k_a'(\theta)}{2\pi} + \left[K_{a,b} \star (n_b \rho_b^t)\right](\theta) \tag{2.22}$$

**Dressing transformation** Before proceeding we proceed to manipulate Eq. (2.20) and formally rewrite it in terms of a new object, the dressing transformation, which will be ubiquitous in many of the calculations presented in this thesis.

We start by observing that Eq. (2.20) is an inhomogeneous linear equation for $\boldsymbol{\rho}^t$. To make this more explicit we can introduce the kernel

$$\Omega_{ab}(\theta, \theta') = \delta_{ab}\delta(\theta - \theta') - K_{ab}(\theta - \theta')\sigma_b n_b(\theta'), \tag{2.23}$$

sometimes more compactly denoted as $\boldsymbol{\Omega} = \mathbf{1} - \boldsymbol{K\sigma n}$, so that

$$\left[\Omega_{ab} \star \rho_b^t\right](\theta) = \frac{k_a'(\theta)}{2\pi}. \tag{2.24}$$

We will always assume that the kernel $\boldsymbol{\Omega}$ admits a unique inverse $\boldsymbol{\Omega}^{-1}$, such that

$$\Omega_{ab}(\theta, \cdots) \star \Omega_{bc}^{-1}(\cdot, \theta') = \Omega_{ab}^{-1}(\theta, \cdots) \star \Omega_{bc}(\cdot, \theta') = \delta_{ac}\delta(\theta - \theta'). \tag{2.25}$$

The kernel $\boldsymbol{\Omega}^{-1}$ is called the dressing kernel and its action upon a rapidity function $f_a(\theta)$ defines its dressed version

$$f_a^{\mathrm{dr}}(\theta) = \left[\Omega_{ab}^{-1} \star f_b\right](\theta). \tag{2.26}$$

Eq. (2.20) can then be conveniently rewritten as

$$\rho_a^t(\theta) = \frac{1}{2\pi} (k')_a^{\mathrm{dr}}(\theta). \tag{2.27}$$

Note that the dressing kernel and the derivative w.r.t. rapidity do not commute, viz. $(f^{\mathrm{dr}})' \neq (f')^{\mathrm{dr}}$, if $\boldsymbol{n}$ is $\theta$-dependent (which is generally the case).

**Thermodynamics** We now proceed to fully specify the structure of equilibrium states. While above we have seen how $\boldsymbol{\rho^t}$ is determined by $\boldsymbol{n}$, we now have to describe how to compute $\boldsymbol{n}$ in an equilibrium setting. For simplicity we start by describing this relation in a grand-canonical ensemble at zero chemical potential, where the density matrix is given by $\hat{\rho} = \frac{1}{Z} \exp(-\beta \hat{H})$.

The idea is that microscopic states, as specified by their set of rapidities, will share the same macroscopic properties if their QP densities are the same on a coarse scale. Consequently, states with the same QP densities $\boldsymbol{\rho}$ (or equivalently the same $\boldsymbol{n}$) will be equally populated at equilibrium. The number of microscopic states corresponding to a given $\boldsymbol{\rho}$ will then give an entropic contribution, as quantified by the Yang-Yang entropy. The balance between the energy density associated to a given $\boldsymbol{\rho}$ and its entropy density will then determine the equilibrium state of the system [193].

We start by discussing the Yang-Yang entropy. We imagine fixing the distribution $\rho_a(\theta)$ up to a scale $d\theta$. This can be done in practice by splitting the rapidity line into segments of length $d\theta$ and requiring that the number of QPs within each segment is fixed to be $\rho_a(\theta)d\theta$. Note that this also fixes the number of unoccupied Bethe roots (holes) in each segments to be $\bar{\rho}_a(\theta)d\theta$. The entropy $\mathfrak{s}_{YY}$, as defined by Yang and Yang [193], is then related to the logarithm of the possible permutations of holes and QP within each interval

$$\mathfrak{s}_{YY} L = \log \left[ \prod_a \prod_{\text{intervals } [\theta,\theta+d\theta]} \frac{(L\rho_a^t(\theta)d\theta)!}{(L\rho_a(\theta)d\theta)!\,(L\bar{\rho}_a(\theta)d\theta)!} \right]. \tag{2.28}$$

By expanding the factorial using Stirling's approximation, one can show that in the limit $d\theta \to 0$, the Yang-Yang entropy has a simple integral representation

$$\mathfrak{s}_{YY} = \sum_a \int d\theta \, \left[ \rho_a^t(\theta) \log \rho_a^t(\theta) - \rho_a(\theta) \log \rho_a(\theta) - \bar{\rho}_a(\theta) \log \bar{\rho}_a(\theta) \right]. \tag{2.29}$$

Finally, using the Yang-Yang entropy, one can define the free energy density as

$$\mathfrak{f}_{YY} = -T\mathfrak{s}_{YY} + \sum_a \int d\theta\, \rho_a(\theta) e_a(\theta) \tag{2.30}$$

The free-energy density can be thought of as a functional of the filling function $n_a(\theta)$. Imposing that the $n_a(\theta)$ of the thermal state is the one that minimizes the free-energy density, one can obtain the TBA equations

$$\log Y_a(\theta) = \beta e_a(\theta) - \sum_b \left[K_{ab} \star \sigma_b \log\left(1 + 1/Y_b(\theta)\right)\right](\theta) \tag{2.31}$$

in terms if the variable $Y_a(\theta) = \frac{1-n_a(\theta)}{n_a(\theta)}$.

As anticipated, this equation completely fixes $\boldsymbol{n}$ for a given inverse temperature $\beta$. Once $\boldsymbol{n}$ is known, all the densities ( $\boldsymbol{\rho}$, $\boldsymbol{\rho^t}$, and $\bar{\boldsymbol{\rho}}$) can then be determined from Eq. (2.20).

**Generalized Gibbs Ensemble (GGE)** In the above discussion of thermodynamics we assumed that the system is described by a grand-canonical density matrix $\hat{\rho}(\beta) \sim \exp(-\beta \hat{H})$ with zero chemical potential. Since most often we consider states with $U(1)$ charge, we can expect that there will be more general family of equilibrium states parameterized by inverse temperature and chemical potential: $\hat{\rho}(\beta, \mu) \sim \exp(-\beta \hat{H} + \beta\mu \hat{Q})$ with $\hat{Q}$ denoting the $U(1)$ charge under consideration. Furthermore the discussion should be extended if additional charges that commute with the Hamiltonian are present.

In fact, it turns out that any Bethe-ansatz-integrable system is endowed with an infinite family of local and quasilocal conserved charges, which we will call $\{\hat{Q}_j\}_{j\in\mathbb{N}}$ [99]. The family of charges includes any $U(1)$ charge (typically labeled as $Q_0$), momentum, and the Hamiltonian itself (often identified with $Q_2$). These charges commute with one-another, viz. $[\hat{Q}_j, \hat{Q}_{j'}] = 0$ , and constitute an infinite family of independent integrals of motions for the Hamiltonian $H$.

By analogy with the case of the $U(1)$ charge, it is sensible to think that the most generic equilibrium state will be one where each charge $\hat{Q}_j$ is associated to a (possibly non-zero) Lagrange multiplier $\beta_j$ playing the role of a generalized inverse temperature relative to $\hat{Q}_j$. Such an equilibrium state is called Generalized Gibbs

Ensemble (GGE) [169, 58] and can be formally written as

$$\hat{\rho}_{\rm GGE}(\boldsymbol{\beta}) = \frac{1}{Z}\exp\left(-\sum_j \beta_j \hat{Q}_j\right). \tag{2.32}$$

The various charges $\hat{Q}_j$ are on the same footing as the Hamiltonian or of the momentum operator in the TBA formalism. In the same way each QP can be associated with a bare momentum eigenvalue $k_a(\theta)$ and a bare energy eigenvalue $e_a(\theta)$, it can also be associated with a bare $\hat{Q}_j$-eigenvalue $q_{j,a}(\theta)$. Equipped with the functions $q_{j,a}(\theta)$, one can repeat many arguments that we encountered so far. For example, the expectation value of a charge $Q_j$ on a state with density $\boldsymbol{\rho}$ is given by

$$\frac{\langle \hat{Q}_j \rangle}{L} = \sum_a \int d\theta\, \rho_a(\theta) q_{j,a}(\theta) + O(1/L) \tag{2.33}$$

Furthermore, from the above equation one can generalize the steps leading to Eq. (2.31) and derive the TBA equation which determines $\boldsymbol{n}$ for a given set of $\beta_j$, thus obtaining

$$\log Y_a(\theta) = \sum_j \beta_j q_{j,a}(\theta) - \sum_b \left[K_{ab} \star \sigma_b \log\left(1 + 1/Y_b(\theta)\right)\right](\theta). \tag{2.34}$$

**Excitation spectrum** The set of results above allow us to fully characterize equilibrium states and compute macroscopic expectation values upon them. A different problem that we can tackle using TBA machinery is the characterization of excitations on top of a given microscopic state.

Imagine starting from a microscopic state $\{(\theta_j, a_j)\}_{j=1,\dots,N}$, which can be also described in terms of TBA quantities like $\boldsymbol{\rho}$. As we mentioned above, from the state we can compute the rapidities of its unoccupied Bethe roots. We can then ask what are the properties, e.g. the momentum and the energy, of the states that can be reached by adding an extra QP in place of an unoccupied Bethe root at $(\tilde{\theta}, \tilde{a})$. If we were dealing with a free-fermion model, the answer would be that the momentum and energy of the excitation are its bare momentum and energy respectively: $k_{\tilde{a}}(\tilde{\theta})$ and $e_{\tilde{a}}(\tilde{\theta})$. However, as we already mentioned above, once the new QP is inserted in $(\tilde{\theta}, \tilde{a})$, the other QP's rapidities shift to a new configuration $\{(\theta'_j, a_j)\}_{j=1,\dots,N}$ with $\Delta\theta_j = \theta_j - \theta'_j = O(1/L)$. Taking into account this shift, sometimes referred to as

backflow, the physical momentum and energy of the QP excitation are

$$k^{\mathrm{ph}}_{\tilde{a}}(\tilde{\theta}) = k_{\tilde{a}}(\tilde{\theta}) + \sum_{j=1}^{N} \Delta\theta_j k'_{a_j}(\theta_j) + O(1/L) \tag{2.35}$$

$$e^{\mathrm{ph}}_{\tilde{a}}(\tilde{\theta}) = e_{\tilde{a}}(\tilde{\theta}) + \sum_{j=1}^{N} \Delta\theta_j e'_{a_j}(\theta_j) + O(1/L), \tag{2.36}$$

where we used the fact that $\theta'_j - \theta_j = O(1/L)$ to expand its dependence up to linear order. More generally, one can write a similar equation for any charge eigenvalue

$$q^{\mathrm{ph}}_{i,\tilde{a}}(\tilde{\theta}) = q_{i,\tilde{a}}(\tilde{\theta}) + \sum_{j=1}^{N} \Delta\theta_j q'_{i,a_j}(\theta_j) + O(1/L). \tag{2.37}$$

$\Delta\theta_j$ can be solved by writing the Bethe equation (2.11) satisfied by $\theta'_j$ and the Bethe equation satified by $\theta_j$. Subtracting the two and neglecting $O(1/L)$ terms, we can obtain

$$Lk'_{a_j}(\theta_j)\Delta\theta_j = -\varphi_{a_j,\tilde{a}}(\theta_j - \tilde{\theta}) - 2\pi \sum_{l\neq j} K_{a_j,a_l}(\theta_j - \theta_l)\,(\Delta\theta_j - \Delta\theta_l) \tag{2.38}$$

Following Ref. [179, 96] we assume that the dependence of $\Delta\theta_j$ on $\theta_j$ is smooth and introduce the backflow function, defined as

$$F_{a_j,\tilde{a}}(\theta_j;\tilde{\theta}) = L\rho^t_{a_j}(\theta_j)\sigma_{a_j}\Delta\theta_j. \tag{2.39}$$

Taking the continuum limit, we immediately find that the backflow function satisfies the equation

$$F_{a,\tilde{a}}(\theta;\tilde{\theta}) = -\frac{\varphi_{a,\tilde{a}}(\theta-\tilde{\theta})}{2\pi} + \sum_b \Big[K \star \sigma_b n_b(\cdot) F_{b,\tilde{a}}(\cdot;\tilde{\theta})\Big](\theta). \tag{2.40}$$

One could in principle solve this equation to obtain the backflow function of a given state, as specified by the filling function $n$. Once $n$ is known, the physical spectrum

of QP excitations on top of the reference state can then be expressed as

$$k^{\rm ph}_{\tilde{a}}(\tilde{\theta}) = k_{\tilde{a}}(\tilde{\theta}) + \sum_a \int d\theta\, k'_a(\theta)\sigma_a n_a(\theta) F_{a,\tilde{a}}(\theta;\tilde{\theta}) \tag{2.41}$$

$$e^{\rm ph}_{\tilde{a}}(\tilde{\theta}) = e_{\tilde{a}}(\tilde{\theta}) + \sum_a \int d\theta\, e'_a(\theta)\sigma_a n_a(\theta) F_{a,\tilde{a}}(\theta;\tilde{\theta}) \tag{2.42}$$

$$q^{\rm ph}_{i,\tilde{a}}(\tilde{\theta}) = q_{i,\tilde{a}}(\tilde{\theta}) + \sum_a \int d\theta\, q'_{i,a}(\theta)\sigma_a n_a(\theta) F_{a,\tilde{a}}(\theta;\tilde{\theta}). \tag{2.43}$$

Finally, we summarize some suggestive connection between the spectrum of excitations and the fundamental TBA results in Eq. (2.20) (2.31). First, by computing the derivative of the backflow function $F$, one can show that $\left(q^{\rm ph}_{i,a}\right)' = \left(q'_{i,a}\right)^{\rm dr}$. Which implies that the density of states can be expressed as

$$\rho^t_a(\theta) = \frac{1}{2\pi}\left(k^{\rm ph}_a\right)'(\theta) \tag{2.44}$$

which is very reminiscent of the free particle expression for the density of states. Furthermore, the TBA equation (2.31) can be rewritten in terms of the physical energy of excitations as [179, 15]

$$n_a(\theta) = \frac{1}{1+e^{\beta e^{\rm ph}_a(\theta)}}, \tag{2.45}$$

which is reminiscent of the usual Fermi distribution, but with the physical energy in place of the bare QP energy.

**Summary** The paragraphs above exhaust the TBA technology that will be used in this thesis. In summary, Eq. (2.20) determines all the densities ($\boldsymbol{\rho}$, $\bar{\boldsymbol{\rho}}$, $\boldsymbol{\rho^t}$) as a functional of $\boldsymbol{n}$. Furthermore Eq. (2.31) and Eq. (2.34) determine the filling function $n$ for thermal states and GGE-states respectively. Finally, once we know the filling function $\boldsymbol{n}$ and all the densities, we can compute macroscopic observables, like the entropy (Eq. (2.29)), the internal energy (Eq. (2.13)). In addition the spectrum of QP excitations on top of a given reference state can also be computed.

## 2.3 Generalized Hydrodynamics (GHD)

The TBA framework outlined above allows one to characterize equilibrium states of integrable systems, but does not offer direct access to correlation functions, transport,

or other dynamical properties. To treat such questions exactly, one is forced to use form-factor expansions that are generally hard to resum for finite-temperature states (nonetheless see Refs. [85, 87, 84, 86, 88] for recent developments). However, the framework of GHD [31, 14] offers a way to leverage the relatively simple TBA solutions to predict the coarse-grained dynamics of integrable systems.

As already mentioned, integrable systems possess an infinite number of quasilocal conserved charges $\{\hat{Q}_j\}$. The quasilocality of the charges means that they admit a representation of the form

$$\hat{Q}_j = \int dx\, \hat{q}_j(x), \tag{2.46}$$

with $\hat{q}_j(x)$ having support centered around position $x$ and rapidly decaying away from $x$. The fact that $[\hat{Q}_j, \hat{H}] = 0$, then implies that there must be a local current density operator $\hat{j}_j(x)$ such that

$$\partial_t \hat{q}_j(x,t) + \partial_x \hat{j}_j(x,t) = 0 \tag{2.47}$$

with the time dependence denoting the evolution in the Heisenberg picture. Taking the expectation value of the above equation on top of a generic out-of-equilibrium state, one can then naturally relate $q_j(x,t) = \langle \hat{q}_j(x,t) \rangle$ and $j_j(x,t) = \langle \hat{j}_j(x,t) \rangle$ via

$$\partial_t q_j(x,t) + \partial_x j_j(x,t) = 0. \tag{2.48}$$

To leverage the continuity equation above, one assumes that the system can be partitioned into mesoscale cells of size $\ell$, each of which is approximately in a local equilibrium state (i.e., one described by a GGE ensemble). Nonetheless, globally, the system can be far away from equilibrium because the generalized inverse temperatures $\beta_j$ vary from cell to cell. Under this hydrodynamic assumption, the coarse-grained dynamics of the system reduces to the dynamics of the parameters that specify a local GGE state, for example the expectation values of the charges $q_j(x,t)$. Finally, if we were able to determine $j_j$ from the set of expectation of the charges $\{q_i\}_{i\in\mathbb{N}}$, then one could in principle solve the continuity equation above for all the functions $q_j(x,t)$ and hence be able to describe the state of the system at all times and at scales larger than $\ell$.

In practice, the set of charge expectations $q_j(x,t)$ is not the most convenient set of variables to work with. A much more convenient set of variables is the density of QPs $\boldsymbol{\rho}(x,t)$ of the space- and time-dependent GGE ensemble, which determines the

set of $q_j(x,t)$ through Eq. (2.33), or, more explicitly

$$q_j(x,t) = \sum_a \int d\theta\, q_{j,a}(\theta)\rho_a(\theta). \tag{2.49}$$

[Note that there are two distinct functions, both denoted as $q_j$, as it is common notation. The convention is that, if the arguments of $q_j$ are space and time coordinates, as in the LHS of the above expression, then this denotes the expectation value of the charge-density operator $\langle \hat{q}_j(x,t)\rangle$. Instead, if the argument of $q_j$ is a rapidity variable, as in the RHS of the above expression, then the function denotes the one-QP eigenvalue of the charge operator.] Assuming that the set of $\{q_{j,a}(\theta)\}_{j\in\mathbb{N}}$ forms a complete basis in the space of functions $f_a(\theta)$, then each GGE state is uniquely determined by $\boldsymbol{\rho}$, in terms of which GHD is more conveniently formulated.

A crucial aspect that is still missing in the description above is then a constitutive relation between $\boldsymbol{\rho}$ and $j_j$ in the same cell. Regarding this problem, it is widely accepted, and there are many complementary proofs [40, 31, 20, 163, 197, 164, 19], that on top of a homogeneous GGE

$$j_j = \sum_a \int d\theta\, q_{j,a}(\theta)\rho_a(\theta)v_a^{\rm eff}(\theta) \tag{2.50}$$

with

$$v_a^{\rm eff}(\theta) = \frac{(e')_a^{\rm dr}(\theta)}{(k')_a^{\rm dr}(\theta)} = \frac{(e_a^{\rm ph})'(\theta)}{(k_a^{\rm ph})'(\theta)}. \tag{2.51}$$

Note that Eq. (2.50) holds exactly only for a homogeneous GGE ensemble. Nonetheless, if the lengthscale $\ell$ at which inhomogeneity appears is large, one can imagine that $j_j(x,t)$ can be expanded in powers of $1/\ell$, or more concretely in a gradient expansion, where Eq. (2.50) will be the leading contributions, viz.

$$j_j(x,t) = \sum_a \int d\theta\, q_{j,a}(\theta)\rho_a(\theta)v_a^{\rm eff}(\theta) + O(\partial_x\boldsymbol{\rho}). \tag{2.52}$$

Neglecting the derivative corrections in the above equation and using completeness of the charges $q_{j,a}(\theta)$ one then obtains the GHD equation

$$\partial_t\rho_a(\theta;x,t) + \partial_x\left(v_a^{\rm eff}[\boldsymbol{\rho}(x,t)](\theta)\rho_a(\theta;x,t)\right) = 0. \tag{2.53}$$

Note that, in spite of its formal simplicity, the above equation is highly nontrivial since $v^{\rm eff}$ at a certain position is a functional of the QP density $\boldsymbol{\rho}(x,t)$ at that position. The

above equation takes a simpler forms if $\boldsymbol{\rho}(x,t)$ is expressed in terms of the occupation functions $\boldsymbol{n}(x,t)$ instead. In terms of this, the GHD equation reads

$$\partial_t n_a(\theta;x,t) + v_a^{\text{eff}}[\boldsymbol{n}(x,t)](\theta)\partial_x n_a(\theta;x,t) = 0. \tag{2.54}$$

[For this reason the fillings $n_a(\theta)$ are sometimes referred to as normal modes in the context of GHD]

Finally, note that the partial differential equation above is amenable to be solved with the method of characteristics. In fact, we can note that the value of $n_a(\theta;x,t)$ is constant along the trajectory $x = r_{a,\theta}(t)$ if $r$ solves the ordinary differential equation

$$\frac{dr_{a,\theta}(t)}{dt} = v_a^{\text{eff}}[\boldsymbol{n}(r_{a,\theta}(t),t)](\theta). \tag{2.55}$$

While this is still too hard to be solved analytically, it gives a very convenient scheme for the numerical solution of the GHD equation

**The Euler scale** From the method of characteristics, we know that the solutions of the GHD equation above are ballistically propagating charge and density profiles. One can exploit this fact and define the Euler scaling limit, i.e., a rescaling of space and time of the form $(x,t) \mapsto (\lambda x, \lambda t)$ in the limit $\lambda \to \infty$. Then, the solution of the GHD equation are still nontrivial in the Euler scaling limit, but the gradient correction $O(\partial_x \boldsymbol{\rho})$ become suppressed by a factor $\lambda^{-1}$. Therefore, in this limit, the gradient corrections can be neglected and the GHD equation become asymptotically exact.

In practice, while Eq. (2.53) determines the ballistic spreading of charge and densities profiles, the gradient corrections will give rise to diffusive corrections and account for a broadening on top of the ballistic motion.

### 2.3.1 Linear response within GHD

One of the easiest application of GHD is the study of linear response functions related to transport on top of a stationary state, i.e. a homogeneous GGE state. The response functions that can be most easily studied are the ones that reduce to two-point correlators of either charge densities $\hat{q}_j$ or current densities $\hat{j}_j$. As we will show their computation is quite straightforward, once all TBA quantities are computed on top of the a stationary GGE state.

We start by discussing in details the case of charge-charge correlators of the form

$$\langle q_i(x,t)q_j(0,0)\rangle_C = \langle q_i(x,t)q_j(0,0)\rangle - \langle q_i(x,t)\rangle\langle q_j(0,0)\rangle. \tag{2.56}$$

In the GHD formalism this correlator can be formally written as [51, 96, 47]

$$\langle q_i(x,t)q_j(0,0)\rangle_C = -\frac{\delta q_i(x,t)}{\delta\beta_j(0,0)}. \tag{2.57}$$

This equation should be interpreted as follows. The starting state is a homogeneous GGE state, characterized by some filling function $\boldsymbol{n_0}$. The GGE ensemble describing the hydrodynamic cell at $(0,0)$ gets perturbed by increasing its generalized inverse temperature $\beta_j$. Under the advection equation (2.54), the perturbation produced at $(0,0)$ will eventually spread out and ultimately affect the local GGE ensemble at $(x,t)$, and consequently affect $q_i(x,t)$. The three steps described in words above can be directly translated into equations as

$$\frac{\delta q_i(x,t)}{\delta\beta_j(0,0)} = \sum_{a,a'}\int d\theta \int d\theta' \, \frac{\delta q_i(x,t)}{\delta n_a(\theta;x,t)}\frac{\delta n_a(\theta;x,t)}{\delta n_{a'}(\theta';0,0)}\frac{\delta n_{a'}(\theta';0,0)}{\delta\beta_j(0,0)} \tag{2.58}$$

Note that the first and second term are purely TBA quantities as they involve the same hydrodynamic cell. These can be straightforwardly computed from the machinery developed in the previous section, obtaining

$$\frac{\delta q_i(x,t)}{\delta n_a(\theta;x,t)} = \frac{1}{2\pi}(k')_a^{\mathrm{dr}}(\theta)q_{i,a}^{\mathrm{dr}}(\theta) \tag{2.59}$$

$$\frac{\delta n_a(\theta;0,0)}{\delta\beta_j(0,0)} = -n_a(\theta)\left[1-n_a(\theta)\right]q_{j,a}^{\mathrm{dr}}(\theta), \tag{2.60}$$

where it is meant that the right hand side is evaluated on the state characterized by $\boldsymbol{n_0}$.

The last object that is left is $\frac{\delta n_a(\theta;x,t)}{\delta n_{a'}(\theta';x,t)}$, describing how perturbations to $\boldsymbol{n}$ propagate. As previously observed the advection equation (2.54) is generally hard to solve due to its nonlinearity. In this context, however, it suffices to consider small fluctuations $\boldsymbol{\delta n}$ about a spatially homogeneous generalized Gibbs state, viz. $\boldsymbol{n}(x,t) = \boldsymbol{n_0} + \boldsymbol{\delta n}(x,t)$. At leading order in $\boldsymbol{\delta n}$, we can then approximate $v^{\mathrm{eff}}[\boldsymbol{n}]$ as $v^{\mathrm{eff}}[\boldsymbol{n_0}]$. This greatly simplifies the solution of the GHD equation. By using the characteristic method, one can see that $\delta n_a(\theta;x,t)$ is constant along rays of the form

$r_{a,\theta}(t) = v_a^{\rm eff}[\boldsymbol{n_0}](\theta)t + x_0$. Therefore

$$\frac{\delta n_a(\theta;x,t)}{\delta n_{a'}(\theta';0,0)} = \delta_{a,a'}\delta(\theta-\theta')\delta(x-v_a^{\rm eff}(\theta)t). \tag{2.61}$$

Putting everything together we then have

$$\langle q_i(x,t)q_j(0,0)\rangle_C = \sum_a \int d\theta \rho_a^t(\theta)n(\theta)\left[1-n_a(\theta)\right] q_{i,a}^{\rm dr}(\theta)q_{j,a}^{\rm dr}(\theta)\delta(x-v_a^{\rm eff}(\theta)t). \tag{2.62}$$

From this results, any two-point function can then be computed through the hydrodynamic projection principle. The idea is that any perturbation to the system can be decomposed as a perturbation of the charges $\{q_j(x,t)\}$ plus perturbation of other degrees of freedom that rapidly relax. The long-time limit of any two-point function can then be obtained by computing how the application of the operators affects the charge expectations. For example, in the case of current densities, we have $\delta j_i(x,t) = \sum_j A_{i,j}\delta q_j(x,t) + \cdots$, where $\cdots$ represents the projection of the current onto rapidly-relaxing operators, and the matrix $A_{ij}$ can be related to the dressing transformation and the effective velocity in hydrodynamics. Along these lines, one can derive the long-time limit of the current-current correlators as

$$\langle j_i(x,t)j_j(0,0)\rangle_C = \sum_a \int d\theta \rho_a^t(\theta)n(\theta)\left[1-n_a(\theta)\right] q_{i,a}^{\rm dr}(\theta)q_{j,a}^{\rm dr}(\theta)\left[v_a^{\rm eff}(\theta)\right]^2\delta(x-v_a^{\rm eff}(\theta)t). \tag{2.63}$$

Importantly, the results and relations described in this subsection are not exact equalities. They, however, become asymptotically exact at the Euler scale after the two-point correlator is averaged over space-time mesoscopic cells to eliminate rapidly oscillating contributions. [2]

A quantity of particular importance is the Drude weight, defined as the long-time limit of the current-current correlation function

$$D_{ij} = \beta \lim_{t\to\infty}\frac{1}{t}\int_{-t}^{t} dt' \int dx \langle j_i(x,t')j_j(0,0)\rangle_C. \tag{2.64}$$

The physical significance of the Drude weight is most clear in the case of a $U(1)$ charge $\hat{q}_0$. Here the Drude weight appears as a zero-frequency singularity of the conductivity

$$\sigma(\omega) = \frac{i}{\omega+i0^+}D_{0,0} + (\text{regular}). \tag{2.65}$$

[2] Nonetheless, the oscillating contributions can also be computed in some cases by appropriately modifying the hydrodynamic projection [184].

Integrating the current-current correlator in Eq. (2.63) we can then obtain

$$D_{ij} = \beta \sum_a \int d\theta \, \rho_a \left[1 - n_a\right] (q_a^i)^{\rm dr} (q_a^j)^{\rm dr} \left[v_a^{\rm eff}\right]^2 , \tag{2.66}$$

providing a closed-form expression for the Drude weight solely from TBA data. Note that this expression has a rather simple physical interpretation: a quasiparticle of type $(a, \theta)$ carries charge $(q^j)^{\rm dr}$ while moving ballistically at a speed $v^{\rm eff}$. Since the quasiparticle never scatters, this current does not relax. The Drude weight is the sum of these persistent currents due to each quasiparticle. [Since most of the times we will be interested with the diagonal component of the Drude weight we will often abbreviate $D_{ii}$ as $D_i$.]

# Chapter 3

# Transport in the 1D Hubbard model

The Hubbard model has a storied history in the study of strong correlations in many-body quantum systems. Originally formulated to model interacting electrons in narrow energy bands [95], it came to renewed prominence following the discovery of the copper-oxide high-temperature (high-$T_c$) superconductors. The ability of the Hubbard model to capture what are believed to be key features of the high-$T_c$ phase diagram [128] — for example, the existence of an antiferromagnetic Mott insulator at half filling that could yield unconventional superconducting states upon doping — have made it an enduring subject of theoretical studies [72], and a favored testbed for new techniques. Numerical approaches [126, 168] such as dynamical mean-field theory [73] and density-matrix renormalization group [173], as well as theoretical frameworks such as quantum spin liquids [172, 21] and quantum criticality [170], were either devised for, or greatly stimulated by, application to the Hubbard model.

An influential line of inquiry pertains specifically to the Hubbard model in *one* spatial dimension, which admits an exact solution via the technique of the Bethe ansatz [59]. This integrability has meant that many subtle features of the model, including non-perturbative effects, can be explored with analytical control — including those, such as the existence of hidden symmetries [194], that extend also to its higher-dimensional counterparts. The one dimensional model can also be experimentally relevant in its own right: for instance, one-dimensional (extended) Hubbard models have been used to describe correlations in carbon nanotubes [7], and as a starting point for the description of materials, such as organic charge-transfer salts [105], that can be approximated as quasi-one-dimensional [75].

More recently, the Hubbard model has also received much attention in a setting quite distinct from its solid-state origins: namely, that of ultracold atomic gases [103, 17, 130]. Over the past two decades, it has been the subject of a concerted experimental effort to build 'optical lattice emulators': systems of cold trapped neutral gases moving in lattice potentials and subject to strong contact interactions. The overarching goal is to engineer artificial systems whose microscopic Hamiltonian is *exactly* that of the Hubbard model, so as to experimentally address and potentially settle the many questions that remain the subject of spirited theoretical debate. This program has had striking successes, such as experimental realization of the *bosonic* Hubbard model [74] and its Mott insulator-superfluid transition [139, 76, 66, 124, 89, 102, 137, 109, 5, 191] and the detection of anomalous transport in 2D quantum Heisenberg magnets [93] — but has also faced unexpected obstacles in accessing the low-temperature regime of the model in its original, fermionic, *avatar*. Another challenge is that much of the theoretical lore on the Hubbard model focuses on observables — such as conductivities and spectral properties — that are naturally accessed in solid-state experiments but are often less tractable from an atomic-physics perspective. Despite these hurdles, over the past few years different groups have been able to access a range of temperature scales in Fermi-Hubbard optical lattices [36, 142], and perfected new techniques, such as quantum gas microscopy [6, 35, 91, 159, 155, 55], that offer direct lattice-scale probes of these systems [185, 195, 18, 153, 60, 127, 2, 22].

Here we apply the techniques of GHD to the one-dimensional Hubbard model. We focus on two characteristic features of the one-dimensional model: (i) temperature-tuned spin-dynamics crossovers in the regime of ballistic transport at strong coupling; and (ii) superdiffusive dynamics at half filling and/or zero magnetization. In the former case, we identify an integrable analog of the crossover between spin-incoherent [63, 34, 141, 64, 65, 156, 101] and spin-coherent dynamics identified within the framework of Luttinger liquid theory [77]. We give a precise characterization of this crossover in the language of integrability, and identify its signature in the spin Drude weight (that characterizes the ballistic transport of spin). We also compute the Drude weights for charge and energy transport, in which the crossover is only manifest in subleading corrections in $1/U$. At half-filling and zero magnetization, some subset of conserved charges are transported sub-ballistically but super-diffusively, with dynamical properties governed by Kardar-Parisi-Zhang (KPZ) scaling [111], while the energy transport remains ballistic. We present analytical, semiclassical, and numerical arguments for KPZ scaling at the special $SO(4)$ symmetric point.We thus give

a comprehensive picture of temperature-dependent transport and response in the one-dimensional Hubbard model. The present discussion thus complements existing studies that have addressed transport in the one-dimensional Hubbard model using rigorous bounds on transport coefficients [114, 199, 12, 30, 29], and via numerical simulations [114, 112, 113, 162, 198, 71, 165, 115, 107, 167]. It also substantially extends previous GHD results [96, 98] by studying superdiffusion, crossovers in spin dynamics, and the associated experimental signatures. We emphasize that many of the distinctive experimental signatures of spin transport in the Hubbard model should be detectable in near-term experiments on ultracold atoms using optical gas microscopes [153].

## 3.1 One-dimensional Hubbard model: overview

### 3.1.1 Model and Symmetries

Our focus throughout this chapter will be the electronic Hubbard model, described by the Hamiltonian

$$\hat{H} = \hat{T} + \hat{V} \tag{3.1}$$

where

$$\hat{T} = -t \sum_{j,\sigma=\uparrow,\downarrow} \left( c^\dagger_{j+1,\sigma} c_{j,\sigma} + \text{h.c.} \right), \tag{3.2}$$

is a nearest-neighbor hopping term (we set $t = 1$ henceforth),

$$\hat{V} = U \sum_j \left( n_{j,\uparrow} - \frac{1}{2} \right) \left( n_{j,\downarrow} - \frac{1}{2} \right) \tag{3.3}$$

is the usual on-site Hubbard interaction (with $n_{j,\sigma} \equiv c^\dagger_{j,\sigma} c_{j,\sigma}$). Furthermore we will be interested in computing linear response functions on top of thermal states of the form

$$\hat{\rho} = \frac{1}{Z} \exp\left( -\beta \hat{H} + \beta\mu \hat{Q} + \beta h \hat{S}^z \right). \tag{3.4}$$

Here the chemical potential $\mu$ and magnetization $h$ couple to the two $U(1)$ conserved quantities, namely the total electric charge

$$\hat{Q} = \sum_j \left( n_{j,\uparrow} + n_{j,\downarrow} \right), \tag{3.5}$$

and total magnetization along the $z$-axis

$$\hat{S}^z = \frac{1}{2}\sum_j \left(n_{j,\uparrow} - n_{j,\downarrow}\right), \tag{3.6}$$

whose transport, along with that of the energy, will be our primary concern below. We have chosen a convention such that for $\mu = 0$ the system is at half-filling, which for a chain of $L$ sites is defined as $\frac{\langle \hat{Q} \rangle}{L} = \frac{1}{L}\sum_{j,\sigma}\langle n_{j,\sigma}\rangle = 1$.

Besides its evident translational invariance, the Hubbard Hamiltonian $\hat{H}$ (3.1) and the state $\hat{\rho}$ (3.4) enjoy several global symmetries; for a complete treatment we refer the reader to Ref. [59] and only summarize those most pertinent to our discussion. First, observe that $\hat{H}$ and $\hat{\rho}$ commute with $\hat{Q}$ and $\hat{S}^z$, and so these are always symmetries: below, we will discuss the transport of the conserved charge and magnetization corresponding to these two $U(1)$ symmetries. However, the global symmetry of the system is enhanced when either $\mu = 0$ or $h = 0$ (or both). For $h = 0$, the $U(1)_s$ spin symmetry of rotations about the $z$ axis extends to a full non-abelian $SU(2)_s$ symmetry of rotations about an arbitrary axis in spin space. This $SU(2)_s$ symmetry can can be made manifest [67] by rewriting the interaction term as $\hat{V} = -\frac{2U}{3}\left(\boldsymbol{S}_j \cdot \boldsymbol{S}_j\right)$, where we have defined $\boldsymbol{S}_j = \sum_{\alpha,\beta} c^\dagger_{j\alpha}\frac{\boldsymbol{\sigma}_{\alpha\beta}}{2}c_{j\beta}$, where $\boldsymbol{\sigma} = (\sigma_x, \sigma_y, \sigma_z)$ is a triplet of Pauli matrices. Evidently, $\hat{S}^z$ coincides with our definition in (3.6), and the other components of $\boldsymbol{S}$ are chosen so as to satisfy the usual $SU(2)_s$ Lie algebra $[\hat{S}^\alpha, \hat{S}^\beta] = i\epsilon^{\alpha\beta\gamma}\hat{S}^\gamma$ of spin rotations. As a consequence of this $SU(2)_s$ symmetry, thermal states for $h = 0$ are not magnetized in any direction. On the other hand, for $\mu = 0$, the nearest-neighbor model has a distinct $SU(2)$ invariance discovered by Yang [194] and dubbed the '$\eta$-pairing' symmetry. [1] The three generators $\hat{\boldsymbol{\eta}} = (\hat{\eta}^x, \hat{\eta}^y, \hat{\eta}^z)$ of the $SU(2)_\eta$ symmetry take the form

$$\hat{\eta}^x = \frac{\hat{\eta}^+ + \hat{\eta}^-}{2}, \hat{\eta}^y = \frac{\hat{\eta}^+ - \hat{\eta}^-}{2i}, \hat{\eta}^z = \sum_j \frac{n_{j\uparrow} + n_{j\downarrow} - 1}{2}, \tag{3.7}$$

where $\hat{\eta}^+ = -\sum_j (-1)^j c^\dagger_{j\uparrow} c^\dagger_{j\downarrow} = (\hat{\eta}^-)^\dagger$. It is straightforward to show that this generates an $SU(2)_\eta$ algebra $[\hat{\eta}^\alpha, \hat{\eta}^\beta] = i\epsilon^{\alpha\beta\gamma}\hat{\eta}^\gamma$ that is distinct from that of spin rotations, since $[\hat{S}^\alpha, \hat{\eta}^\beta] = 0$. From the relation $\hat{Q} = 2\hat{\eta}^z + 1$, it is clear that for $\mu \neq 0$, the

[1] The $\eta$-pairing symmetry is most conveniently understood by performing a particle-hole (or 'Shiba') transformation on a single spin species. This interchanges charge and spin, and maps the Hamiltonian $\hat{H}$ (upto unimportant constants) to another Hamiltonian $H'$ of the same form as (3.1) but with $U' = -U$, $h' = -\mu$ and $\mu' = -h$. The interchange of $SU(2)_\eta$ and $SU(2)_s$ generators reveals that $SU(2)_\eta$ invariance of $H$ is equivalent to an $SU(2)_s$ invariance of its single-spin-Shiba-transform $H'$.

system only has the $U(1)$ symmetry generated by $\hat{\eta}^z$, which coincides with that of charge conservation. However, when $\mu = 0$, the system enjoys the full $SU(2)_\eta$ symmetry generated by the above operators. Therefore as in the case when $h = 0$, the extra $SU(2)_\eta$ symmetry has implications for the thermal states, as $\langle \eta^z \rangle = 0$, thermal states for $\mu = 0$ are at half-filling.

Finally, at the special point $\mu = h = 0$ which lies at the intersection of the lines of $SU(2)_s$ and $SU(2)_\eta$ symmetry, the system enjoys an extended $SO(4) \simeq SU(2)_s \times SU(2)_\eta/\mathbb{Z}_2$ symmetry. [2]

Note that the symmetries discussed up to this point are not necessarily specific to the nearest-neighbor Hubbard model or to its one-dimensional setting. Absent an explicit breaking of spin rotation (e.g. by the introduction of spin-orbit coupling), even extended Hubbard models continue to enjoy $U(1)_s$ ($SU(2)_s$) symmetry for $h \neq 0$ ($h = 0$). Similarly, the global $U(1)_c$ symmetry is generically a feature of Hubbard-like models, unless an explicit superconducting pairing term is introduced, for instance in order to capture the effects of externally induced superconductivity. Finally, for any *bipartite* [3] hopping $\hat{T}$ we expect the full $SU(2)_\eta$ symmetry.

However, as previously noted, the one-dimensional nearest-neighbor Hubbard model – unlike its generalizations and higher-dimensional counterparts — is an integrable model that hosts an extensive set of conserved quantities. Consequently we may determine its full spectrum of eigenstates *exactly* for any fixed system size $L$, particle number $N$, and magnetization $M$ via the (nested) Bethe ansatz. By taking the thermodynamic limit of the resulting Bethe equations and using the framework of generalized hydrodynamics, we can extract transport coefficients such as Drude weights and d.c. conductivities. Henceforth, we focus on the one-dimensional model; in the remainder of this section we summarize the TBA data of the Hubbard model.

## 3.2 TBA data for the Hubbard Model

Here we give a brief summary of the TBA data for the one-dimensional Hubbard model, as can be derived through nested coordinate Bethe ansatz. Much of this material may be found in classic monographs [Refs. [179, 59]]; to our knowledge its

[2] The $\mathbb{Z}_2$ quotient reflects the fact that although $[\hat{S}^\alpha, \hat{\eta}^\beta] = 0$, the allowed irreducible representations of $SU(2)_s$ and $SU(2)_\eta$ are not independent: either both are integer or both are half-odd-integer. Note that this distinction is only important in considering the global Lie group structure rather than the Lie algebra, and is hence unimportant to our semiclassical analysis in Section 3.4.2.

[3] By bipartite hopping we mean that the lattice may be divided into two disjoint sets of sites $A, B$ such that $\hat{T}$ has no matrix elements between the two sets.

first application in conjunction with the GHD formalism is in Ref. [96], of which we will follow the notation.

First, since $U(1)$ charge and spin conservation are valid symmetries for any $\mu, h$, we can work in sectors with fixed particle number $N = N_\uparrow + N_\downarrow$ and magnetization $M = \frac{N_\uparrow - N_\downarrow}{2}$, where $N_\uparrow$, $N_\downarrow$ are the number of up and down spin electrons respectively. Then, exploiting particle-hole symmetry $\mathcal{P} : c_{j,\sigma} \mapsto (-1)^j c^\dagger_{j,\sigma}$ (under which $\mu \mapsto -\mu$), we can restrict ourselves to sectors with the total number of particles $N$ satisfying $N < L$. Similarly, exploiting the discrete symmetry $S^z \mapsto -S^z$ (under which $h \mapsto -h$), we can limit our study to sectors for which the magnetization $M > 0$, Under these assumptions, we can build a basis of Bethe ansatz states by starting with states of $N$ spin-up electrons, whose rapidity we denote by $u_j$ (where $1 \leq j \leq N$), and adding $N_\downarrow$ magnon-like excitations, with rapidities $w_j$ (where $1 \leq j \leq N_\downarrow$). We can also associate each root with a definite charge under the two $U(1)$ symmetries: each $u_j$ root has charge $q = 1$ and $z$-magnetization $m = 1/2$, while each $w_j$ root has charge $q = 0$ and $z$-magnetization $m = -1$.

Note that there is formally a slight subtlety with the Bethe ansatz states constructed in this manner: they correspond to only the 'highest weight' states in each $SU(2)_s$, $SU(2)_\eta$ sector (as defined in the $h = \mu = 0$ limit). In each sector the remaining states in the spectrum must be generated by acting on the Bethe-ansatz states with $\hat{S}^- = \hat{S}^x - i\hat{S}^y$ and $\hat{\eta}^-$. However, this is unimportant in the thermodynamic limit as the 'missed' states only contribute a logarithmically vanishing correction to the free energy density. To see that this error is negligible, let us consider a generic $L$-site system with an even number $N$ of $SU(2)$ degrees of freedom each in the spin-1/2 representation, and assume that $N/L$ is held fixed as $N, L \to \infty$. The eigenspectrum can be decomposed into $SU(2)$ multiplets, with each representation $r \in \{0, 1, 2, \ldots, N/2\}$ appearing $n_r$ times, with energies $\epsilon_{r,j}$, where $j = 1, 2, \ldots, n_r$. Then the *exact* free energy per site at inverse temperature $\beta = 1/k_B T$ is given by $\beta f_{\text{ex}} = -\frac{1}{L} \ln \left[ \sum_{r=0}^{N/2} (2r+1) \sum_{j=0}^{n_r} e^{-\beta \epsilon_{r,j}} \right]$, whereas the TBA result $\beta f_{\text{TBA}} = -\frac{1}{L} \ln \left[ \sum_{r=0}^{N/2} \sum_{j=0}^{n_r} e^{-\beta \epsilon_{r,j}} \right]$ neglects the degeneracy factors. However, the free energy difference per site, $\beta \delta f \equiv |\beta f_{\text{ex}} - \beta f_{\text{TBA}}| \leq \frac{\ln(N+1)}{L}$, which vanishes in the thermodynamic limit since $N$ is $O(L)$. Consequently, any quantity that can be derived from TBA is not affected by the degeneracy factors.

Assuming the string hypothesis, the Bethe ansatz spectrum of the Hubbard model is built of an infinite number of quasiparticles/strings species that can be broadly classified into one of three types:

**$y$-particles** Spin-up electrons not bound into larger objects. $q_y = 1$ and $m_y = 1/2$; these come in two branches, [4] labeled $\pm$

**$M|w$-strings** with $M \in \mathbb{N}$, $M \geq 1$. Strings of $M$ $w$-roots, corresponding to a magnon of length $M$. $q_{M|w} = 0$ and $m_{M|w} = -M$.

**$M|uw$-strings** with $M \in \mathbb{N}$, $M \geq 1$. Strings of $2M$ $u$-roots and $M$ $w$-roots, forming a spin-singlet object. $q_{M|uw} = 2M$ and $m_{M|uw} = 0$.

We will refer to these three objects in the TBA spectrum as '$y$-particles', 'magnons' and 'singlets' , respectively. Note that there is an infinite number of magnon and singlet species, indexed by positive integers.

As noted above, each quasiparticle/string is labeled by its species and by a rapidity that describes the position of the corresponding Bethe root. The advantage of working with strings rather than individual Bethe roots is that string centres (which we denote by $\theta$) are real, and hence easier to handle than the full set of complex Bethe roots. Note that for each species there is a specific interval of possible rapidities, that will eventually determine the domain of the corresponding distribution functions, e.g. $\rho_a(\theta)$, $\rho_a^t(\theta)$, or $n_a(\theta)$. The relevant spectral data are summarized in Table 3.1.

To complete the TBA description, we also require the scattering kernels $K_{ab}(\theta)$ for every pair of string species. These are summarized in Table 3.2, and depend on the pair of functions,

$$K_M(\theta) = \frac{1}{2\pi} \frac{UM}{2\left(\theta^2 + M^2U^2/16\right)} \tag{3.8}$$

$$K_{MN}(\theta) = K_{M+N}(\theta) + K_{N-M}(\theta) + 2\sum_{j=1}^{M-1} K_{N-M+2j}(\theta).$$

## 3.3 Ballistic transport, Drude weights, and spin-coherence crossovers at strong coupling

We are now ready to address one of our two main objectives: to analyze the structure of transport processes in the Hubbard model in the strong coupling regime $U/t \gg 1$. As previously noted, the lines $h = 0$, $\mu = 0$ require special consideration due

[4] Note that the fact that there are two branches is because we have chosen to label particles by rapidities; quasimomenta are multivalued functions of rapidity, and so we need an extra label to keep track of the relevant quasi-momentum branch when working with rapidities.

Table 3.1: TBA Spectrum for the Hubbard model. As is customary, we employ units in which the hopping strength, $t = 1$.

| **Species $a$** | **$\theta$ domain** | $\sigma_a$ | $q_a$ | $m_a$ | $k'(\theta)$ | $e_a(\theta)$ |
|---|---|---|---|---|---|---|
| $y$ ($\pm$-branch) | $[-1, 1]$ | $\mp 1$ | $1$ | $\frac{1}{2}$ | $\mp\frac{1}{\sqrt{1-\theta^2}}$ | $\pm 2\sqrt{1-\theta^2} - \frac{U}{2}$ |
| $M\|uw$ | $\mathbb{R}$ | $-1$ | $2M$ | $0$ | $-\frac{1}{\sqrt{1-(\theta+MiU/4)^2}} - \frac{1}{\sqrt{1-(\theta-MiU/4)^2}}$ | $2\sum_{\alpha=\pm 1}\sqrt{1-(\theta+\alpha MiU/4)^2} - MU$ |
| $M\|w$ | $\mathbb{R}$ | $+1$ | $0$ | $-M$ | $0$ | $0$ |

Table 3.2: TBA Scattering kernels for the Hubbard model. Functions $K_M, K_{MN}$ are defined in Eqn. (3.8).

| $\boldsymbol{K_{ab}}$ | $\boldsymbol{y_\pm}$ | $\boldsymbol{N\vert w}$ | $\boldsymbol{N\vert uw}$ |
|---|---|---|---|
| $\boldsymbol{y_\pm}$ | 0 | $K_N$ | $K_N$ |
| $\boldsymbol{M\vert w}$ | $K_M$ | $-K_{MN}$ | 0 |
| $\boldsymbol{M\vert uw}$ | $K_M$ | 0 | $K_{MN}$ |

to the presence of non-Abelian symmetries, which lead to a transport regime that is intermediate between ballistic transport with nonzero Drude weight, and simple diffusion. Accordingly, we discuss this regime in the next section and for now focus on the case when $\mu \neq 0$ and $h \neq 0$.

In the strong coupling limit, a hierarchy of well-separated energy scales can be identified, allowing us to distinguish four different regimes (Fig. 3.1) depending on the temperature $T$. [Note that since we have fixed $\mu, h \neq 0$, within each regime we must be careful to compare the temperature scale with those set by the chemical potential and the field; we provide further details on this below.]

Starting from high temperature, the first transport regime we encounter is

(i) $\boldsymbol{T \gtrsim U \gg t}$: this corresponds to 'generic' high temperature transport, to which all string types contribute. Systems at weak- and strong-coupling show qualitatively similar behavior in this limit.

We access the remaining regimes by lowering the temperature so that $U \gg T$. Transport in these regimes can be approximately understood by projecting out double occupancies to obtain an effective $t-J$ model [59] with $J \sim t^2/U \ll t$, which we can subdivide further into three regimes:

(ii) $\boldsymbol{U \gg T \gg t \gg J}$: in this case, away from half filling we have $\mu = -O(U)$, so that $uw$-strings are not thermally occupied and drop out of transport; therefore, we expect transport properties to be comparable to that of the $t-J$ model at $T = \infty$.

(iii) $\boldsymbol{U \gg t \gg T \gg J}$: this ordering of scales leads to an unusual situation in which charge degrees of freedom are in the low-temperature phase (effectively at $T \simeq 0$), whereas the spin degrees of freedom remain high-temperature (i.e. approximately at $T = \infty$.) A similar regime has been identified in the context of generic Luttinger liquid theory (i.e., without any assumption of integrability) where it has been dubbed the spin-incoherent Luttinger liquid (SILL) [63].

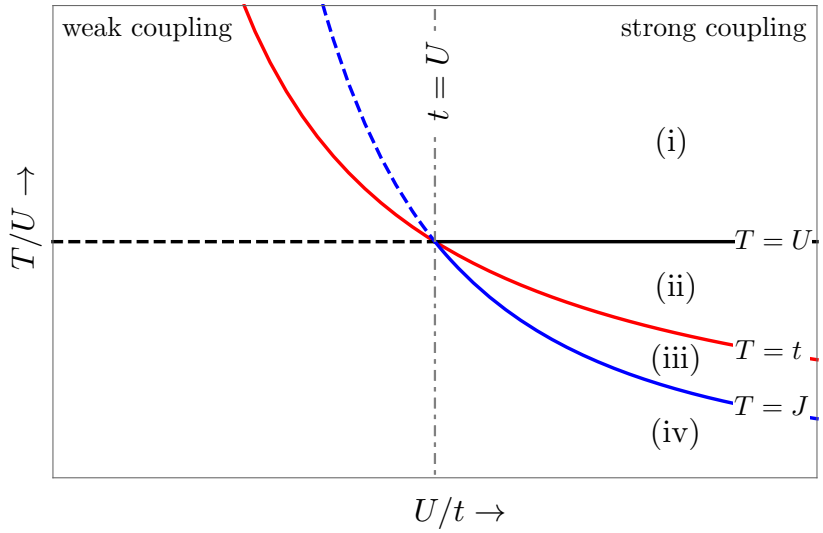


Figure 3.1: Regimes of transport for the Hubbard model. At strong coupling $U \gg t$ we can distinguish four temperature regimes delineated by sharp crossovers (indicated by the solid lines) in dynamics. In descending order of temperature $T$ these are (i) the 'high temperature Hubbard' regime, where $T$ is the biggest energy scale; (ii) the high-temperature $t - J$ regime, where we can effectively ignore double-occupancies since $U \gg t$, but $T$ still exceeds both the charge scale $t$ (i.e., the holon bandwidth) and the effective spin-exchange scale $T \gg J \sim t^2/U$; (iii) the 'spin-incoherent' regime, where the charge fluctuations of the $t - J$ model are cold ($T \ll t$) but the spins remain hot, ($T \gg J$); and finally, the low-temperature regime where the system is described as spin-charge separated Luttinger liquid of coherent charge and spin degrees of freedom, where $T$ is the lowest energy scale. At weak coupling, regimes (i) and (iv) are broadly similar and we expect a crossover at $T \sim t$. In this chapter we will focus on the strong coupling regime and will not discuss the weak-coupling crossovers further.

(iv) $\boldsymbol{U \gg t \gg J \gg T}$: when $T$ is the lowest scale in the problem, we expect to recover normal Luttinger liquid-like behavior including the identification of two distinct speeds that control ballistic propagation of spin and charge, as in simpler integrable models [144] (see also Ref. [16, 15]). As in the case of regime (i), we do not expect a qualitative distinction between weak and strong coupling in this low-temperature regime.

For completeness, we briefly comment on the physics at weak coupling, $t \gg U$. First, as noted above behavior in the regimes (i) (which now emerges when $T \gg t$ and is again the largest energy scale) and (iv) (where $T$ is the smallest scale in the problem) are broadly similar to that seen in the strong-coupling limit. There is no analog of the 'high-temperature $t - J$ model' regime (ii), and the spin-incoherent

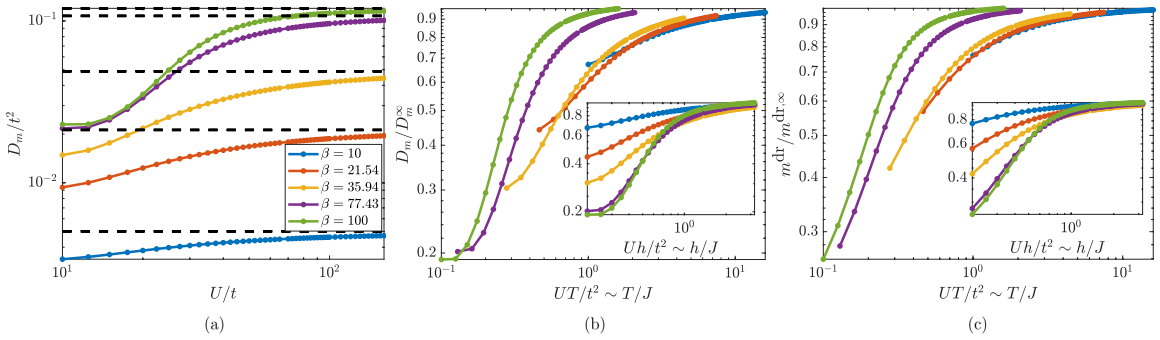


Figure 3.2: Spin Drude weight $D_m$ at the thermal crossover between spin-incoherent and spin-coherent regimes ((iii) and (iv) respectively in Fig. 3.1). We fix $\langle \hat{Q} \rangle / L = 0.3$ and $h/t = 0.04$. (a) $D_m$ as a function of $U$ for various $\beta$. Dashed line indicates the asymptotic value $D_m^\infty$ for $U \to \infty$ in regime (iii). (b) The same data as in panel (a). We observe that for $\beta h \lesssim 1$, $D_m/D_m^\infty$ departs from 1 when $J \sim T$. Instead, if $\beta h \gtrsim 1$, $D_m/D_m^\infty$ departs from 1 when $J \sim h$ (inset). (c) We highlight that the crossover in the Drude weight is a consequence of a change of the dressed magnetization of the $y$-particles at the Fermi points.

regime (iii) is also absent in the sense discussed above.[5] We do not address this regime further in the present work (but see Ref. [59])

### 3.3.1 Spin transport and spin-coherence crossovers

Away from the lines $\mu = 0, h = 0$, the density is fixed away from half-filling $\langle \hat{Q} \rangle / L \neq 1$ and the magnetization is fixed and non-zero $\langle \hat{S}_z \rangle / L \neq 0$. Charge and energy transport are completely unaffected by the crossover from (iii) to (iv), in agreement with a general conjecture [64], and confirmed by explicit calculation below. However, spin transport is sensitive to the crossover, as we now show. In a non-integrable model the crossover would be very clear-cut, as in regime (iii) spin transport would not be ballistic, while in the Luttinger liquid regime (iv) we expect a non-zero spin Drude weight. What happens at the crossover in the integrable Hubbard model is less obvious, since we expect the spin transport to have a ballistic (Drude) response at all temperatures. Surprisingly, the spin-incoherent to spin-coherent crossover has a sharp signature in the spin Drude response itself, as we now demonstrate.

In both regimes the leading contribution in $t/U$ to the spin Drude weight comes from the $y$-particles and is given by (see Sec. 3.3.2 and Appendix 3.C for the deriva-

[5] However, there is an intermediate regime in which $U \ll T \ll t$. In this regime spin excitations are effectively at high temperature, since their characteristic energy scale at weak coupling is the exchange scale $U$. We expect this regime to have some thermodynamic and transport features in common with the SILL.

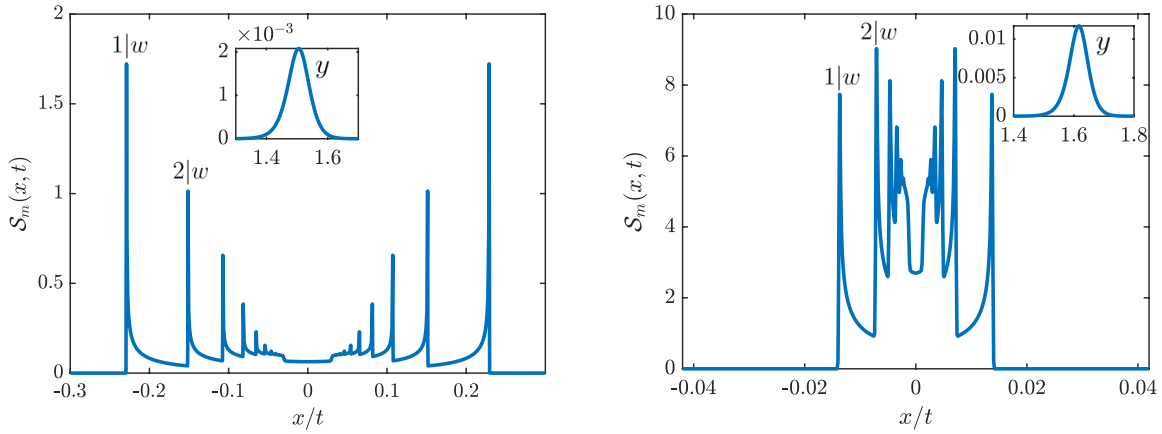


Figure 3.3: Dynamical spin-spin correlation function in (a) the spin-coherent regime ($U = 10$) and (b) the spin-incoherent regime ($U = 160$). In each panel, the main figure displays the rich structure due to slow magnon modes, while the insets show the fast-moving leading front due to $y$-particles. The peaks corresponding to $1|w$ and $2|w$ magnons are marked in the figure. In both figures $h = 0.04$, $\beta = 35.9$, and $\langle \hat{Q} \rangle / L = 0.3$.

tion)

$$D_m = \frac{v_F}{\pi} (m_F^{\mathrm{dr}})^2. \tag{3.9}$$

Here $v_F$ is the Fermi velocity of the $y$-particles and $m_F^{\mathrm{dr}}$ is the dressed magnetization at the Fermi points. At leading order in $t/U$, $v_F$ is the same in the two regimes, whereas $m_F^{\mathrm{dr}}$ undergoes a crossover between regime (iii) and (iv). In regime (iii) we can straightforwardly obtain that $m_F^{\mathrm{dr}} = \tanh(\beta h/2)/2$. Regime (iv) is difficult to understand analytically due to the presence of a non-zero field, especially if $\beta h \lesssim 1$. Thus, we first analyze which parameters can affect the crossover and then rely on numerical solution of the TBA equation in cases where there can be a non-trivial crossover.

The parameters relevant to the characterization of spin transport are $\beta h$ and $h/J$, with the crossover (iii)-(iv) taking place at $\beta J \sim 1$. A first consequence of this observation is that the crossover (iii)-(iv) is more naturally observed by varying $U$ at a fixed $\beta$, since otherwise spin transport will already have a non-trivial dependence due to the variation of $\beta h$. We first analyze the case where $\beta h \gtrsim 1$. In this situation, regime (iii) is practically spin-coherent since the external field $h$ dominates the exchange scale $J$. As a consequence, we do not expect to see a sharp signature in spin transport at the (iii)-(iv) crossover, since the exchange scale is no longer relevant to the spin physics. Instead, we expect a crossover when, as $U$ decreases, $J$ becomes

comparable with $h$ – which occurs inside regime (iv) (see inset of Fig. 3.2b). However, we do expect non-trivial behavior at the (iii)-(iv) crossover when $\beta h \lesssim 1$. In Fig. 3.2, we demonstrate that around this parameter regime a crossover is indeed observable in the spin-Drude weight, as determined by numerically solving the TBA equations (see Appendix 3.A).

In order to shed further light on this crossover, it is useful to examine its qualitative features in the dynamical spin-spin correlators

$$\mathcal{S}_m(x,t) = t\langle S^z_x(t) S^z_0(0)\rangle_C, \tag{3.10}$$

which can be computed through Eq. (2.62) in the Euler-scale limit. The numerical solution of the TBA equation then give the results shown in Fig. 3.3. In both regimes, as noted above, the current response is dominated by fast $y$-particles, which produce a peak at $x/t \simeq v_F$ (see insets). However, the spin-spin correlators also present a rich structure at smaller $x/t$, which is produced by the slow magnons. First, in the spin-incoherent regime (iii) a hierarchy of magnons (truncated at a length $M \sim T/h$) produces a structure which is overall peaked at small $x/t$ (see Fig. 3.3b): in other words, the longest and slowest magnons (with $M \sim T/h$) give the dominant contributions to $\mathcal{S}_m$. In this regime we expect to observe similar phenomenology to that discussed in Ref. [83] for the Heisenberg XXX chain. In contrast, in the spin coherent regime (iv), the amplitudes of the peaks due to $M|w$-magnons with $M > 1$ tend to 0 as $T$ decreases. This happens irrespective of the field $h$: if $h/T \gtrsim 1$, $n_{M|w} \simeq 0$ for $M > 2$, otherwise, if $h/T \lesssim 1$, $\rho^t_{M|w} \to 0$ as $T$ is lowered [59, 39]. Thus, deep in regime (iv), $\mathcal{S}_m$ is dominated by $y$-particles and $1|w$-magnons alone, as can already be seen for the parameters in Fig. 3.3a. However, as these results are most clearly manifest in the long-time limit (recall that the magnons are slow!) they might not be easy to observe in real-time dynamics on shorter timescales. Note that the change in the magnon properties across the crossover is not *directly* visible in the spin Drude weight, which is dominated by $y$-particles in both regimes (iii) and (iv). Instead, they affect the spin Drude weight indirectly, via the the change in the nature of the dressing of the $y$ particles as they scatter off the magnons (see Fig. 3.2c). There is possibly a more direct signature of this crossover in *single-particle* spectral functions that can be measured, e.g. by tunneling experiments. In the Luttinger liquid setting, this allows the extraction of the charge Luttinger parameter, which is effectively doubled in the spin-incoherent regime relative to its low-temperature, spin-coherent value. However these quantities are extremely difficult to compute via

the TBA, as they involve form factors that do not admit the manifold simplifications of GHD. Furthermore, while natural in solid-state systems, they are less well-suited to the cold-atom setting. However, in optical lattice emulators of the Hubbard model, quantum-gas microscopy techniques may allow the measurement of correlation functions and Drude weights [116]. Our work therefore leverages integrability to provide a complementary set of diagnostics for the crossover to those previously known. We expect that the basic structure is likely to survive, with minor modifications, in systems with weak integrability breaking [69, 53] – for instance, the $\delta$-function peak in the Drude response is broadened into a narrow Lorentzian with a decay time set by the scale of integrability breaking. Further investigations of the crossover regime in experimentally-relevant systems and observables seem warranted.

### 3.3.2 Charge and energy transport

To complete the discussion, we now briefly summarize results for charge and energy transport away from half filling. Both can be understood analytically in most of the regimes identified above by using appropriate expansions of the TBA and dressing equations; details are provided in Appendices 3.A, 3.B, and 3.C, but we summarize the intuition behind the expansions for clarity. Formally, the TBA and dressing equations for the strings (i.e., the magnons, and the singlets) as presented in Chapter 2 are highly nonlocal in the species index, as they couple every species of string to every other species. This makes their solution computationally challenging even from a numerical perspective. However, they simplify in both the high-temperature and low-temperature regimes, as we now discuss. At high temperatures, long strings have appreciable filling, so that $n_{M|s}$ decays slowly for $M \to \infty$ (where $s = w$ or $s = uw$). In this limit, it is useful to recast the TBA and dressing equations into an alternative "quasi-local" form discussed in Appendix 3.A. At low-temperatures, only short strings contribute and so it is safe to truncate the TBA equations even in their nonlocal form. In certain cases – notably, in the spin-incoherent regime (iii) – it is convenient to use a 'hybrid' form of the TBA that invokes the nonlocal form for some species and the quasilocal form for others. (Heuristically, this can be understood by thinking of the magnons as being at high-temperature and tractable in the quasilocal form, and the singlets and $y$-particles being amenable to the low-temperature nonlocal description.)

In regime (i), we can can first perform a high-temperature expansion of the TBA equations and retain the first few terms to determine $n_a(\theta)$, and then expand in $t/U$ to solve for the density, the effective velocity and the dressed charges. Regimes (ii)

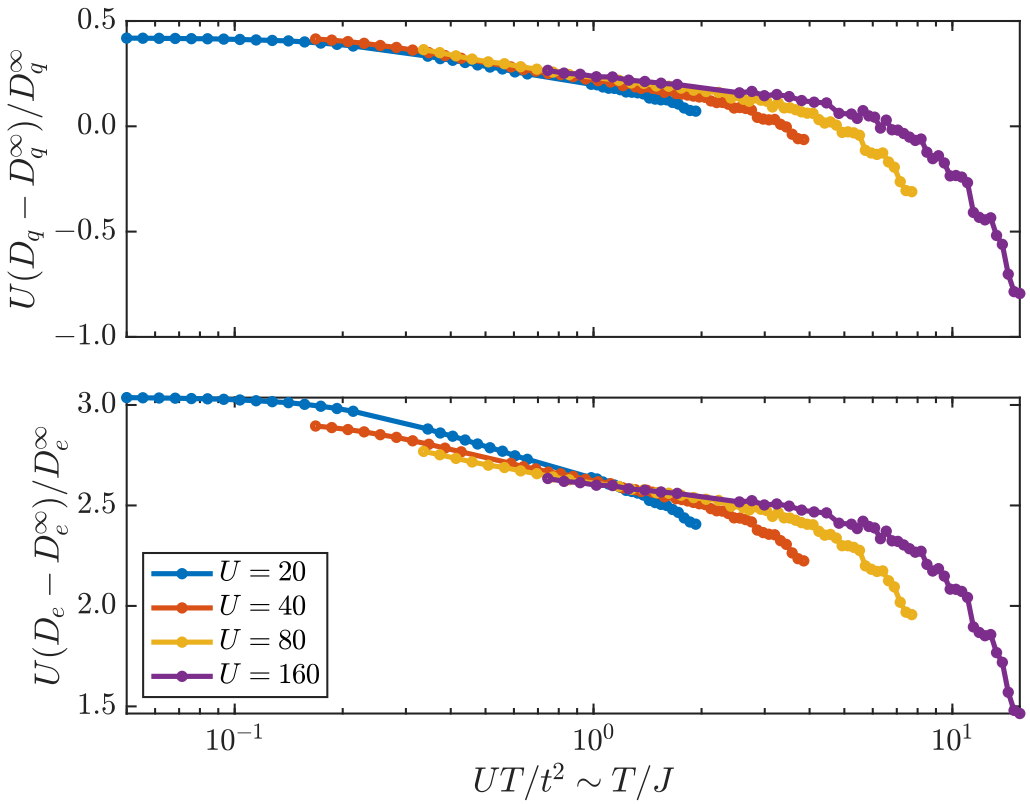


Figure 3.4: The crossover between the spin-incoherent regime (iii) and spin-coherent regime (iv) is also visible in subleading corrections to the charge and energy Dude weights. The plots show the magnitude of the relative correction to the Drude weight compared to the leading order expressions in $t/U$ ($D_q^\infty$ and $D_e^\infty$) given by Eq. (3.11). Apart from a tail at large $T$, which is due to the crossover to regime (ii), we see that the corrections indeed scale like $t/U$ and depend on the ratio $T/J$, signaling that their change is really a consequence of the (iii)-(iv) crossover. Numerical parameters: $h = 0$ and $\langle n \rangle = 0.3$.

and (iii) can be accessed instead by expanding directly in $t/U$. (Note however that since the $T \to \infty$ and $U \to \infty$ limits commute, regimes (i-iii) can be treated in a unified way. [6] The $t/U$ expansion breaks down in regime (iv), where we can, however, exploit the $T \to 0$ limit in the presence of a finite magnetic field.

In all regimes, we find that the dominant contribution to the charge and energy Drude weights in the strong coupling limit is from the $y$-particles

$$D_{\mathcal{O}} \simeq \frac{\beta}{2\pi} \sum_{a=y_\pm} \int d\theta \, n_a(\theta) \left(1 - n_a(\theta)\right) \left[\mathcal{O}_a^{\mathrm{dr}}(\theta)\right]^2 \frac{\left[e_a'(\theta)\right]^2}{|k_a'(\theta)|} \tag{3.11}$$

where $\mathcal{O} = q, e$. To obtain this strong-coupling expression for the Drude weight we used the fact that in the large-$U$ limit, and for $y$-particles, all quantities apart from some dressed charges $\mathcal{O}_a^{\mathrm{dr}}(\theta)$ are not dressed to leading order in $t/U$, and applied the identity $|k_a'(\theta)| = 2\pi\rho_a^t(\theta)$. Furthermore, it is understood that in (3.11) the filling factor $n_\pm(\theta)$ is controlled by the bare energies. For energy transport $e_\pm^{\mathrm{dr}}(\theta)$ is always dominated by its bare value $e_\pm(\theta)$ (Table 3.1). To discuss the dressed electric charge, we need to distinguish regime (i), where

$$q_\pm^{\mathrm{dr}} = \tanh(\beta\mu) < 1 \tag{3.12}$$

with $\beta\mu$ implicitly determined by the filling, and regimes (ii), (iii), and (iv) where

$$q_\pm^{\mathrm{dr}} = 1. \tag{3.13}$$

Finally, the expression for the Drude weights can be further simplified in regimes (iii) and (iv), using the fact that $t \gg T$. In this situation, the Fermi factors $n_\pm(\theta)$ are step-like functions, jumping from 0 to 1 at two Fermi points $u_F$. Calling $v_F$ the bare (group) velocity at those points, we find

$$D_{\mathcal{O}} = \frac{v_F}{\pi} \mathcal{O}_F^2, \tag{3.14}$$

where $\mathcal{O}_F$ is the operator evaluated at the Fermi points.

Expanding the TBA equations in regime (iv), we note that charge and energy transport do not change to leading order in $t/U$ during the the crossover from the

[6] Indeed, in the TBA, the energy bandwidth of both $w$ and $uw$-strings is of order $J$, and the expansion is valid as long as $J/T \ll 1$. The crossover between regimes (i) and (ii), is instead due to the chemical potential. Working at a fixed charge density and away from half filling requires $\mu = O(U)$, and therefore the crossover takes place when $\mu/T \sim 1$.

spin-incoherent regime (iii) to the spin-coherent regime (iv). This was postulated in the context of Luttinger liquid theory by Ref. [64] and was used to infer an effective theory of transport in the SILL. Using GHD, we have now verified that this statement is correct up to $t/U$ corrections (see Appendix 3.C). Going beyond the leading terms, we also compute the exact charge and energy Drude weights by numerically solving the GHD equations; these are reported in Fig. 3.4, which clearly shows that these subleading corrections are sensitive to the crossover. An analytical estimate of the corrections in regime (iii) can be found in Appendix 3.C.

## 3.4 Transport at $h = 0$ or $\mu = 0$: KPZ universality and superdiffusion

We now turn to a generic feature of transport expected for all $t/U$, along special high-symmetry lines of the model. As noted above, the Hubbard model hosts an $SU(2)_s$ symmetry whenever $h = 0$ and an $SU(2)_\eta$ symmetry when $\mu = 0$. Along these high-symmetry lines, reasoning in analogy with the case of the isotropic Heisenberg (XXX) spin chain [135, 134, 98, 82, 25, 46, 43], we expect spin and/or charge transport respectively to be transported super-diffusively with length-time scaling governed by the Kardar-Parisi-Zhang (KPZ) dynamical universality class [111], meaning that

$$\langle S^\mu(x,t)S^\mu(0,0)\rangle = \frac{\chi_h}{[\lambda^{(S)}_{\rm KPZ}t]^{2/3}} f_{\rm KPZ}\left(\frac{x}{[\lambda^{(S)}_{\rm KPZ}t]^{2/3}}\right), \tag{3.15}$$

$$\langle n(x,t)n(0,0)\rangle = \frac{\chi_\mu}{[\lambda^{(\eta)}_{\rm KPZ}t]^{2/3}} f_{\rm KPZ}\left(\frac{x}{[\lambda^{(\eta)}_{\rm KPZ}t]^{2/3}}\right), \tag{3.16}$$

where $\chi_h$ and $\chi_\mu$ are respectively the spin and charge susceptibilities, $f_{\rm KPZ}$ is a universal scaling function, and $\lambda^{(S)}_{\rm KPZ}, \lambda^{(\eta)}_{\rm KPZ}$ are characteristic energy scales for the KPZ dynamics. The possibility of superdiffusion in the Hubbard model was first identified in Ref. [98], that used bounding arguments to show that the diffusion constant diverged in the $h \to 0$ limit. However, a detailed analysis of superdiffusive transport has not been previously attempted; also, the $SO(4)$ invariant point $h = \mu = 0$ has not been directly studied. Therefore, here we address these lacunae by providing arguments for KPZ scaling both along the high-symmetry lines and at the $SO(4)$ point, deploying both kinetic-theory approaches [82], and a classical analysis of soft gauge modes [25, 46]. Although physically motivated, neither of these two approaches is mathematically rigorous. Therefore, we then proceed to confirm our predictions using

state-of-the-art numerical simulations using time-evolving Matrix-Product-Operators (MPOs).

We note that after the publication of Ref. [62], on which this chapter is based, Refs. [97, 196] showed that KPZ scaling is a generic feature of many integrable systems with non-abelian symmetry groups.

### 3.4.1 Kinetic theory of superdiffusion

We begin our discussion of superdiffusion of charge and spin by extending to the Hubbard model the analysis presented in Ref. [82] for the XXX model. Focusing for definiteness on spin transport at $h = 0$, we will show here that the spin Drude weight vanishes, signaling the absence of ballistic spin transport. Incorporating diffusive corrections to the linearized GHD framework we then demonstrate the divergence of the spin diffusion constant (see also Ref. [98]). Finally, following the self-consistency argument of Ref. [82], we argue that the specific divergence of the spin diffusion constant can be interpreted as the emergence of superdiffusive transport with dynamical scaling exponent $z = 2/3$. Before proceeding to the Hubbard model, we review the arguments for the simpler case of the XXX model.

**XXX model** The string content of the XXX chain is composed of an infinite number of strings, which can be labeled by their length $M$ [179]. [For many practical purposes they are very similar to the $M|w$ strings of the Hubbard model.] We begin by observing that the spin-spin Drude weight $D_m$, as can be computed through Eq. (2.66), i.e.

$$D_m = \sum_{M=1}^{\infty} \int d\theta \, \rho_M(\theta) n_M(\theta)[1 - n_M(\theta)][v_M^{\text{eff}} m_M^{\text{dr}}(\theta)]^2, \tag{3.17}$$

vanishes in the $h \to 0$ limit. This is because as $h \to 0$, $m_M^{\text{dr}} \to 0$ and more precisely

$$m_M^{\text{dr}} \approx \frac{\beta h}{3} M^2 \tag{3.18}$$

for small $\beta h$ and large $M$. Intuitively this means that the ballistically-moving QPs do not transport spin in the Euler-scale limit.

The zero spin-spin Drude weight signals that the system does not support persistent spin currents and therefore spin transport is sub-ballistic at long times. Therefore, a reasonable expectation is that spin transport takes place diffusively when $h = 0$. In principle, one should then consider GHD with diffusive corrections [41, 152, 79]

to determine the spin diffusion constant. Ref. [82] proposed an approximate argument to compute the spin diffusion constant that becomes exact in the $h \to 0$ limit [45]. This approach is simpler and has the advantage of allowing a self-consistent interpretation of the divergence of the spin diffusion constant taking place at $h = 0$. The starting point is the Euler-scale value of the average square displacement of spin, as can be computed through Eq. (2.62)

$$\langle p^2 \rangle = \sum_j j^2 \langle S_j^z(t) S_0^z(0) \rangle = t^2 \sum_{M=1}^{\infty} \int d\theta \, \rho_M^t(\theta) n_M(\theta)[1 - n_M(\theta)][v_M^{\rm eff}(\theta) m_M^{\rm dr}(\theta)]^2. \tag{3.19}$$

This is a useful quantity since it is directly related to the spin diffusion constant $\mathcal{D}_m$ in the long-time limit by

$$\langle p^2 \rangle \sim 4\chi_h t \mathcal{D}_m \tag{3.20}$$

with $\chi_h = \frac{\partial \langle S_0^z \rangle}{\partial h}$ denoting the static susceptibility in the thermal state.

Intuitively, one can imagine that diffusive corrections will be produced by fluctuations on top of the integral in the RHS of Eq. (3.19). As previously stated, $m_M^{\rm dr} = 0$ on top of an homogeneous ensemble with $h = 0$. However, a typical thermal state will not be uniform and, as a QP moves, it will go through regions with different polarizations, whose contribution ultimately averages to zero. One can therefore introduce an effective fluctuating magnetic field $\tilde{h}(x, t)$ describing the local polarization of the state. In terms of this

$$\langle p^2 \rangle = t^2 \sum_k \frac{1}{k!} \sum_{M=1}^{\infty} \int d\theta \, \rho_M^t(\theta) n_M(\theta)[1 - n_M(\theta)][v_M^{\rm eff}(\theta)]^2 \partial_{\tilde{h}}^k \left[ m_M^{\rm dr}(\theta) \right]^2 \langle \tilde{h}^k \rangle_t \tag{3.21}$$

and therefore

$$\mathcal{D}_m = \frac{t}{4\chi_h} \sum_k \frac{1}{k!} \sum_{M=1}^{\infty} \int d\theta \, \rho_M^t(\theta) n_M(\theta)[1 - n_M(\theta)][v_M^{\rm eff}(\theta)]^2 \partial_{\tilde{h}}^k \left[ m_M^{\rm dr}(\theta) \right]^2 \langle \tilde{h}^k \rangle_t, \tag{3.22}$$

where $\langle \cdot \rangle_t$ denotes the average up to time $t$ along the trajectory of the quasi-particle under consideration.

At long times, the above equation only receives contributions from the $k$ for which $\langle \tilde{h}^k \rangle_t \propto 1/t$, i.e. when $\langle \tilde{h}^k \rangle_t$ is proportional to the inverse of the distance $l = |v^{\rm eff} t|$ traveled by the particle. Assuming Gaussian fluctuations of quasiparticle occupations

(central limiting behavior) we have that

$$\langle \tilde{h}^2 \rangle = \frac{1}{4\chi_h l}. \tag{3.23}$$

with all higher moments scaling giving subleading corrections. Therefore, the diffusion constant is asymptotically given by

$$\mathcal{D}_m = \frac{1}{16\chi_h^2} \sum_{M=1}^{\infty} \int d\theta \, \rho_M^t(\theta) n_M(\theta)[1 - n_M(\theta)] \left| v_M^{\text{eff}}(\theta) \right| \partial_{\tilde{h}}^2 \left[ m_M^{\text{dr}}(\theta) \right]^2. \tag{3.24}$$

By evaluating the above equation within the TBA formalism, one finds the following scaling behavior

$$n_M \sim M^{-2} \tag{3.25}$$

$$\partial_{\tilde{h}}^2 \left[ m_M^{\text{dr}}(\theta) \right]^2 \sim M^4 \tag{3.26}$$

$$\int d\theta \, \rho_M^t(\theta) \left| v_M^{\text{eff}}(\theta) \right| \sim M^{-2}. \tag{3.27}$$

Therefore, $\mathcal{D}_m$ diverges. More precisely, we can define a regularized diffusion constant $\mathcal{D}_m^*(M^*)$, which can be obtained by the previous expression by replacing the sum $\sum_{M=1}^{\infty}$ with $\sum_{M=1}^{M^*}$, and see that $\mathcal{D}_m^*(M^*) \sim M^*$. The divergence of $\mathcal{D}_m$ signals that spin transport is superdiffusive. In this case, we can therefore expect to find a dynamical scaling exponent $z$, defined by the scaling $D \sim t^{2z-1}$, with $1/2 < z < 1$.

As detailed in Ref. [82], $z$ can be computed self-consistently from the scaling behavior derived above. The key observation is that in the above derivation of $\mathcal{D}_m$ we have always assumed that quasiparticles move fast enough such that the magnetic background $\tilde{h}(x,t)$ can be approximately considered fixed and its variance simply scales like $\langle \tilde{h} \rangle_t \sim 1/l$. At a given time $t$, this assumption fails to be true for strings longer than a certain $M^*$ because $\left| v_M^{\text{eff}} \right| \sim M^{-1}$. More specifically, we expect the above assumption to break down for strings such that the distance traveled by the string $v_M^{\text{eff}} t$ is much smaller than the distance travelled by the superdiffusive spin transport $t^z$. Therefore the natural cutoff $M^*$ in the above analysis scales like

$$M^* \sim t^{1-z}. \tag{3.28}$$

Using the fact that $\mathcal{D}_m^* \sim M^*$, we can determine $z$ self-consistently through

$$t^{2z-1} \sim \mathcal{D} \simeq \mathcal{D}_m^* \sim M^* = t^{1-z} \tag{3.29}$$

yielding $z = 2/3$.

**Hubbard model** The arguments above can be translated to the Hubbard model, as we now demonstrate. Focusing for concreteness on the case where $h = 0$, we see that the spin-spin Drude weight vanishes because $m_a^{\rm dr} = 0$ for all QP species $a$ in the model. We can then proceed to estimate the effective spin diffusion constant following Refs. [82, 43]. At time $t$, this will be given by $\mathcal{D}_m(t) = \sum_a \mathcal{D}_a(t)$ where

$$\mathcal{D}_a(t) = \frac{t}{4\chi_h} \int d\theta\, \rho_a(\theta) \left[1 - n_a(\theta)\right] \left[v_a^{\rm eff}(\theta)\right]^2 \times \sum_{j,k} \frac{1}{j!k!} \partial_{\tilde{\mu}}^j \partial_{\tilde{h}}^k \left[m^{\rm dr}(\tilde{\mu}, \tilde{h})\right]^2 \langle \tilde{\mu}^j \tilde{h}^k \rangle_t, \tag{3.30}$$

where $\langle \cdot \rangle_t$ denotes the average up to time $t$ along the trajectory of the QP under consideration, and $\tilde{\mu}$ and $\tilde{h}$ are fluctuations in the effective chemical potential and effective magnetic field perceived by a propagating QP about their mean values (respectively, $\mu/2$ and 0).

At long times, (3.30) only receives contributions from $(j, k)$ for which $\langle \tilde{\mu}^j \tilde{h}^k \rangle_t \propto 1/t$, i.e. when $\langle \tilde{\mu}^j \tilde{h}^k \rangle_t$ is proportional to the inverse of the distance $l = |v^{\rm eff} t|$ traveled by the particle. As for the XXX model we expect that

$$\langle \tilde{h}^2 \rangle = \frac{1}{4\chi_h l}, \qquad \langle \tilde{\mu}^2 \rangle = \frac{1}{4\chi_\mu l}, \tag{3.31}$$

where $\chi_h$ and $\chi_l$ are the magnetic and charge susceptibilities respectively, while all higher moments scaling as higher inverse powers of $t$, and all cross terms vanishing due to the $S^z \to -S^z$ symmetry present for $h = 0$.

Hence, the diffusion constant is asymptotically given by the $t \to \infty$ limit of (3.30), i.e. $\mathcal{D}_m = \sum_a \mathcal{D}_a^\infty$, with

$$\begin{aligned} \mathcal{D}_a^\infty &\equiv \lim_{t\to\infty} \mathcal{D}_a(t) \\ &= \frac{1}{4\chi_h} \int d\theta\, \rho_a(\theta) \left[1 - n_a(\theta)\right] \left|v_a^{\rm eff}(\theta)\right| \\ &\quad \left\{ \frac{1}{4\chi_h} \partial_h^2 \left[m_a^{\rm dr}(\theta)\right]^2 + \frac{1}{4\chi_\mu} \partial_\mu^2 \left[m_a^{\rm dr}(\theta)\right]^2 \right\}. \end{aligned} \tag{3.32}$$

For $h = 0$, we see that the second term containing $\partial_\mu^2 \left[m_a^{\rm dr}(\theta)\right]^2$ vanishes since $\left[m_a^{\rm dr}(\theta)\right]^2$ is identically zero at $h = 0$ due to the $SU(2)_s$ invariance, leaving us with

the final result that

$$\mathcal{D}_a^{\infty} = \int d\theta\, \rho_a(\theta)\left[1-n_a(\theta)\right]\left|v_a^{\rm eff}(\theta)\right| \frac{\partial_h^2\left[m_a^{\rm dr}(\theta)\right]^2}{16\chi_h^2}. \tag{3.33}$$

It remains to analyze this result for $h=0$.

We start by considering the case with $\mu<0$. As pointed out in Ref. [98], the behavior at large $M$ can be understood from the asymptotic form [180] of $Y$ at large $M$

$$Y_{M|w}(\theta) = \left[\frac{\sinh\left(f(\theta)+M\right)\beta h/2}{\sinh(\beta h/2)}\right]^2 - 1, \tag{3.34}$$

$$Y_{M|uw}(\theta) = \left[\frac{\sinh\left(g(\theta)+M\right)\beta \mu}{\sinh(\beta \mu)}\right]^2 - 1, \tag{3.35}$$

for some $O(1)$ functions $f$ and $g$, which will generally depend on $\beta$, $h$ and $\mu$. Specifically, at $h=0$ and $\mu\neq 0$ we have for the magnons

$$Y_{M|w}(\theta) \sim \left(f(\theta)+M\right)^2 - 1, \tag{3.36}$$

while large singlet ($uw$) strings do not contribute to transport as their occupation is exponentially suppressed in $\beta\mu$. Then, using the result that $m_a^{\rm dr} = \partial_{\beta h}\log Y_a$, it follows that

$$m_{M|w}^{\rm dr}(\theta) \sim \frac{1}{3}\left(f(\theta)+M\right)^2\beta h. \tag{3.37}$$

Combining this with the fact that

$$n_{M|w} \sim \left(f(\theta)+M\right)^{-2}, \tag{3.38}$$

and that

$$\int d\theta\, \rho_{M|w}^t(\theta)\left|v_{M|w}^{\rm eff}(\theta)\right| \sim \alpha/M^2, \tag{3.39}$$

for $h=0$ and large $M$ as in the XXX spin-chain (see Appendix 3.B), we have that $\mathcal{D}_{M|w}^{\infty}$ tends to a constant as $M\to\infty$. This produces a divergence in the spin diffusion constant. Since this mechanism is formally identically to the case of the XXX chain, following the self-consistent argument in Ref. [82] we deduce that spin transport is superdiffusive with KPZ scaling exponent.

We now focus on the case at $\mu=0$ (while keeping $h=0$ fixed), to examine if there is a possible different structure to the divergence of $\mathcal{D}_m$ in this case. When $\mu=0$, the magnons ($M|w$ strings) follow exactly the same scaling, and so would give rise to the

same divergence in the diffusion constant; but now the singlets ($M|uw$ strings) are no longer exponentially suppressed and in principle could yield an additional divergent contribution to $\mathcal{D}_m$. As it happens, however, using the fact (cf. (3.35)) that for large $M$

$$Y_{M|uw}(\theta) \sim (g(\theta) + M)^2 - 1, \tag{3.40}$$

we find that $m^{\mathrm{dr}}_{M|uw} \sim (\partial_{\beta h} g)/(g + M)$ with $\partial_{\beta h} g = 0$ at $h = 0$. We combine this with the analogs of Eqs. (3.38) and (3.39) for the $uw$ strings (which have similar scaling at large $M$, see Appendix 3.B) to conclude that $\mathcal{D}_{M|uw} = O(M^{-6})$ and hence that $\sum_M \mathcal{D}_{M|uw}$ converges. This strongly suggests that $z = 3/2$ also for the $SO(4)$ case when $\mu = h = 0$. (Note that we obtain similar results by swapping the order of limits, suggesting that there is a well-defined $(\mu, h) \to (0, 0)$ limit.) If we assert that the scaling function is $f_{\mathrm{KPZ}}$ also at $\mu = 0$, it follows that $\lambda^{(S)}_{\mathrm{KPZ}}(\mu = 0)$ is smooth around $\mu = 0$.

Finally, the above arguments about spin transport apply *mutatis mutandis*, for charge transport, interchanging, e.g. the role of $h/2$ and $\mu$ and magnons and singlets ($w$- and $uw$-strings).

### 3.4.2 "Soft gauge modes" and KPZ universality from classical spin fluctuations

While the kinetic approach predicts KPZ-like exponents, it does not readily provide access to the KPZ scaling function. Therefore we take the lead of recent work Ref. [25] which proposed that super-diffusion emerges from the classical hydrodynamics of "soft gauge modes". The Bethe ansatz is built on a choice of pseudovacuum, which in our case is the fermionic vacuum, and quasi-particle excitations are characterized on top of this pseudovacuum. Evidently the fermionic vacuum preserves all microscopic symmetries. However, the choice of the pseudo-vacuum for the spin singlets necessarily breaks the $SU(2)_\eta$ symmetry, and similarly the choice of the pseudo-vacuum for the magnons explicitly breaks $SU(2)_s$ symmetry [59]. "Soft gauge modes" —in the language of Ref. [25]— are dynamical space-dependent fluctuations of the pseudovacuum choice. In the XXX model, their classical dynamics – governed by the Landau-Lifshitz equations — was able to properly account for KPZ scaling. They have also been identified identified as "giant" (large $M$) quasiparticles in recent work [43], providing a microscopic understanding of the emergence of superdiffusion via the GHD formalism; however at present we focus on the classical soft gauge approach.

If either $\mu$ or $h$ are non-zero, the discussion proceeds identically as in Ref. [25, 46]. We thus focus on the case $h = 0$ and $\mu = 0$, where we have two soft gauge modes, associated to the breaking of $SU(2)_\eta$ and $SU(2)_s$ by our choice of pseudovacuum. We can parametrize this choice in terms of a pair of vector fields $\boldsymbol{\eta}(x,t)$ and $\boldsymbol{S}(x,t)$, that indicate respectively the expectation value of the operators $\boldsymbol{\eta}$ and $\boldsymbol{S}$ in the pseudo-vacuum. Working directly in the continuum limit, the dynamics of $\boldsymbol{S}(x,t)$ and $\boldsymbol{\eta}(x,t)$ will be described by a classical Hamiltonian $\mathcal{H}$, that produces Landau-Lifshitz dynamics, viz.

$$\partial_t \boldsymbol{S}(x,t) = \boldsymbol{S} \times \frac{\delta \mathcal{H}[\boldsymbol{S},\boldsymbol{\eta}]}{\delta \boldsymbol{S}(x)} \tag{3.41}$$

$$\partial_t \boldsymbol{\eta}(x,t) = \boldsymbol{\eta} \times \frac{\delta \mathcal{H}[\boldsymbol{S},\boldsymbol{\eta}]}{\delta \boldsymbol{\eta}(x)}. \tag{3.42}$$

On symmetry grounds, we consider the most general $\mathcal{H}$ that is invariant under all the relevant symmetries, and particularly under the transformations generated by the $su(2)_s \oplus su(2)_\eta$ algebra. This is the symmetry class of two independent spin chains, invariant under independent rotations of the spin in each chain. This means that the only terms that can appear in the Hamiltonian are rotational scalar intra-chain couplings, and inter-chain scalar-scalar couplings.

Focusing first on the intra-chain coupling, the most relevant terms (i.e. those with the lowest number of derivatives) in the equations of motion are then given by

$$\partial_t \boldsymbol{S}(x,t) = J_S \boldsymbol{S} \times \partial_x^2 \boldsymbol{S} \tag{3.43}$$

$$\partial_t \boldsymbol{\eta}(x,t) = J_\eta \boldsymbol{\eta} \times \partial_x^2 \boldsymbol{\eta}. \tag{3.44}$$

These equation becomes particularly simple once expressed using Frenet-Serret variables [125]

$$\kappa_S = \sqrt{(\partial_x \boldsymbol{S})^2} \tag{3.45}$$

$$\tau_S = \frac{1}{\kappa_S^2} \boldsymbol{S} \cdot \left(\partial_x \boldsymbol{S} \times \partial_x^2 \boldsymbol{S}\right) \tag{3.46}$$

and similarly for $\boldsymbol{\eta}$. Here $\kappa_S$ gives the curvature of the vector field $\boldsymbol{S}(x)$, while $\tau_S$ gives its torsion. In term of these, we have

$$\partial_t \kappa_a^2 = -J_a \partial_x \left(\kappa_a^2 \tau_a\right) \tag{3.47}$$

$$\partial_t \tau_a = -J_a \partial_x \left(\tau_a^2 - \kappa_a^2/2 - \partial_x^2(\kappa_a)/\kappa_a\right) \tag{3.48}$$

with $a = \eta,\ S$. Upon coarse-graining over a length scale $l$, $\kappa_a^2 \sim 1/l^2$ and is transported ballistically; the latter follows from the fact that $\kappa_a^2$ is proportional to the energy density and is hence ballistic because of integrability. Meanwhile, as we argue self-consistently below $\tau$ will be transported super-diffusively. Therefore, the two equations effectively dynamically decouple [25, 46]. Focusing on the second equation, we insert a phenomenological diffusion coefficients $D_a$ and white noise terms $\xi_a$, and thereby obtain a pair of uncoupled noisy Burger equations for the $\tau_a$,

$$\partial_t \tau_a = J_a \partial_x \left( -\tau_a^2 + D_a \partial_x \tau_a + \xi_a \right). \tag{3.49}$$

The solutions of these independent equations each obey KPZ scaling. From the perspective of the Burgers equations, the only relevant terms we can write that couple the two equations are of the form $\partial_x(\tau_S \tau_\eta)$. Although this term could under special cases produce different scaling exponents (see e.g. Ref. [56]) and could more generally produce a renormalization of the KPZ scaling function [176], it is not *a priori* obvious if such a coupling can arise under the restriction of the $SU(2)_\eta \times SU(2)_s$ symmetry and from local lattice Hamiltonian dynamics. Indeed, we will argue below that regular scalar-scalar couplings cannot give rise to a term of this form. This then leads us to conclude that the scaling of spin-spin and charge-charge correlators is strictly KPZ also at the $SO(4)$ point (though there may be significant finite-size effects relative to the single-KPZ case since there are additional irrelevant 'interchain' couplings that must flow to zero before the two Burgers equations decouple).

The terms in the continuum that admit an obvious regularization on the lattice are polynomials of $\boldsymbol{S}$, $\boldsymbol{\eta}$, $\partial_x^n \boldsymbol{S}$ and $\partial_x^n \boldsymbol{\eta}$. Rotational scalars can then be constructed either by taking the scalar product of two derivatives of the vector field (e.g. $\partial_x^n \boldsymbol{S} \cdot \partial_x^m \boldsymbol{S}$), or as triple products (e.g. $\partial_x^n \boldsymbol{S} \cdot \left( \partial_x^m \boldsymbol{S} \times \partial_x^l \boldsymbol{S} \right)$).

In order to show that such terms cannot produce a $\tau_S \tau_\eta$ coupling, we recapitulate the Frenet-Serret formalism. Focusing for specificity on the spin dynamics, the key idea is to fix a space and time dependent frame (Frenet-Serret frame) characterized by the 3 unit vectors $\boldsymbol{e}_{S,1} = \boldsymbol{S}$, $\boldsymbol{e}_{S,2} = (\partial_x \boldsymbol{S})/\kappa_S$ and $\boldsymbol{e}_{S,3}$. Since the frame is space-dependent, its spatial variation can be described via the pseudo-vector $\boldsymbol{\Omega}_S(x,t)$, i.e. $\partial_x \boldsymbol{e}_{S,j} = \boldsymbol{\Omega}_S \times \boldsymbol{e}_{S,j}$. Similarly the time-variation of the frame can be described in terms of its angular velocity $\boldsymbol{\omega}_S(x,t)$. From these two pseudo-vectors we can describe

any derivative of a vector $\boldsymbol{v}$ as

$$\partial_x \boldsymbol{v} = \partial_x^{(\mathrm{FS})} \boldsymbol{v} + \boldsymbol{\Omega}_S \times \boldsymbol{v} \tag{3.50}$$

$$\partial_t \boldsymbol{v} = \partial_t^{(\mathrm{FS})} \boldsymbol{v} + \boldsymbol{\omega}_S \times \boldsymbol{v}, \tag{3.51}$$

with $\partial^{(\mathrm{FS})}$ denoting the partial derivative in the Frenet-Serret frame. To determine the dynamics of $\tau_S$, we exploit that [125] in the Frenet-Serret frame $\boldsymbol{\Omega}_S = (\tau_S, 0, \kappa_S)$ and that [125, 46] $\partial_t \tau_S = \partial_x \omega_{S,1} - \kappa_S \omega_{S,2}$. Finally $\boldsymbol{\omega}_S$ is determined by the classical Hamiltonian dynamics of the system as

$$\omega_{S,i} = -\left( \frac{\delta \mathcal{H}[\boldsymbol{S}, \boldsymbol{\eta}]}{\delta \boldsymbol{S}(x)} \right)_i \qquad i = 2, 3 \tag{3.52}$$

$$\omega_{S,1} = \frac{\partial_x^{(\mathrm{FS})} \omega_{S,2} + \tau_S \omega_{S,3}}{\kappa_S}. \tag{3.53}$$

Here the last equation can be derived by computing $\partial_t \boldsymbol{e}_{S,2}$ by commuting the order of the space and time derivative and relating it to $\boldsymbol{\omega}_S$. Therefore, even if the Hamiltonian $\mathcal{H}$ includes terms of the form

$$F\left(\boldsymbol{S}, \partial_x \boldsymbol{S}, \cdots\right) G\left(\boldsymbol{\eta}, \partial_x \boldsymbol{\eta}, \cdots\right), \tag{3.54}$$

the final equation of motion for spin torsion $\tau_S$ will be of the form

$$\begin{aligned} \partial_t \tau_S = {} & \partial_x \left( J_1[\kappa_S, \tau_S] G\left(\boldsymbol{\eta}, \partial_x \boldsymbol{\eta}, \cdots\right) \right) \\ & + \partial_x \left( J_2[\kappa_S, \tau_S] \right) G\left(\boldsymbol{\eta}, \partial_x \boldsymbol{\eta}, \cdots\right) \end{aligned} \tag{3.55}$$

for some functionals $J_1$ and $J_2$ which can be computed from $F$. Crucially, the function $G$ is left unaltered in computing the equation of motion for $\tau_S$. To obtain $\partial_t \tau_S = \cdots + \partial_x(\tau_S \tau_\eta)$ then we would need $G = \tau_\eta$, which is not possible to achieve using only polynomials of the derivatives of $\boldsymbol{\eta}$, but would require a continuum Hamiltonian which would not admit a trivial lattice regularization.

Thus, we conclude that no lattice-regularizable classical Hamiltonian can produce a coupling between the Burgers equations for $\tau_S$ and $\tau_\eta$ that is relevant under KPZ scaling. As a consequence, the scaling of spin-spin and charge-charge correlators is of the "$(\mathrm{KPZ})^2$" form given in Eqs. (3.15) and (3.16).

Finally, once ascertained that the correlators have the KPZ scaling form (3.16), the constants $\lambda_{\mathrm{KPZ}}^{(S)}$ and $\lambda_{\mathrm{KPZ}}^{(\eta)}$ can in principle be computed through a modification of the kinematic theory presented in the previous subsection [44].

### 3.4.3 Numerical Simulations

We confirm the double-KPZ scaling scenario presented above by means of state-of-the-art time-evolving block-decimation (TEBD) numerical simulations using the matrix product operator (MPO) formalism. We focus on spin dynamics at $h = \mu = 0$ and $T = \infty$, and compute the dynamic correlator $\langle S^z(x_j, t)S^z(0, 0)\rangle$, where $j$ indexes the sites. To do this, we represent $S^z(0, 0)$ as a bond-dimension-1 MPO, which we subsequently evolve in the Heisenberg picture using TEBD techniques. All evolutions are done with a fourth-order Trotter step of size $\delta t = 0.2$. Truncations are done initially with a fixed discarded weight $\varepsilon = 10^{-8}$ and a growing bond dimension — however, once the bond dimension surpasses a threshold, subsequent truncations keep at most $\chi_{\max}$ states, with $\chi_{\max}$ ranging from 256 to 1024. Our conclusions are quantitatively consistent across bond dimensions.

Once we have $S^z(0, t)$, we exploit translational invariance to access $S^z(x_j, t)$, at which point the correlator can be easily computed. To reduce the error coming from the trotterization and the SVD truncation, we exploit the sum rule

$$\sum_j \langle S^z(x_j, t)S^z(0, 0)\rangle = \chi_h, \tag{3.56}$$

to correctly normalize $\langle S^z(x_j, t)S^z(0, 0)\rangle$ at each time $t$.

We consider two different methods to extract the dynamical exponent $z$ and $\lambda^{(S)}_{\mathrm{KPZ}}$. First, we analyze the return probability $\langle S^z(0, t)S^z(0, 0)\rangle$ as a function of time; second, we analyse the growth of the profile width

$$\sqrt{\sum_j x_j^2 \langle S^z(x_j, t)S^z(0, 0)\rangle}. \tag{3.57}$$

with $j$ indexing the sites and $x_j$ measured in units of lattice spacings. At each time $t$, we take a window of size $\Delta \log t = 1$ centered around $t$ and fit the outcome of the TEBD simulations within that time window to the predicted KPZ scaling form. The results we obtain are presented in Fig. 3.5 for $U/t = 1, 2$, and 4. Our analysis suggests that $z$ and $\lambda^{(S)}_{\mathrm{KPZ}}$ converge more quickly in time when the return probability is analysed. Both approaches, however, seem to be compatible with $z = 3/2$ at sufficiently late times.

Note that, especially at $U/t = 4$, the fit for $z$ seems to converge rather quickly, suggesting that the exponent $z$ could be accessed in the timescale of a typical cold-atom

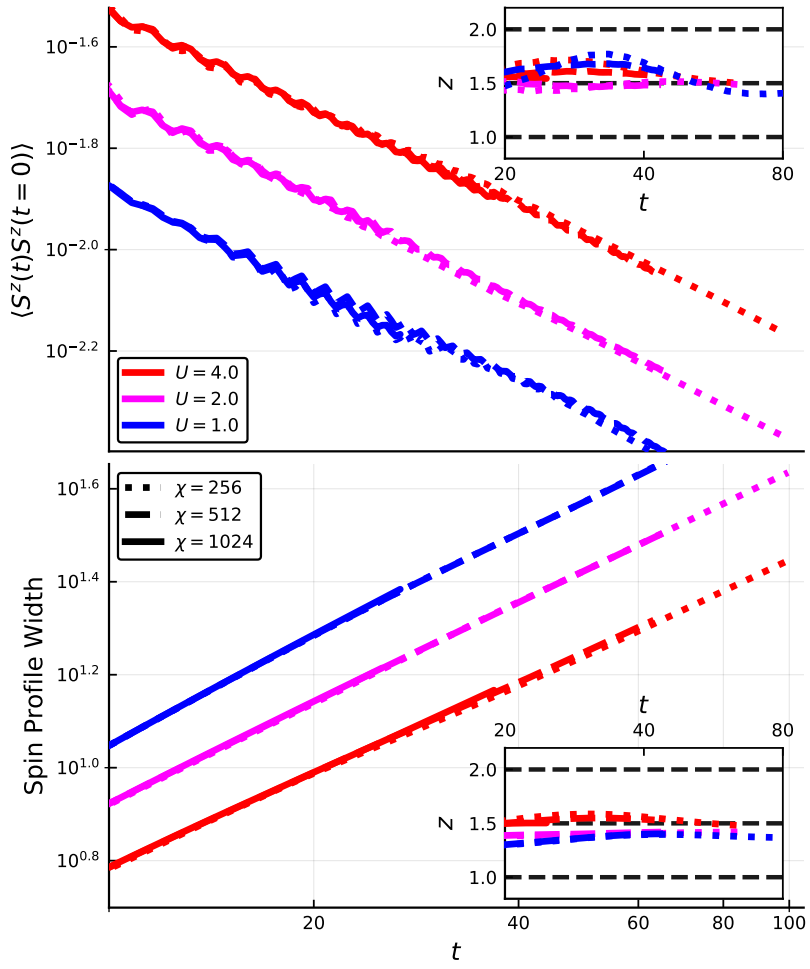


Figure 3.5: TEBD data for the Hubbard model at $h = \mu = 0$ and $U/t = 1, 2, 4$ and for various maximum-bond-dimensions $\chi_{\max} = 256, 512, 1024$. From the return probability (top), and from the profile width (bottom), we have fit the dynamical exponent $z$ (insets) as described in the main text. [Numerical simulations performed by Brayden Ware.]

experiment. To further highlight the accessibility to quantum microscope experiments, we used TEBD to analyze finite size effects, finite temperature effects, and the effects of small $SU(2)_s$ symmetry breaking field $h$ and $SU(2)_\eta$ symmetry breaking chemical potential $\mu$ around the $U/t = 4$ point.

For short chains, the clearest signature of $z = 3/2$ scaling is in the autocorrelator for a spin near the middle of the chain, which shows $t^{-2/3}$ scaling before eventually saturating to $0.5/L$ in a time that scales like $L^{3/2}$ (Fig. 3.6). Upon decreasing the temperature from $T = \infty$ to $T = 2t$, the $z = 3/2$ scaling remains (Fig. 3.7).

Moving away from the $SU(2)_s$ symmetric line by adding a small field $h$, the spin structure factor $\langle S^z(x_j, t)S^z(0, 0)\rangle_c$ immediately develops ballistically moving

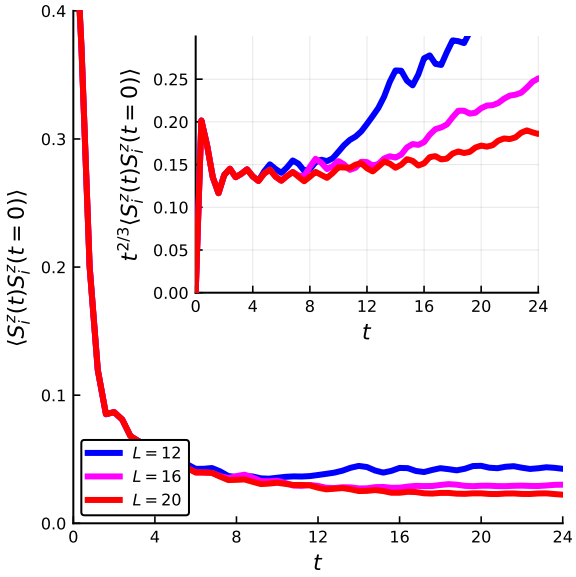


Figure 3.6: Signatures of superdiffusion in small Hubbard chains directly accessible in current quantum microscope experiments. TEBD data for the Hubbard model at $U/t = 4$ for finite chains of size $L = 12, 16, 20$. The return probability saturates due to the finite size effects, cutting off the $t^{-2/3}$ scaling. [Numerical simulations performed by Brayden Ware.]

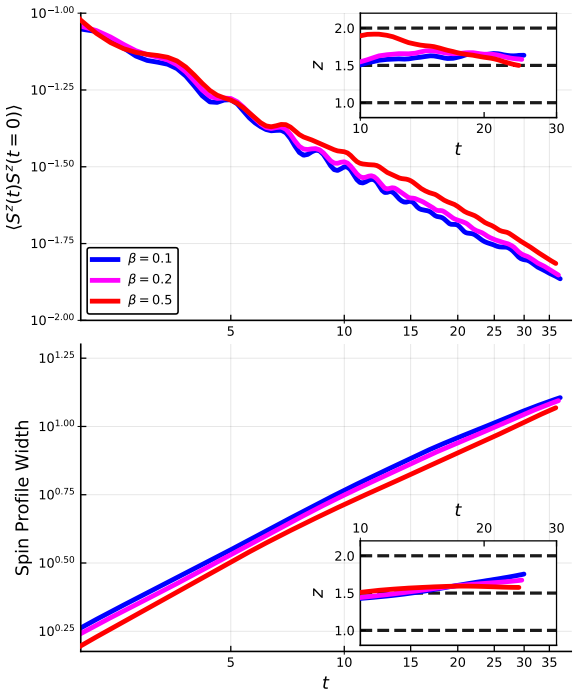


Figure 3.7: Superdiffusion at finite temperature. TEBD data for the Hubbard model at $U/t = 4$ for $\beta t = 0.1, 0.2, 0.5$. [Numerical simulations performed by Brayden Ware.]

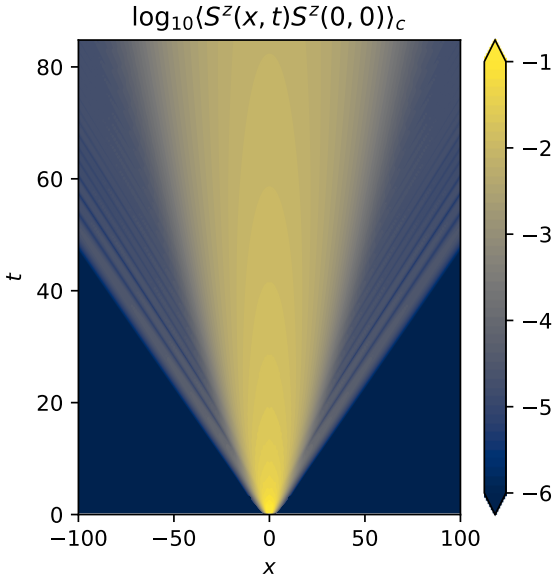


Figure 3.8: TEBD data for the Hubbard model at $h = 0.1, \mu = 0$ and $U/t = 4$. Ballistically moving peaks coexist with a superdiffusive central peak that lasts for a time scale $\sim h^{-3}$. [Numerical simulations performed by Brayden Ware.]

peaks corresponding to light magnons (Fig. 3.8), which coexist with a superdiffusive peak at $x = 0$, which we expect [83] will cross over to a ballistic scaling at times $\gg h^{-3}$. Indeed, as $h \to 0$ the spin Drude weight $D_m$ scales as as $h^2|\log h|$, since the contributions of $M|w$ strings to $D_m$ scale like $h^2/M$ up to $M \sim 1/h$, beyond which the $n_{M|w}$ is exponentially suppressed (see Ref. [98] for a more detailed discussion). Thus, in the ballistic regime, the spatial variance of the spin profile is proportional to $Dt^2 \sim h^2|\log h|t^2$ at long times. At short times, instead, $h$ is effectively 0 and the variance of the spatial profile is given by the KPZ scaling form, i.e. it is proportional to $t^{4/3}$. Therefore, the crossover from anomalous diffusion to ballistic transport takes place when these two lengthscales becomes comparable, i.e. on a timescale $t^* \sim h^{-3}$ (up to logarithmic corrections).

In the parameter regime of these numerics, adding a small chemical potential $\mu$ also has no effect on the $z = 3/2$ scaling of $\langle S^z(x_j,t)S^z(0,0)\rangle_c$; this is consistent with our analysis in Sec. 3.4.1 above, since as we have discussed $\mu$ breaks the $SU(2)_\eta$ symmetry but preserves $SU(2)_s$. Thus we expect that the $z = 3/2$ scaling should be accessible to currently available experimental platforms (see e.g. Ref. [185]), with the biggest limitation being imposed by the finite length of the chains.

Finally, we analyze the full profile of $\langle S^z(x_j,t)S^z(0,0)\rangle$ at different times (Fig. 3.9), assuming $z = 3/2$, with the goal of determining if the scaling function is of the KPZ

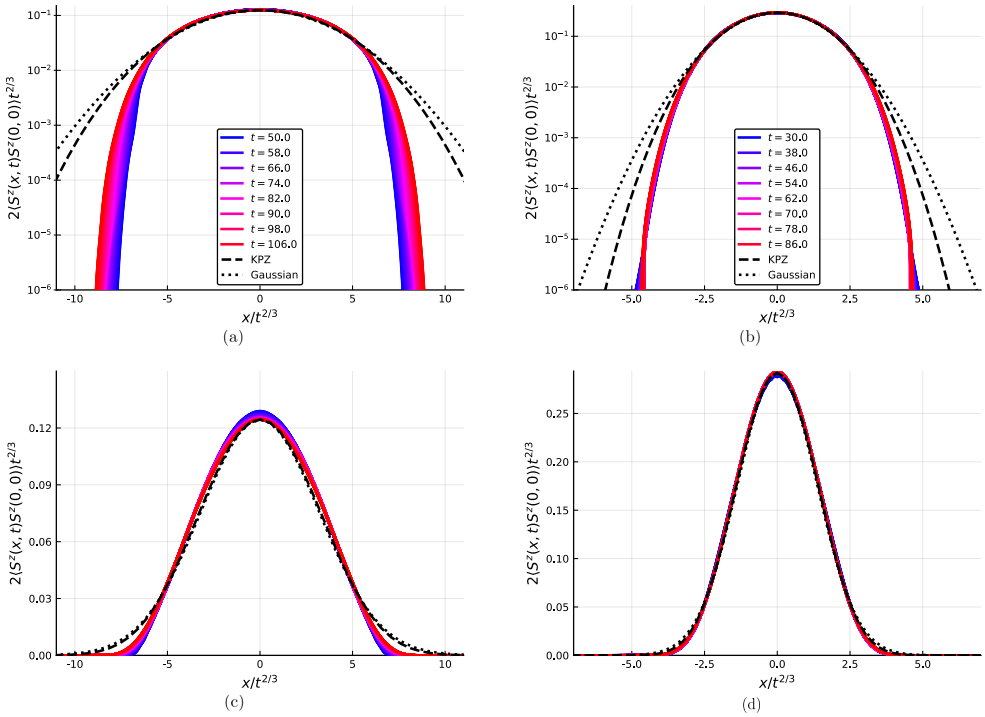


Figure 3.9: (a) Collapsed profile of $\langle S^z(x_j,t)S^z(0,0)\rangle$ for $U/t = 1$ assuming $z = 3/2$. We can observe that the tails of the correlators did not converge yet up to the maximum time we were able to reach in our simulations. (b) Same as panel (a), but for $U/t = 4$. The drift of the profile with time is less pronounced than in (a), making it harder to understand if the profile is converged in $t$. If convergence has been reached, this would indicate that the profile are described by $f_{\mathrm{KPZ}}$, in contrast with our previous analysis. Panel (c) and (d) report the same data of (a) and (b) respectively, but in a linear scale. [Numerical simulations performed by Brayden Ware.]

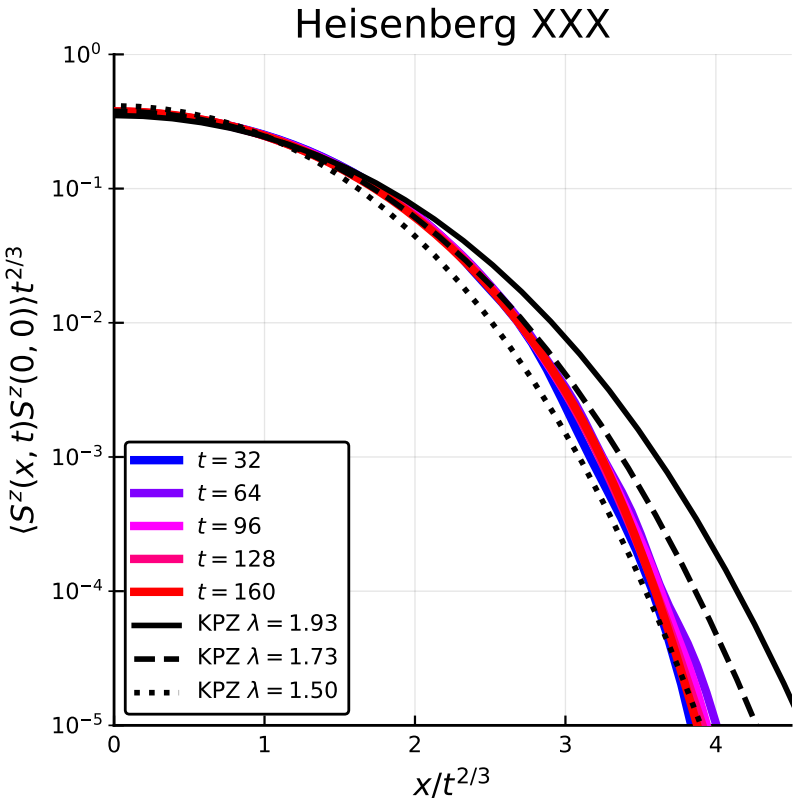


Figure 3.10: Collapsed profile of $\langle S^z(x_j,t)S^z(0,0)\rangle$ for the Heisenberg XXX chain assuming $z = 3/2$, computed using TEBD with bond dimension $\chi = 512$. Significant deviations in the tails from $f_{\mathrm{KPZ}}$ persist to accessible timescales. [Numerical simulations performed by Brayden Ware.]

form $f_{\mathrm{KPZ}}$, as indicated by our soft gauge mode-treatment. At the latest times for which our TEBD truncation errors are controlled, the profiles are not converged in the tails; these tails seem to fall off faster than $f_{\mathrm{KPZ}}$. Therefore we cannot definitively conclude that the scaling function is of KPZ form. Note that coupled noisy Burgers equations can give rise to non-KPZ scaling functions consistent with the exponent $z = 3/2$ [56]. Our numerical results do not rule out this possibility. We emphasize, however, that we see strong similarities between our numerical data for the scaling function in the Hubbard model at $U/t = 4$ and our data for the Heisenberg spin chain, shown in Fig. 3.10, computed using the same TEBD approach. Whether convergence to the KPZ scaling function appears on larger time scales is an interesting question for future work.

## 3.5 Concluding Remarks

In this work we revisited transport in the paradigmatic Hubbard model, in one dimension, in light of recent developments in understanding transport in integrable systems using generalized hydrodynamics. The GHD framework allowed us to capture the crossover between the low temperature Luttinger liquid, the intermediate-temperature spin-incoherent Luttinger liquid, and the high temperature regime. Away from half filling (zero magnetic field), charge (spin) transport is primarily ballistic. We explored the crossovers between various ballistic regimes, focusing on the Drude weight and the dynamic structure factor as diagnostics. The sharpest crossovers away from the $SO(4)$ point are in spin transport, as one might expect. In all regimes, when $\mu \neq 0$, spin transport is dominated by the fast-moving $y$-particles, whose dressed magnetization is sensitive to the crossover. The long time spin structure factor $\mathcal{S}_m(x,t)$ reflects the spin-incoherent to spin-coherent crossover more directly. In the former case, $\mathcal{S}_m(x,t)$ displays a hierarchy of peaks of increasing height as $x/t$ decreases. Instead, in the latter, $\mathcal{S}_m(x,t)$ is dominated by $1|w$-magnons. Less pronounced signatures are seen in energy and charge transport away from half filling. Finally, we turned to the case of half filling and/or zero magnetic field: in this limit, ballistic transport vanishes, and instead one has superdiffusive charge and spin transport, which we argued belongs to the KPZ universality class. We presented extensive numerical evidence for $z = 3/2$ dynamical scaling.

We close with two remarks. First, the most striking qualitative phenomena we have found (such as charge and spin superdiffusion) are observable in quite small systems of $L \lesssim 22$ at times $t \lesssim 20$. These can easily be realized in experiments using quantum gas microscopes, as well as other existing or near-term experiments. The GHD framework—built on physically reasonable but unrigorous assumptions—makes exact, zero-parameter predictions for such experiments, which it is important to test. Second, one can regard the quasiparticle picture presented here as the starting point for a broader analysis of high-temperature transport in the Hubbard model, perturbed slightly away from integrability. Integrability-breaking creates decay channels for all the quasiparticle types we have considered; however, owing to their very different kinematics, we expect a family of well-separated quasiparticle lifetimes, and consequently a sequence of dynamical crossovers that persist in the nonintegrable limit as well.

# Appendix

## 3.A Solving the TBA Equations

We now describe how to solve the TBA and dressing equations numerically in various regimes. The generic form of the TBA equations (see Chapter 2) involve the kernels reported in Table 3.2. Given that $K_{MN}$ is non-zero for every pair $(M, N)$, the equations in this form contain a direct coupling among all magnon/singlet strings, making their interpretation and solution difficult. We refer to this as the "non-local" formulation of the TBA, in contrast with the one we are about to introduce. It is well known [59, 179, 98] that there is an equivalent "quasi-local" formulation where each string species is coupled to at most other 3 string species. We now sketch the derivation of this quasilocal formulation of the TBA and the GHD dressing equations for the Hubbard model. Our notation closely parallels that of Ref. [96], who first derived the quasi-local form for the dressing equations.

We begin by defining the kernel $(\mathbf{1} + K)^{-1}_{MN}$ as the inverse under convolution of $(\mathbf{1} + K)_{MN}$, i.e.

$$(\mathbf{1} + K)^{-1}_{MN'} \star (\mathbf{1} + K)_{N'M} = \mathbf{1}_{MN}, \tag{3.58}$$

with $\mathbf{1}_{MN}(\theta) = \delta_{MN}\delta(\theta)$. Exploiting the explicit expression for $K_{MN}$, it can be shown that [179, 59]

$$(\mathbf{1} + K)^{-1}_{MN}(\theta) = \delta_{MN}\delta(\theta) - I_{MN}s(\theta), \tag{3.59}$$

where we define

$$s(\theta) = [(\delta + K_2)^{-1} \star K_1](\theta) = \frac{1}{U\cosh(2\pi\theta/U)} \tag{3.60}$$

$$I_{MN} = \delta_{M,N+1} + \delta_{M,N-1}. \tag{3.61}$$

Table 3.A.1: Quasi-local form of the TBA equations for different functions $f_a(\theta)$ corresponding to TBA variables labeled by species and rapidity. Here $\mathcal{O}_a(\theta)$ corresponds to the projection of one of the two $U(1)$ conserved charges (the electric charge or the $z$-magnetization) onto quasiparticle species $a$ at rapidity $\theta$. $g_a(\theta)$ is meant to be either $e_a(\theta)$ or $k'_a(\theta)$.

| $\boldsymbol{f_a}$ | **TBA/Dressing Equations for $\boldsymbol{f_a}$** | $\boldsymbol{\lim_{M\to\infty} \frac{f_a}{M}}$ |
|---|---|---|
| $\log Y_\pm$ | $\log Y_\pm = \beta\left(e_\pm - s\star e_{1\|uw}\right) - s\star\log\left(\frac{1+Y_{1\|w}}{1+Y_{1\|uw}}\right)$ | — |
| $\log Y_{M\|w}$ | $\log Y_{M\|w} = s\star I_{MN}\log\left(1+Y_{N\|w}\right) - \delta_{M1}s\star\log\left(\frac{1+1/Y_-}{1+1/Y_+}\right)$ | $\beta h$ |
| $\log Y_{M\|uw}$ | $\log Y_{M\|uw} = s\star I_{MN}\log\left(1+Y_{N\|uw}\right) - \delta_{M1}s\star\log\left(\frac{1+Y_-}{1+Y_+}\right)$ | $-2\beta\mu$ |
| $\mathcal{O}^{\rm dr}_\pm$ | $\mathcal{O}^{\rm dr}_\pm = -s\star\left[\bar n_{1\|uw}\mathcal{O}^{\rm dr}_{1\|uw} - \bar n_{1\|w}q^{\rm dr}\right]$ | — |
| $\mathcal{O}^{\rm dr}_{M\|w}$ | $\mathcal{O}^{\rm dr}_{M\|w} = s\star I_{MN}\bar n_{N\|uw}\mathcal{O}^{\rm dr}_{N\|uw} - \delta_{M1}s\star\left[n_-\mathcal{O}^{\rm dr}_- - n_+\mathcal{O}^{\rm dr}_+\right]$ | $\lim_{M\to\infty}\frac{\mathcal{O}_{M\|w}}{M}$ |
| $\mathcal{O}^{\rm dr}_{M\|uw}$ | $\mathcal{O}^{\rm dr}_{M\|uw} = s\star I_{MN}\bar n_{N\|uw}\mathcal{O}^{\rm dr} - \delta_{M1}s\star\left[n_-\mathcal{O}^{\rm dr}_- - n_+\mathcal{O}^{\rm dr}_+\right]$ | $\lim_{M\to\infty}\frac{\mathcal{O}_{M\|uw}}{M}$ |
| $g^{\rm dr}_\pm$ | $g^{\rm dr}_\pm = g_\pm - s\star g_{1\|uw} - s\star\left[\bar n_{1\|uw}g^{\rm dr}_{1\|uw} - \bar n_{1\|w}g^{\rm dr}_{1\|w}\right]$ | — |
| $g^{\rm dr}_{M\|w}$ | $g^{\rm dr}_{M\|w} = s\star I_{MN}\bar n_{N\|w}g^{\rm dr}_{N\|w} - \delta_{M1}s\star\left[n_-g^{\rm dr}_- - n_+g^{\rm dr}_+\right]$ | $\lim_{M\to\infty}\frac{g_{M\|w}}{M}$ |
| $g^{\rm dr}_{M\|uw}$ | $g^{\rm dr}_{M\|uw} = s\star I_{MN}\bar n_{N\|uw}g^{\rm dr}_{N\|uw} + \delta_{M1}s\star\left[\bar n_-g^{\rm dr}_- - \bar n_+g^{\rm dr}_+\right]$ | $\lim_{M\to\infty}\frac{g_{M\|uw}}{M}$ |

From this, it is also easy to show that

$$(\mathbf{1}+K)^{-1}_{MN}\star K_N=(\mathbf{1}+Is)^{-1}_{MN}\star K_N=\delta_{M1}s \tag{3.62}$$

Another property which will be useful in deriving the following equations is that for $f_M\in\{e_{M|uw},k'_{M|uw}\}$, we have

$$(\mathbf{1}+K)^{-1}_{MN}\star f_M=\delta_{M1}s\star(f_+-f_-)\,, \tag{3.63}$$

while for $g_M=\alpha M$ for any $\alpha$ we have

$$(\mathbf{1}+K)^{-1}_{MN}\star g_M=0 \tag{3.64}$$

We now act from the left with $(\mathbf{1}+K)^{-1}_{MN}$ on all terms in the set of equations

$$\begin{aligned}\log Y_{M|w}&=\beta e_{M|w}+\beta hM+K_{MN}\log\left(1+1/Y_{N|w}\right)\\&\quad-K_M\star\log\left(\frac{1+1/Y_-}{1+1/Y_+}\right)\end{aligned} \tag{3.65}$$

$$\begin{aligned}\log Y_{M|uw}&=\beta e_{M|uw}-2\beta\mu M+K_{MN}\log\left(1+1/Y_{N|uw}\right)\\&\quad-K_M\star\log\left(\frac{1+1/Y_-}{1+1/Y_+}\right)\end{aligned} \tag{3.66}$$

and use the above identities to obtain quasi-local TBA equations for the singlets and the magnons strings, listed in Table 3.A.1.

The case of the $y$-particles must be treated more carefully. Here, we first define $\boldsymbol{e}$ as the bare energy for $h=\mu=0$, and write the TBA equation explicitly as

$$\begin{aligned}\log Y_\pm&=\beta\left(e_\pm-\mu-h/2\right)\\&\quad+K_M\star\log\left(\frac{1+1/Y_{M|uw}}{1+1/Y_{M|w}}\right).\end{aligned} \tag{3.67}$$

We now first manipulate $K_M\star\log(1+1/Y_{M|w})$ in order to remove the coupling to all $M|w$ strings in favor of just the first, i.e. $1|w$. To do so, we fix a cutoff $\tilde{M}$, and for

$M < \tilde{M}$ we rewrite

$$\begin{aligned}\log(1+1/Y_{M|w}) &= \log(1+Y_{M|w}) - \log Y_{M|w} \\ &= \log(1+Y_{M|w}) \\ &\quad - I_{MN} s \star \log\left(1+Y_{N|w}\right) \\ &\quad - \delta_{M1} s \star \log\left(\frac{1+1/Y_-}{1+1/Y_+}\right)\end{aligned} \tag{3.68}$$

where we have used the quasi-local expression for $\log Y_{M|w}$ from Table 3.A.1. We now substitute (3.68) into $K_M \star \log(1+1/Y_{M|w})$ in (3.67). We then manipulate the part coming from the first term in (3.68) as[7]

$$\begin{aligned}K_M \star \log(1+Y_{M|w}) &= I_{MN} s \star K_N \star \log(1+Y_{M|w}) \\ &\quad + \delta_{M1} s \star \log(1+Y_{M|w})\end{aligned} \tag{3.69}$$

In this way most of the terms cancel out and (after remembering to include the terms above the cutoff) we are left with

$$\begin{aligned}&\sum_M K_M \star \log(1+1/Y_{M|w}) = \\ &= \sum_{M>\tilde{M}} K_M \star \log(1+1/Y_{M|w}) \\ &\quad - K_1 \star s \star \log\left(\frac{1+1/Y_-}{1+1/Y_+}\right) + s \star \log(1+Y_{1|w}) \\ &\quad - K_{\tilde{M}} \star s \star \log(1+Y_{\tilde{M}+1|w}) + K_{\tilde{M}+1} \star s \star \log(1+Y_{\tilde{M}|w})\end{aligned} \tag{3.70}$$

Finally, using that $\log(1+1/Y_{M|w}) = o(1/M^2)$ and that the last line in the previous expression converges to [8]

$$\frac{1}{2} \lim_{\tilde{M}\to\infty} K_1 \star \log(Y_{\tilde{M}|w}) - \log(Y_{\tilde{M}+1|w}) = -\frac{\beta h}{2}, \tag{3.71}$$

[7] Note that the convolution product is associative.

[8] See for example the discussion in Ref. [179] concerning the XXX chain.

we arrive at

$$\begin{aligned}\log Y_{\pm} = \beta\,(\tilde{e}_{\pm} - \mu) \\ + K_M \star \log\left(1 + 1/Y_{M|uw}\right) - s \star \log(1 + Y_{1|w}) \\ + K_1 \star s \star \log\left(\frac{1 + 1/Y_{-}}{1 + 1/Y_{+}}\right).\end{aligned} \tag{3.72}$$

Finally, repeating the same procedure, but acting on $uw$-strings, we arrive at the quasi-local TBA equation for $y$-particles in Table 3.A.1. The derivation for the quasi-local form the dressing equations closely follows those for the TBA equations [96].

To numerically solve the TBA equations, we truncate the hierarchy of $w$ strings ($uw$-strings) at some maximum length $\tilde{M}_w$ ($\tilde{M}_{uw}$). We introduce a rapidity cutoff for the $w$ and $uw$ strings, requiring $\theta \in [-\theta_{\max}, \theta_{\max}]$, and apporximate $Y_a(\theta)$ with $|\theta| > \theta_{\max}$ as $Y_a\left(\text{sign}(\theta)\theta_{\max}\right)$. We then discretize rapidity space into a regularly spaced grid containing $\tilde{m}_{\text{rap}}$ points per string. Finally, we solve the TBA and dressing equations iteratively. For example, focusing on the TBA equations, we take an initial guess $Y^{(0)}$ for $Y$. We plug it in the right-hand side of the TBA equations to compute the next approximation $Y^{(1)}$. We proceed in this way until $\left\|Y^{(j)} - Y^{(j-1)}\right\|_{\mathbb{L}^1}$ is less than the desired accuracy $\epsilon_{\text{acc}}$. We solve the equations for dressed quantities in a similar fashion (see also Ref. [154]).

While truncating the hierarchy of strings, in the non-local formulation we can just approximate all terms outside the cutoff with 0. However this truncation requires more care in the quasi-local formulation, where the asymptotic condition (the final column of Table 3.A.1) is crucial to identify a unique solution. For the solution of the TBA equation, the issue is discussed in detail in Ref. [180]. For the dressed quantities, we employ the following scheme. In order to compute the dressing of (for example) $f_{M|w}(\theta)$ with the asymptotic condition $\lim_{M\to\infty} f^{\text{dr}}_{M|w}/M = \alpha_w$, we approximate

$$f^{\text{dr}}_{\tilde{M}_w+1|w}(\theta) \simeq K_1 \star f^{\text{dr}}_{\tilde{M}_w|w}(\theta) + \alpha_w. \tag{3.73}$$

Finally, we mention that in the spin-incoherent regime when $\beta\mu \lesssim -1$ and $\beta h \lesssim 1$, both formulations of the TBA equation presented above seem to be poorly suited to numerics. Instead, we find that the option that works best in this case is to employ a 'hybrid' combination of Eq. (3.66), (3.72) and the quasi-local form for $w$-strings reported in Table 3.2.

## 3.B Asymptotic results at large $M$

In this section, building on Ref. [180] and standard TBA results [59, 179], we expand the TBA equations at large string length $M$, with the goal of showing that

$$\int d\theta\, \rho^t_{M|w}(\theta) \left|v^{\text{eff}}_{M|w}(\theta)\right| \sim \alpha/M^2 \quad \text{at } h = 0 \tag{3.74}$$

$$\int d\theta\, \rho^t_{M|uw}(\theta) \left|v^{\text{eff}}_{M|uw}(\theta)\right| \sim \tilde{\alpha}/M^2 \quad \text{at } \mu = 0, \tag{3.75}$$

for two real numbers $\alpha$ and $\tilde{\alpha}$. For definiteness we focus on (3.74), but the argument proceeds identically for (3.75).

First of all, using the definition of $v^{\text{eff}}$ we have

$$\int d\theta\, \rho^t_{M|w}(\theta) \left|v^{\text{eff}}_{M|w}(\theta)\right| = \int \frac{d\theta}{2\pi} \left|\left(e'_{M|w}\right)^{\text{dr}}\right|. \tag{3.76}$$

Now, using the fact that that $e^{\text{ph}}_{M|w}(\theta)$ is even under $\theta \mapsto -\theta$ to halve the domain of integration, and the observation (see below) that $e_{M|w}(\theta)$ is monotonically increasing from 0 to $+\infty$, we can finally re-express (3.76)

$$\frac{1}{\pi\beta}\left(\log Y_{M|w}(+\infty) - \log Y_{M|w}(0)\right) \tag{3.77}$$

Therefore we analyse the TBA equation for large ($M \gg 1$) magnons in quasi-local form

$$\log Y_{M|w} = s \star \left[\log(1 + Y_{M-1|w}) + \log(1 + Y_{M+1|w})\right] \tag{3.78}$$

The solution of these equations at large $M$ and $h = 0$ can be approximated by [180, 98]

$$Y_{M|w} \simeq \left(f_M(\theta) + M\right)^2 - 1, \tag{3.79}$$

with $f_{M|w} = o(M)$ and $\lim_{\theta\to\infty} f_{M|w}(\theta) = 0$. Plugging this form back into the TBA equation, we find that $f_M$ satisfies

$$f_M = s \star (f_{M-1} + f_{M+1}) \tag{3.80}$$

$$\lim_{M\to\infty} f_M/M = 0, \tag{3.81}$$

where we have neglected terms of $o(f_M)$ and $O(1/M^4)$. One can verify that the

recurrence relation can be rewritten as

$$f_M = K_1 \star f_{M-1}. \tag{3.82}$$

Thus $f_M \sim K_M \star \tilde{f}$ for some function $\tilde{f}$ with $\lim_{\theta\to\infty} \tilde{f}(\theta) = 0$. As $M \to \infty$, we can neglect the width of $\tilde{f}$ relative to that of $K_M$. Therefore, the overall shape of $f_M$ is approximately given by a Lorentzian with width proportional to $M$ and maximum height proportional to $1/M$.

Finally, plugging this estimate into Eq. (3.79) and expanding to leading order in $1/M$, we obtain the final result that $\log Y_{M|w}(+\infty) - \log Y_{M|w}(0)$ scales as $1/M^2$.

## 3.C Large-$U$ expansions of the TBA

At large $U$, the TBA and dressing equations are considerably simplified, as was pointed out in Ref. [179]. In this section we provide the complete solutions at leading order in $1/U$ in the strong-coupling regimes (i), (ii), and (iii), and a partial solution in regime (iv). The crucial observation which allows for exact solutions is that the kernels $s$ and $K_M$ have a width of order $U$ and an height of order $1/U$, and that $y$-particle rapidities are bounded in the $[-1, 1]$ interval. We observe that for a function $f$ with domain $[-1, 1]$, we can expand

$$\begin{aligned}(s \star f)(\theta) = &\left(\int_{-1}^{+1} dw\, f(w)\right) s(\theta) \\ &- \left(\int_{-1}^{+1} dw\, w f(w)\right) s'(\theta) + O(1/U^3).\end{aligned} \tag{3.83}$$

On the other hand, for a function $g$ with domain in $\mathbb{R}$, we can expand

$$\begin{aligned}(s \star f)|_{[-1,1]}(\theta) = &\int dw\, K(-w) g(w) \\ &+ \theta \int dw\, K'(-w) g(w) + O(|g|/U^2).\end{aligned} \tag{3.84}$$

Note that the same expansion holds also if $s$ is replaced by $K_M$.

### 3.C.1 Regimes (i), (ii) and (iii): $U \gg 1 \gg \beta$

In this case, it is convenient to work with the quasi-local formulation of the TBA and dressing equations. From Eq. (3.83), we see that

$$\log Y_{\pm}(\theta) = \beta\left(e_{\pm}(\theta) - \mu - h/2\right) + \alpha_Y + O(1/U^3), \tag{3.85}$$

where $\alpha_Y$ is $\theta$-independent. Furthermore the strings satisfy the equations

$$\log Y_{M|w} = s \star I_{MN} \log\left(1 + Y_{N|w}\right) + \delta_{M1}\gamma_Y s \tag{3.86}$$

$$\log Y_{M|uw} = s \star I_{MN} \log\left(1 + Y_{N|uw}\right) + \delta_{M1}\tilde{\gamma}_Y s \tag{3.87}$$

$$\gamma_Y = -\int_{-1}^{+1} \log\left(\frac{1 + 1/Y_-}{1 + 1/Y_+}\right) \tag{3.88}$$

$$\tilde{\gamma}_Y = -\int_{-1}^{+1} \log\left(\frac{1 + Y_-}{1 + Y_+}\right). \tag{3.89}$$

The key observation is that $\|s\|_\infty = O(1/U)$, so that at leading order we can just neglect the terms $\gamma_Y s$ and $\tilde{\gamma}_Y s$, in which case (3.86) and (3.87) are simply the $T = \infty$ TBA equations for the strings. Their solution is known to be given by [179]

$$Y_{M|w} = \chi_M^2 - 1, \qquad \chi_M = \frac{\sinh\left[(M+1)\beta h/2\right]}{\sinh\left(\beta h/2\right)} \tag{3.90}$$

$$Y_{M|uw} = \tilde{\chi}_M^2 - 1, \qquad \tilde{\chi}_M = \frac{\sinh\left[(M+1)\beta\mu\right]}{\sinh\left(\beta\mu\right)}. \tag{3.91}$$

Plugging $Y_{1|w}$ and $Y_{1|uw}$ into the equation for $\log Y_{\pm}$, we can now determine

$$\alpha_Y = \log\tilde{\chi}_1 - \log\chi_1, \tag{3.92}$$

thus completing the solution of the TBA equation.

Nonetheless, it will be convenient compute dressed charges using

$$\tilde{m}^{\mathrm{dr}} = \frac{1}{\beta}\frac{\partial \log Y}{\partial h}, \tag{3.93}$$

$$\tilde{q}^{\mathrm{dr}} = \frac{1}{\beta}\frac{\partial \log Y}{\partial \mu}, \tag{3.94}$$

$$e^{\mathrm{dr}} = \left.\frac{\partial \log Y}{\partial \beta}\right|_{\beta\mu,\beta h}, \tag{3.95}$$

from $Y$-functions and $(e')^{\mathrm{dr}} = \left(e^{\mathrm{ph}}\right)'$ from $Y_a(\theta) = \exp[\beta e_a^{\mathrm{ph}}(\theta)]$ and . Then to obtain

a non-zero result we need to expand to next order and take into account the source term $\gamma_Y s$ and $\tilde{\gamma}_Y s$. We then expand $\log Y = \beta e^{\mathrm{ph}} = \log Y^{(0)} + \beta\varepsilon^{(1)} + O(1/U^2)$ with $\varepsilon^{(1)} = O(1/U)$. Plugging this ansatz into the Eq. (3.86) (3.87), we obtain

$$\varepsilon^{(1)}_{M|w} = s \star I_{MN} \left(1 - n_{N|w}\right) \varepsilon^{(1)}_{N|w} + \delta_{M1} \frac{\gamma_Y}{\beta} s, \tag{3.96}$$

$$\varepsilon^{(1)}_{M|uw} = s \star I_{MN} \left(1 - n_{N|uw}\right) \varepsilon^{(1)}_{N|uw} + \delta_{M1} \frac{\tilde{\gamma}_Y}{\beta} s, \tag{3.97}$$

where we can substitute $n_a$ with its approximate form to leading order in $1/U$,

$$n_a = \frac{1}{1 + \exp(\log Y^{(0)}_a)}. \tag{3.98}$$

This set of equations has been solved exactly [98] and yields

$$\varepsilon^{(1)}_{M|w} = \gamma_Y \frac{\chi_M}{\chi_1} \left( \frac{K_M}{\chi_{M-1}} - \frac{K_{M+1}}{\chi_{M+1}} \right), \tag{3.99}$$

$$\varepsilon^{(1)}_{M|uw} = \tilde{\gamma}_Y \frac{\tilde{\chi}_M}{\tilde{\chi}_1} \left( \frac{K_M}{\tilde{\chi}_{M-1}} - \frac{K_{M+1}}{\tilde{\chi}_{M+1}} \right). \tag{3.100}$$

This directly allows for the computation of dressed charges by taking derivatives.

The last quantity left to compute is $(k^{\mathrm{dr}})'$, which also yields $\rho^t$. This can be solved in a similar fashion to the TBA equations, yielding

$$\left(k'_{\pm}\right)^{\mathrm{dr}} = k'_{\pm}, \tag{3.101}$$

$$\left(k'_{M|w}\right)^{\mathrm{dr}} = \gamma_k \frac{\chi_M}{\chi_1} \left( \frac{K_M}{\chi_{M-1}} - \frac{K_{M+1}}{\chi_{M+1}} \right), \tag{3.102}$$

$$\left(k'_{M|uw}\right)^{\mathrm{dr}} = \tilde{\gamma}_k \frac{\tilde{\chi}_M}{\tilde{\chi}_1} \left( \frac{K_M}{\tilde{\chi}_{M-1}} - \frac{K_{M+1}}{\tilde{\chi}_{M+1}} \right), \tag{3.103}$$

$$\gamma_k = \int_{-1}^{+1} d\theta \, \left( n_- k'_- - n_+ k'_+ \right), \tag{3.104}$$

$$\tilde{\gamma}_k = \int_{-1}^{+1} d\theta \, \left[ (1 - n_-) k'_- - (1 - n_+) k'_+ \right]. \tag{3.105}$$

Note that in practice this expansion is valid across regimes (i-iii), although conceptually regimes (ii-iii) can be accessed more easily using a hybrid form (see Appendix 3.A), where $uw$-strings explicitly drop out of the problem. While this does not affect the analytical solution, it is extremely convenient numerically, as it allows use to retain a very low cutoff on the length of $uw$-strings and hence improves the convergence of the iterative solution.

From the data above we can explicitly compute Drude weights and correlators. The Drude weights are always dominated by $y$-particles since

$$\int d\theta\, \rho^t_{M|w}(\theta) \left(v^{\rm eff}_{M|w}(\theta)\right)^2 = O(1/U^2). \tag{3.106}$$

and similarly for $uw$-strings. Furthermore, the contribution of $w$-strings energy and charge correlators is again suppressed since

$$\left(q^{\rm dr}_{M|w}(\theta)\right)^2 = O(1/U^2), \tag{3.107}$$

and similarly for the component of the dressed energy from $\tilde{e}$ (Table 3.1). Finally, as shown above the dressed quantities for $y$-particles are unaffected by the dressing to leading order in $1/U$.

As mentioned in the main text, the expression Eq. (3.11) for the Drude weight can be further simplified in regime (iii), where $\beta n_\pm(1-n_\pm)$ is significantly non-zero only over an interval of width $T$ around the fermi points $u_F$ where $e_\pm(u_F)=0$. Linearising $e_\pm(u_F)=0$ around the Fermi points, and explicitly performing the integral over rapidity we obtain the low-temperature form of the Drude weight in Eq. (3.14).

We now proceed to estimate the order of the corrections to the Drude weights in regime (iii). The main source of these corrections is given by the feedback of $\varepsilon^{(1)}$ and $(k')^{\rm dr}$ of $w$-strings (and $uw$-strings in regime (i)) in the TBA equation and dressing equations. For definiteness we focus on $(k')^{\rm dr}$, but the reasoning is the same for $\varepsilon^{(1)}$ in the TBA equations. Looking at Eq. 3.84, and noticing that $\left(k'_{M|uw}\right)^{\rm dr}(\theta)$ is even under $\theta \mapsto -\theta$, we conclude that the leading correction is constant in $\theta$ and is of order $O(1/U)$. A similar consideration applies to $e^{\rm ph}_\pm$. The corrections we obtain at order $1/U$ can be obtained by making the following replacements in Eq. (3.14)

$$\begin{aligned} e_\pm \to e_\pm &+ \gamma_Y \int d\theta \left(\frac{K_1(\theta)}{\chi_0} - \frac{K_2(\theta)}{\chi_2}\right) s(\theta) \\ &- \tilde{\gamma}_Y \int d\theta\, s(\theta) K_1(-\theta), \end{aligned} \tag{3.108}$$

$$\begin{aligned} k'_\pm \to k'_\pm &+ \gamma_k \int d\theta \left(\frac{K_1(\theta)}{\chi_0} - \frac{K_2(\theta)}{\chi_2}\right) s(\theta) \\ &- \tilde{\gamma}_k \int d\theta\, s(\theta) K_1(-\theta), \end{aligned} \tag{3.109}$$

and modifying the Fermi velocity and the dressed charges accordingly. As anticipated,

the corrections are $O(1/U)$, due to

$$\int d\theta\, K_M(\theta) s(\theta) = O(1/U) \tag{3.110}$$

### 3.C.2 Regime (iv): $\beta \gg U \gg 1$

In this regime, we deploy the standard technology of $T \to 0$ TBA expansions [179, 59, 39, 144, 15]. The fundamental idea behind the simplification of the TBA equations in this limit is to express them in terms of dressed energy $e^{\rm ph} = \log Y/\beta$ which remain finite as $\beta \to \infty$. In non-local form, the equations for the dressed energies then become (at leading order in $\beta^{-1}$)

$$e_a^{\rm ph} = e_a - \mu - h/2 - K_{ab} \star \left[e_b^{\rm ph}\right]^-, \tag{3.111}$$

with $[f]^- = f\theta_H(-f)$, denoting the Heaviside-$\theta$ function with $\theta_H$. Furthermore $n_a = \theta_H(-e_a^{\rm ph})$.

The first consequence is that singlets ($uw$-strings) always have [179, 59] $n_{M|uw} = 0$. Specifically in the high-$U$ limit, from Eq. (3.84) it follows again that energy, momentum and charge of $y$-particles are dominated by bare quantities. On the other hand, Eq. (3.83) implies that $e^{\rm ph}_{M|w}(\theta)$ are functions with height $O(1/U)$ and rapidity-width $O(U)$, and similar considerations hold for $(k'_{M|w})^{\rm dr}(\theta)$. Thus, the velocities of $w$-strings are again suppressed by factors of $1/U$, implying that in regime (iv) as well the Drude weight is dominated by $y$ particles. These same considerations lead us also to conclude that the dressed charge and energy of $y$ particles are dominated by their bare value. Therefore, the crossover between regimes (iii) and (iv) cannot be observed in the (reduced) energy or charge Drude weights. However, the magnetization of $y$-particles is significantly corrected relative to its bare value due to scattering off the magnons, and the spin Drude weight picks up the crossover due to the change in magnon properties.

Although a full analytical solution in this regime is generally hard [59], we focus on the $h \ll t$ regime to show that the leading corrections to the charge and energy Dude weight in Eq. (3.14) are different than those in regime (iii). When $h \ll t$, the dressed energy of the "elementary" magnon (i.e. the $1|w$ string) is negative in a large rapidity interval centred around 0. Approximating this interval by the whole real axis, the TBA equation becomes linear in $e^{\rm ph}_{1|w}$, and furthermore all higher magnons ($M|w$ strings with $M > 1$) strings drop out of the problem. The TBA equation can

then be readily solved (to leading order in $1/U$)

$$e_{\pm}^{\mathrm{dr}} = e_{\pm} - \mu - h/2, \tag{3.112}$$

$$e_{1|w}^{\mathrm{dr}} = \gamma_Y s(\theta) < 0. \tag{3.113}$$

The dressing equation for $\left(k^{\mathrm{dr}}\right)'$ yields a similar result

$$\left(k'_{\pm}\right)^{\mathrm{dr}} = k'_{\pm}, \tag{3.114}$$

$$\left(k'_{1|w}\right)^{\mathrm{dr}} = \gamma_k s(\theta) < 0. \tag{3.115}$$

The correction to the Drude weight can then be computed similarly to that in case (iii), by the following substitutions in Eq. (3.14)

$$e_{\pm} \to e_{\pm} + \gamma_Y \int d\theta\, K_1(\theta) s(\theta), \tag{3.116}$$

$$k'_{\pm} \to k'_{\pm} + \gamma_k \int d\theta\, K_1(\theta) s(\theta), \tag{3.117}$$

where, again

$$\int d\theta\, K_1(\theta) s(\theta) = O(1/U). \tag{3.118}$$

# Chapter 4

# Nonlinear transport in generalized hydrodynamics

In this chapter, we develop and apply an asymptotically exact framework for computing the nonlinear response of interacting integrable systems to an external potential accelerating QPs. Given that the perturbation can only move QPs, we refer to these type of nonlinear response functions as nonlinear transport.

The framework we develop is itself rooted within GHD. Ultimately it allows us to compute nonlinear response functions or multipoint correlators as a sum of terms, each of which can be associated to a diagram. Therefore the calculation of nonlinear response function is reduced to the enumeration of certain diagrams and the evaluation of each of these (either analytically or numerically). Each element of the diagram can in fact be converted into an expression involving only TBA quantities.

We discuss in detail the diagrams contributing to second-order response and how these closely correspond to actual physical processes. Within this context we argue that the nonlinear response of integrable systems contains information that is absent from (or subleading in) linear response: while the spectral functions of free and interacting integrable systems are qualitatively similar (with only subtle differences in the broadening around their ballistic light-cones [80, 42]), we find that spatially resolved nonlinear response reveals clear, qualitative distinctions between interacting and noninteracting integrable systems. We exemplify the discussion by studying the second-order response of the Lieb-Liniger model.

Furthermore, we consider the effect of uniform electric fields and study the nonlinear analog of the Drude weights. Here we demonstrate the validity of our method by comparing our theory with exact diagonalization studies of the XXZ spin chain in

the easy-axis regime. Finally we discuss the XXX chain and show that at the $SU(2)$ symmetric point, nonlinear Drude weights of order higher than 3 diverge.

In this chapter, in order to simplify the already heavy notation, we will write all expressions for a system with only one QP species. Generalizations to systems with multiple species is immediate.

## 4.1 Setup

We consider general one-dimensional systems whose dynamics is governed by some integrable Hamiltonian $\hat{H}_0$. The dynamics under $\hat{H}_0$ is treated within Euler-scale GHD: we partition the system into hydrodynamic cells each of mesoscopic size and linked to some spacetime point $(x,t)$, and assume that each cell is always instantaneously in some local GGE, characterized by the vector of occupation factors of available quasiparticle states, $\boldsymbol{n}(x,t) = \{n_\theta(x,t)\}$.

To simplify the notation, we specialize to the case where the perturbation couples to a global $U(1)$ charge-density $\hat{q} = \hat{q}_0$. Thus, the perturbed Hamiltonian is

$$\hat{H}(t) = \hat{H}_0 + \int dx\, V(x,t)\hat{q}(x). \tag{4.1}$$

Response theory is concerned with computing the expectation value of some local observable $\hat{O}$—taken here to be a charge density $\hat{q}_j$ or current density $\hat{j}_j$—following the application of the field $V(x,t)$. Formally, the connected order-$N$ response is then given by

$$\chi^{(N)}_{\hat{O}}\left(\{x_n,t_n\}\right) = \prod_{n=0}^{N-1} \frac{\delta}{\delta E(x_n,t_n)} \langle \hat{O}(x_N,t_N)\rangle \Big|_{E\to 0} \tag{4.2}$$

with $t_0 < t_1 < \cdots < t_N$, and $E(x,t) = -\partial_x V(x,t)$ denoting the electric field. Here the expectation value is taken with respect to the nonuniform state at time $t_N$ generated by perturbing the initial uniform GGE state with external fields at times $t_1, \dots t_{N-1}$.

Equivalently $\chi^{(N)}_{\hat{O}}$ can be defined in term of the electric field operator

$$\hat{E}(x) = -\int dx' \,\mathrm{sign}(x'-x)\hat{q}_0(x), \tag{4.3}$$

in terms of which

$$\chi^{(N)}_{\hat{O}}\left(\{x_n,t_n\}\right) = \left\langle \Big[\hat{E}(x_0,t_0), \Big[\dots\Big[\hat{E}(x_{N-2},t_{N-2}), \Big[\hat{E}(x_{N-1},t_{N-1}), \hat{O}(x_N,t_N)\Big]\Big]\dots\Big]\Big]\right\rangle \tag{4.4}$$

A natural approach to computing $\chi^{(N)}$ could be the following. Expand the nested commutator as a linear combination of $(N+1)$-point functions containing $N$ $\hat{q}_0$ operators and one $\hat{O}$ operator. Compute the various $(N+1)$-point correlators and take their linear combination to compute the response function. Unfortunately, such an approach is bound to fail as correlation functions at the Euler scale do not depend on the order of the operators, as explained in Ref. [47]. In other words, commutators are suppressed at the Euler scale and the computation of their expectation value goes beyond the leading order achievable through GHD without diffusive corrections. In linear response this obstacle is usually overcome through the fluctuation dissipation theorem, which relates the expectation value of the commutator to the expectation value of a single time-ordered two-point function. However, as discussed in Chapter 1, such an approach does not easily generalize to nonlinear response, since the fluctuation-dissipation theorem is not as powerful in this context.

To circumvent this problem, we therefore use an extension of GHD, which incorporates external inhomogeneous potentials [52, 9]. Assuming $V$ varies slowly in space and time, the Euler-scale time evolution of the system is described by [52, 28, 9, 11, 32, 147, 117]

$$\partial_t n_\theta + v_\theta^{\mathrm{eff}} \partial_x n_\theta + E a_\theta^{\mathrm{eff}} \partial_\theta n_\theta = 0, \tag{4.5}$$

where $a_\theta^{\mathrm{eff}}[\boldsymbol{n}] = \boldsymbol{q}_j^{\mathrm{dr}}/(\partial_\theta k)^{\mathrm{dr}}$ is the effective acceleration of the quasiparticles, and the sole dependence on the potential is via the electric field $E(x,t) \equiv -\partial_x V(x,t)$.

We remark that Eq. (4.5), and thus our method, is believed to be exact at the Euler scale for any finite temperature and it can be applied to the computation of correlation functions of the density of any conserved charge in any integrable system. A caveat is that the response to sharply localized potentials could contain oscillations in space and time that the GHD approach automatically averages out and hence cannot properly capture (see e.g. Ref. [184]).

## 4.2 Summary of the technique

As previously mentioned, we will consider Eq. (4.5) and expand it perturbatively in $E(x,t)$. Our strategy is to express the expectation value in (4.2) in terms of quasiparticle occupations, perform all the functional derivatives, and then set $E=0$, yielding an expression that we evaluate in the *uniform* GGE. An expectation value $\langle O(x,t)\rangle$ is a nonlinear functional of the local state $\boldsymbol{n}(x,t)$. It can be affected by perturbations at other spacetime points only through the advection of those perturbations to $(x,t)$,

which is captured by the propagator $D(\theta,\theta';z,z') = \frac{\delta n(\theta;z)}{\delta n(\theta';z')}$, where we have defined $z \equiv (x,t)$. One can express this dependence in the following compact form, suggestive of a chain rule: [47]

$$\frac{\delta\langle O(z_1)\rangle}{\delta E(z_0)} = \int d\theta d\alpha \frac{\delta\langle O(z_1)\rangle}{\delta n(\alpha;z_1)} \frac{\delta n(\alpha;z_1)}{\delta n(\theta;z_0)} \frac{\delta n(\theta;z_0)}{\delta E(z_0)}, \tag{4.6}$$

Eq. (4.6) simply says that expectation values at spacetime point $z_0$ depend on fields at $z_1 \neq z_0$ purely via the process by which the fields perturb the quasiparticle distribution at $z_0$ and this perturbation is advected over to $z_1$.

We are interested in generalizing Eq. (4.6) to the case of higher-order functional derivatives. To organize these more complicated expressions we have developed a diagrammatic framework, which relies on the observation that any functional derivative can be composed of the following types of elementary object. First, there are propagators, defined above, connecting perturbations at different spacetime points; in a uniform GGE, the propagators take the simple form $D(\theta,\theta';x_0,t_0;x_1,t_1) = \delta(\theta-\theta')\delta\left[(x_0-x_1) - v^{\rm eff}(\theta)(t_0-t_1)\right]$ [47]. Second, there are functional derivatives of observables at a point with respect to the quasiparticle distribution at the same point, which can be evaluated using TBA techniques [48]. We call these "measurement vertices." Third, there are derivatives of the quasiparticle distribution at a spacetime point with respect to fields at the same point. To find these we invert (4.5) using Green's function techniques, and thereby find $\frac{\delta n(\theta;z)}{\delta E(z)} = -a^{\rm eff}(\theta)[\boldsymbol{n}]\partial_\theta n_\theta$. These objects are called "field vertices." These three types of objects appear in Eq. (4.6). Finally, response functions at order $N > 1$ will also involve expressions of the form $\Gamma^{(p)} = \frac{\delta^p n_\theta(z_0)}{\delta n_{\theta_1}(z_1)\ldots\delta n_{\theta_p}(z_p)}$. These capture the modification of the spacetime propagator by scattering events, and can be computed by repeatedly differentiating (4.5) with $V = 0$ with respect to $n$, which yields a recursive formula, that allows us to express $\Gamma^{(p)}$ in terms of $\partial_x\Gamma^{(1)}$ and functional derivatives of the $v^{\rm eff}[\boldsymbol{n}]$ with respect to quasiparticle occupations. These objects are "scattering vertices." All other types of object can be expressed in terms of these: e.g., functional derivatives of the form $\frac{\delta^k\langle\hat{O}\rangle}{\delta n(\theta_1;z_1)\ldots\delta n(\theta_k;z_k)}$, can be rewritten in terms of measurement or scattering vertices and propagators, which advect all occupation factors to the point where the functional derivative is taken. We may verify that for $N = 1$ this procedure yields the standard expressions for linear response. Higher-order response functions can then be computed recursively from (4.2).

We now exemplify the general discussion above by showing explicitly the expression for $\chi^{(2)}$ in terms of these objects. As mentioned above, the starting point is the

expression for $\chi^{(1)}$ in Eq. (4.6), which we rewrite here as

$$\frac{\delta\langle O(z_2)\rangle}{\delta E(z_1)} = \int d\theta_1 d\alpha_1 \frac{\delta n(\theta_1; z_1)}{\delta E(z_1)} \frac{\delta n(\alpha_1; z_2)}{\delta n(\theta_1; z_1)} \frac{\delta\langle O(z_2)\rangle}{\delta n(\alpha_1; z_2)}, \tag{4.7}$$

When taking a further functional derivative w.r.t. $E(z_2)$ we then obtain the sum of three terms, depending on which of the three factors appearing in (4.6) the functional derivative acts upon

$$\frac{\delta^2\langle O(z_2)\rangle}{\delta E(z_0)\delta E(z_1)} \tag{4.8}$$

$$\begin{aligned}
&= \int d\theta_0 d\alpha_0 d\theta_1 d\alpha_1 \frac{\delta n(\theta_0; z_0)}{\delta E(z_0)} \frac{\delta n(\alpha_0; z_1)}{\delta n(\theta_0; z_0)} \frac{\delta^2 n(\theta_1; z_1)}{\delta n(\alpha_0; z_1)\delta E(z_1)} \frac{\delta n(\alpha_1; z_2)}{\delta n(\theta_1; z_1)} \frac{\delta\langle O(z_2)\rangle}{\delta n(\alpha_1; z_2)} + \\
&+ \int d\theta_0 d\theta_1 d\alpha_1 \frac{\delta n(\theta_0; z_0)}{\delta E(z_0)} \frac{\delta n(\theta_1; z_1)}{\delta E(z_1)} \frac{\delta^2 n(\alpha_1; z_2)}{\delta n(\theta_0; z_0)\delta n(\alpha_1; z_1)} \frac{\delta\langle O(z_2)\rangle}{\delta n(\alpha_1; z_2)} \\
&+ \int d\theta_0 d\alpha_0 d\theta_1 d\alpha_1 \frac{\delta n(\theta_0; z_0)}{\delta E(z_0)} \frac{\delta n(\alpha_0; z_2)}{\delta n(\theta_0; z_0)} \frac{\delta n(\theta_1; z_1)}{\delta E(z_1)} \frac{\delta n(\alpha_1; z_2)}{\delta n(\theta_1; z_1)} \frac{\delta\langle O(z_2)\rangle}{\delta n(\alpha_0; z_2)\delta n(\alpha_1; z_2)}
\end{aligned} \tag{4.9}$$

Note that only the objects discussed above appear in the expression for $\chi^{(2)}$. In particular, in the second line, we can recognize a factor $\Gamma^{(2)}$. Given that manually deriving this expressions becomes increasingly more complex as $N$ increases, we develop a diagrammatic framework to generate the various term in the next section.

Although the formal expressions rapidly become unwieldy with increasing $N$, they have a transparent physical interpretation, as we now exemplify for $N = 2$. The external field can affect the system via two distinct physical processes, each corresponding to a distinct field vertex (represented by a box with a wavy line in Fig. 4.1): it can accelerate a thermal quasiparticle from rest within a spacetime cell (the first field vertex in Fig. 4.1a), or else accelerate a quasiparticle previously acted upon by the field at an earlier time (the second field vertex in Fig. 4.1a). In a non-interacting integrable system, all connected nonlinear response functions result solely when a single quasiparticle is repeatedly accelerated by the field, and then measured, as in Fig. 4.1a. However, in interacting integrable systems, quasiparticles influence each other via forward-scattering phase shifts. Consequently, the ability of the field to excite a quasiparticle in a given spacetime cell $z$ is also sensitive to the presence of quasiparticles excited by the field in all spacetime cells in the past light-cone of $z$ under the advective dynamics of GHD, leading to additional connected contributions (as in Fig. 4.1b). Quasiparticles excited by the field acting at distinct spacetime cells

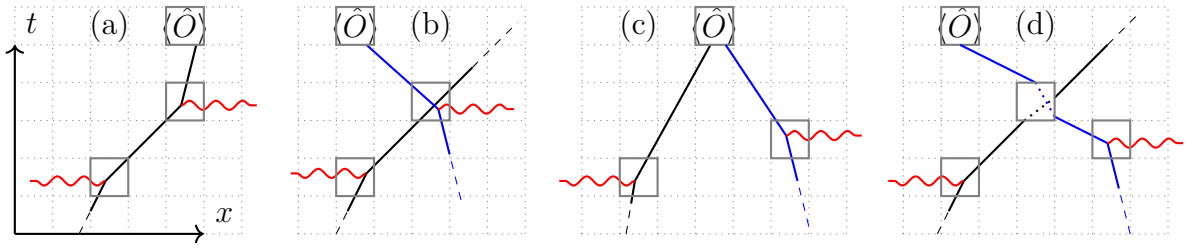


Figure 4.1: Four distinct physical processes contributing to the second-order response $\chi^{(2)}$. (a) A thermal quasiparticle (QP; black line) is accelerated twice by the electric field (red wavy line), and modifies the expectation value $\langle\hat{O}\rangle$ in the final space-time cell. (b) First a thermal QP is accelerated; a second thermal QP (blue line) is later accelerated when the first is in its space-time cell, thus modifying the effective acceleration perceived by the second; both QPs proceed ballistically and the second modifies $\langle\hat{O}\rangle$. (c) Two thermal QPs are independently accelerated by two pulses of the electric field; after travelling to the same space-time cell, and together they modify $\langle\hat{O}\rangle$. (d) As in (c), two thermal QPs are independently accelerated but one scatters off the other before influencing $\langle\hat{O}\rangle$. Only (a) is relevant to free systems but all four processes contribute in interacting integrable systems.

can also propagate to a single cell where they jointly modify the measured observable (Fig. 4.1c). Interactions thus lead to an infinite hierarchy of field and measurement vertices, that are sensitive to the presence of an increasing number of previously-excited quasiparticles in the spacetime cells where quasiparticles are accelerated or measured. Finally, the nonlinear response also receives contributions from scattering vertices, again of arbitrary order, due to the phase shift experienced by the measured quasiparticle as it propagates between the acceleration and measurement cells in the presence of other excited quasiparticles in the system (Fig. 4.1d). The $N^{\text{th}}$ order response in an interacting integrable system involves $N$ field vertices and a single measurement vertex, linked by advection propagators $D(\theta, \theta'; z, z')$ and scattering vertices, and can be organized using spacetime diagrams. Crucially, at fixed $N$, only vertices below some finite order can contribute: for instance Fig. 4.1 contains all processes contributing to $\chi^{(2)}$.

## 4.3 Diagrammatic rules

In this section we explain in more detail the diagrammatic rules mentioned above. A full derivation of these rules requires two further elements, which are deferred to the appendix of this chapter: the derivation of the two distinct classes of field vertices is discussed in Appendix 4.A; similarly, the proof that $\Gamma^{(p)}$ can be constructed by

considering connected diagrams formed by propagators and scattering vertices is left for Appendix 4.B.

As explained above, the starting point of the formalism is the definition of $\chi^{(n)}$ in terms of functional derivatives (Eq. (4.2)) and the chain rule in Eq. (4.6). Combining these allows us to identify the following elementary objects that appear in any response calculation:

- the **propagator** evaluated on the thermal background $D(\theta, \theta'; z, z')$, describing the linearized advection of quasiparticles
- the **non-linear generalization of the propagator** $\Gamma^{(p)}$ with $p > 1$, describing multi-particle processes which modify the linear advection given by $D(\theta, \theta'; z, z')$
- the **field vertices**, corresponding $\delta n(\theta, x, t+0^+)/\delta E_j(x, t)$ and its higher, functional derivatives w.r.t. $\boldsymbol{n}(\cdot, x, t)$. These reflect the perturbation in the normal modes produced by the field $E_j$. As noted in the main text, field vertices come in two varieties, depending on whether they excite a quasiparticle from rest, or accelerate a previously-excited quasiparticle.
- the **measurement vertices**, i.e. the expectation value $\langle \hat{O}(x, t) \rangle$ and the functional derivatives w.r.t. $\boldsymbol{n}(x, t)$.

Crucially, each vertex only involves quantities within the same space-time cell, so that it can be computed within the TBA formalism. The only object that is non-trivial to compute is the non-linear generalization of the propagator $\Gamma^{(p)}$. As we will show in Appendix 4.B, $\Gamma^{(p)}$ can be expressed in terms of the *linear* propagator $D(\theta, \theta'; z, z')$ and a new class of vertices, namely

- the **scattering vertices**, corresponding to functional derivatives of $v^{\text{eff}}[\boldsymbol{n}(x, t)](\theta)$ w.r.t. $\boldsymbol{n}(x, t)$.

With the above definitions, the calculation of $\chi^{(N)}$ can be represented diagrammatically as follows. Each vertex corresponds to a vertex in the diagram. The set of possible vertices is reported in table in Table 4.1, together with a cartoon of the corresponding process in the same schematic language used in Fig. 4.1. Note that field and scattering vertices have a 'marked' incoming leg. In order to diagrammatically indicate the distinction between unmarked and marked legs, we place them respectively to the left and right of a 'notch' on these vertices; therefore, at most one line can enter the vertex to the right of the notch. For a field vertex, there can either

be no incoming line to the right of the notch, corresponding to the case when a field accelerates a quasiparticle previously at rest, or a single incoming line, corresponding to the case where the field accelerates a quasiparticle that was already disturbed from the thermal distribution at a previous time. The remaining 'unmarked' incoming lines to the left of the notch describe any other excited quasiparticles in the same cell that modify the effective acceleration induced by the field. A scattering vertex always has an incoming line on the right of the notch, representing the quasiparticle whose effective velocity is modified by scattering at the spacetime cell due to its scattering against the other excited quasiparticles in the cell, which are represented by the lines entering the unmarked legs to the left of the notch. Diagrams are then formed by joining the vertices reported in the table with lines, corresponding to linearized propagators. Finally, $\chi^{(N)}$ is given by the sum of all connected diagrams that can be constructed with one measurement vertex and with $N$ field vertices. To fully describe the diagrammatic calculation we must then specify the rules for how to associate a real number to each diagram.

Before reporting these rules, we stress that at any given $N$ only a finite number of diagrams can contribute. This follows from two facts: each field vertex can increase the number of propagators *at most* by 1, while all other vertices *decrease* the number of propagators. Consequently one can see that that any scattering or measurement vertex that can enter a diagram contributing to $\chi^{(N)}$ can have at most $N$ incoming legs, while a field vertex contributing to such a diagram can have at most $N-1$ incoming legs.

The *recursive* procedure for computing the weight of a given diagram to do this may be summarized as follows:

1. Label the rapidity of each line. Assign different rapidity labels to different lines, unless the rapidity is constrained to be the same according to the graphical rules in Table 4.1. This happens when a line enters the rightmost/marked leg of a field, scattering, or potential node, in which case the outgoing line needs to have the same rapidity of the line entering the marked leg.

2. Recursively evaluate the weight of each [sub-]diagram using the following procedure:

   (a) Identify the uppermost object in the diagram, i.e. the one corresponding to the latest time. In the first recursive step this will be the measurement vertex; in later steps it can be any other vertex or a propagator.

(b) Remove this object. This will split the diagram into one or more connected sub-diagrams.

(c) Evaluate the weight of each connected sub-diagram generated by the removal in the previous step.

(d) The weight of the sub-diagram under consideration is given by the product of two terms: (i) the expression $I_1$ of the removed object (as in Table 4.1) and (ii) a second term $I_2$, coming from the weight of the sub-diagrams, as detailed below

- If the removed object is a propagator, $I_2$ is the weight of the remaining sub-diagram
- If the removed object is either a measurement node or a field node without lines entering the marked leg (as on the second row of Table 4.1), $I_2$ is the product of the weights of the remaining sub-diagrams.
- If the removed object is a field node with one line entering the marked leg (as the on the third row of Table 4.1), $I_2$ is the product of the weights of the sub-diagrams ending in the non-marked leg -i.e. the one denoted by $\theta_1,\ldots,\theta_k$ in the table- times the derivative w.r.t. $\alpha$ of the weight of the sub-diagram entering the marked leg.
- If the removed object is a scattering vertex (fifth row), $I_2$ is the product of the weights of the sub-diagrams ending in the unmarked legs —i.e., those denoted by $\theta_1,\ldots,\theta_k$ in the table — multiplied by the spatial derivative of the weight of the sub-diagram entering the marked leg w.r.t. the position of the removed vertex. Operationally, this simply replaces the propagator $\delta\left(x-x'-v^{\text{eff}}(\alpha)(t-t')\right)$ entering the marked leg, with its derivative $\delta'\left(x-x'-v^{\text{eff}}(\alpha)(t-t')\right)$.

3. Integrate over each rapidity label.

4. Integrate over the space and time coordinates of all scattering vertices.

As an example we report the diagrams contributing to $\chi^{(2)}$ in Fig. 4.C.1. For an example on how to evaluate these and how to compute the first few functional derivatives, see Sec. 4.C. Evidently, the diagrammatic formalism is simply a schematic representation of the physical processes in Fig. 4.1, but in a form that is more conveniently transcribed into a concrete calculation, and is hence more suited to systematic computation of higher-order responses.

Table 4.1: List of all vertices composing a non-linear response diagram. The "Cartoon" depicts the process in the same style used in Fig. 4.1, while the "Diagram" column reports a more schematic representation, which is more convenient in actual diagrammatic calculations— see e.g. Fig 4.C.1. In all vertices the space-time position of the $\delta n$ perturbations coincide with the position of the vertex. The two version of the field vertex reflect the possibility of evaluating $\partial_\alpha n$ of the thermal background, i.e. accelerating a previously thermal quasiparticle, or take the functional derivative of $\partial_\alpha n$ with one incoming line, i.e. accelerating a quasiparticle already acted upon by the field (see also Fig. 4.1). The scattering vertex has a similar bipartite structure, where $k > 1$ incoming legs act with a functional derivative on $v^{\text{eff}}$, while one acts on $\partial_{x'} n(\alpha, x', t')$, where $z' = (x', t')$ is the space-time position of the vertex and must be integrated upon.

| **Process** | **Cartoon** | **Diagram** | **Expression** |
|---|---|---|---|
| Linearized propagation, $D(\theta; z, z')$ | | 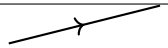 | $\theta_H(t-t')\delta\left(x - x' - v^{\text{eff}}(\theta)(t-t')\right)$ |
| Field accelerates thermal quasiparticle | 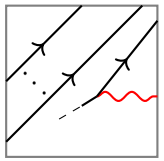 | 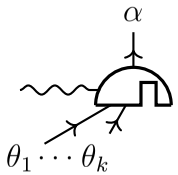  | $-\dfrac{\delta^k a^{\text{eff}}(\alpha)}{\delta n(\theta_1)\cdots\delta n(\theta_k)}\partial_\alpha n(\alpha),\ k \geq 0$ |
| Field accelerates excited quasiparticle | 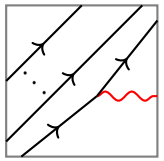 | 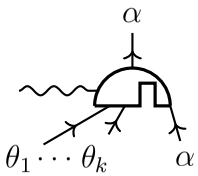  | $-\dfrac{\delta^k a^{\text{eff}}(\alpha)}{\delta n(\theta_1)\cdots\delta n(\theta_k)},\ k \geq 0$ |
| Measurement | |   | $\dfrac{\delta^k \langle\hat{O}\rangle}{\delta n(\theta_1)\cdots\delta n(\theta_k)},\ k \geq 1$ |
| Scattering | 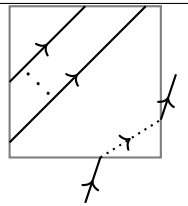 | 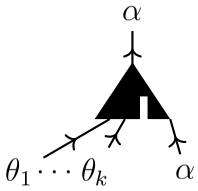  | $-\dfrac{\delta^k v^{\text{eff}}(\alpha)}{\delta n(\theta_1)\cdots\delta n(\theta_k)},\ k \geq 1$ |

## 4.4 Measuring Interactions in the Lieb-Liniger Gas

As an example of this approach, we apply it to the Lieb-Liniger model of 1D bosons with contact interactions, previously introduced in Sec. 2,

$$\hat{H}_0 = \frac{1}{2}\sum_j \hat{p}_j^2 + c\sum_{i\neq j}\delta(\hat{x}_i - \hat{x}_j), \tag{4.10}$$

where $\hat{x}_j$ and $\hat{p}_j$ are the position and momentum of particle $j$. The bare group velocity $v$ of a particle is equal to its momentum $p$. The effective velocity $v^{\text{eff}}$ can be obtained from $v$ as the solution to an integral equation, as discussed in Chapter 2. An additional fact, peculiar to the Lieb-Liniger gas and perturbations coupling to the particle density, is that the effective acceleration $a^{\text{eff}}$ is not renormalized by interactions; with our choice of conventions, $a^{\text{eff}} = 1$. For $c \to 0$, $\hat{H}_0$ is a free Bose gas, while for $c \to \infty$ it can be described as a theory of free fermions. This can be recognized, for example, by studying $v^{\text{eff}}$, which in both limits tends to the bare group velocity $v$. Consequently *linear* response in these two limits approximates that of free bosons or fermions respectively, with only quantitative corrections from interactions. This hinders a precise measurement of $c$ based only on linear response. We now demonstrate that a spatially-resolved measurement of $\chi^{(2)}$ —or higher-order responses— carries direct information about the interactions. For concreteness, we consider a specific charge response of the form $\tilde{\chi}^{(2)}(x,t,\tau) \equiv \chi^{(2)}_{\hat{q}_0}(0,0;x,\tau;0,\tau+t)$ where the first perturbation and the measurement coincide spatially, and the system is perturbed at an intermediate time at position $x$. In the free boson or free fermion limits, we know from the discussion in the previous section that the only process contributing to $\chi^{(2)}$ is one where a single quasiparticle is repeatedly accelerated by the subsequent field applications (Fig. 4.1a). Furthermore, as previously noted, this process can take place only if all the points in which the perturbation is applied and the measurement point lie on the same ray. Thus, in the two non-interacting limits $\tilde{\chi}^{(2)}(x,t,\tau)$ will vanish everywhere except at $x = 0$. Conversely, if $c = O(1)$, quasiparticles are strongly interacting, and each influences the dynamics of the others. For example, processes such as those in Fig. 4.1d will be non-zero since $v^{\text{eff}}$ of a quasiparticle with momentum $p$ will depend on all the quasiparticles in the same region. We thus expect that $\chi^{(2)}$ is generically finite and non-zero for arbitrary perturbation and measurement points.

To summarize: if we focus on the region away from $x = 0$, i.e. chosen to exclude the case where all points lie along the same ray, we expect $\tilde{\chi}^{(2)}(x,t,\tau)$ to be directly sensitive to the interactions, and hence generically will have a nonzero value away

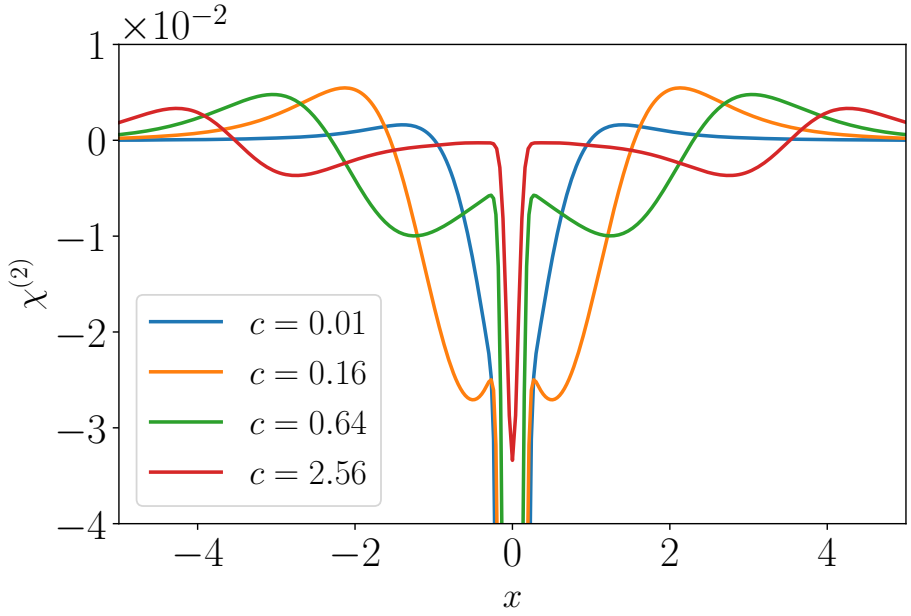


Figure 4.2: $\chi^{(2)}(0,0;x,\tau;0,\tau+t)$ in the Lieb-Liniger model for various interaction strengths $c$. We take $T=2$, $\bar{n}=1$, $\tau=t=1$ and regularize the $\delta$-function GHD propagator as a Gaussian of width $\eta=0.1$. In a noninteracting system, the only response would come from the resolution-limited spike at $x_1=0$; everything else is a signature of interactions.

from the free limits $c\to 0$ or $c\to\infty$. An immediate corollary is that in these limits, $\tilde{\chi}^{(2)}(x\neq 0,t,\tau)$ should respectively vanish as $O(c)$ or $O(1/c)$. This should be contrasted with linear response measurements where $\chi^{(2)}=O(1)$ in all these cases and the effect of interactions is to determine sub-leading corrections.

Indeed, this response is readily computed using the above formalism (as detailed in the previous section); Fig. 4.2 shows the results for various interaction strengths, at fixed temperature $T$ and boson density $\bar{n}$. As $c$ decreases we see that the signal moves closer to $x=0$. This is because for $c\to 0$ the system is proximate to a Bose-Einstein condensate at $c=0$ and $T=0$ (see e.g. Refs. [179, 106]), and hence only slow, low momentum quasiparticle states are occupied. Furthermore, note that the signal starts to decrease either for $c\lesssim 10^{-2}$ or $c\gtrsim 1$, as expected. [Recovering free boson response as $c\to 0$ requires studying very low $c$; as $c$ decreases, the density of states initially *increases* due to the incipient Bose condensation, enhancing interaction effects.] These observations are not restricted to the protocol analyzed above: any protocol which separates the same-ray 'free' contribution from the regular part of the response would yield similar results. Thus, nonlinear correlators provide a more direct window into the interacting Lieb-Liniger gas than linear response.

## 4.5 Nonlinear Drude weights

So far, we have focused on spatially-resolved response. While this can be measured in cold-atom experiments, most solid-state spectroscopic techniques only access spatially integrated quantities. At the Euler scale, the most natural integrated quantity is the generation of a persistent current in response to a uniform electric field. This follows from the fact that the current operator in an integrable system generically has some part that is strictly conserved under time evolution, so the current generated in response to an electric field will not decay over time. For example, specializing to first-order response, $\int dx\, \chi^{(1)}_{\hat{j}_0}(0,0;x,t)$ will tend to a constant as $t \to \infty$; this limiting value is called the Drude weight [13, 166]. Alternatively, in frequency space, the conductivity goes as $\sigma(\omega) = \pi D\delta(\omega) + \ldots$. Drude weights extend to nonlinear response: a field $E$ applied to the system for a finite time $\Delta t$ drives a persistent current $j_0(\varphi)$, where $\varphi \equiv E\Delta t$ is the vector potential variation due to the field. By expanding $j_0(\varphi)$ as a series in its argument and taking derivatives, we may define a sequence of nonlinear Drude weights [190, 189].

Our diagrammatic approach can straightforwardly be used to compute $N^{\text{th}}$ order Drude weights $D^{(N)}$, by integrating the $N^{\text{th}}$ order response over the positions of the field insertions [1]

$$D^{(N)} = \lim_{\{\tau_j \to \infty\}} \int dx_0 \cdots \int dx_{N-1} \chi^{(N)}_{\hat{j}_0}(x_0, 0; x_1, \tau_1; x_2, \tau_1 + \tau_2; \cdots). \tag{4.11}$$

When performing the integral over all spatial coordinates, we see that the diagrams that contain scattering vertices vanish, because they contain a spatial derivative of a propagator. Meanwhile, in all other diagrams the propagators integrate to 1. This can be easily seen as follows. Imagine integrating over $x_j$ in order of increasing $j$. In this way, when we need to integrate over $x_j$, there is a single propagator depending on $x_j$: the propagator of the $\delta n$ perturbation produced in $x_j$, while all other propagators entering $x_j$ have already been integrated. Then, if the propagator has not been differentiated, the integral gives 1; instead, if the propagator has been differentiated (i.e. it terminates in the 'marked leg' of a scattering vertex), then the integral is zero.

This observation enormously simplifies the recursive computation of the Drude weights. Since the Drude weights are just the product of nodes in the diagrams, we can recognize that the whole diagrammatic construction is just a book-keeping

[1] At the Euler-scale the integral over space is time-independent and taking the limit $\tau_j \to \infty$ only eliminates sub-leading corrections to the Euler-scale result.

method to compute the recursive relation

$$D^{(N)} = -\int d\theta_N a^{\rm eff}(\theta_N)\partial_{\theta_N} n(\theta_N)\frac{\delta}{\delta n(\theta_N)} D^{(N-1)} \tag{4.12}$$

with $D^{(0)} = \langle \hat{j}_0 \rangle$. This recursive formula allows us to obtain a closed-form expression for non-linear Drude weight of arbitrary order only using TBA technology. For example, the second-order Drude weight is given by

$$\begin{aligned} D^{(2)} = &\int d\theta_1\, a^{\rm eff}(\theta_1)\tilde{J}(\theta_1)\partial_{\theta_1}\left[a^{\rm eff}(\theta_1)\partial_{\theta_1} n(\theta_1)\right] \\ &+ \int d\theta_2\, a^{\rm eff}(\theta_2)\left[\partial_{\theta_2} n(\theta_2)\right]\int d\theta_1\, \frac{\delta\left[a^{\rm eff}(\theta_1)\tilde{J}(\theta_1)\right]}{\delta n(\theta_2)}\partial_{\theta_1} n(\theta_1), \end{aligned} \tag{4.13}$$

where

$$\tilde{J}(\theta) = \frac{\delta\langle \hat{j}_0\rangle}{\delta n(\theta)} = \frac{1}{2\pi}\left(\partial_\theta e(\theta)\right)^{\rm dr} q^{\rm dr}(\theta). \tag{4.14}$$

By applying the recursion formula once more we obtain the following expression for the third-order Drude weight

$$\begin{aligned} D^{(3)} = &-\int d\theta\, a^{\rm eff}(\theta)\tilde{J}(\theta)\partial_\theta\left[a^{\rm eff}(\theta)\partial_\theta\left[a^{\rm eff}(\theta)\partial_\theta n(\theta)\right]\right] + \\ &- 2\int d\theta_2\, a^{\rm eff}(\theta_2)\partial_{\theta_2} n(\theta_2)\int d\theta_1\, \frac{\delta\left[a^{\rm eff}(\theta_1)\tilde{J}(\theta_1)\right]}{\delta n(\theta_2)}\partial_{\theta_1}\left[a^{\rm eff}(\theta_1)\partial_{\theta_1} n(\theta_1)\right] + \\ &- \int d\theta_2\, a^{\rm eff}(\theta_2)\partial_{\theta_2} n(\theta_2)\int d\theta_1\, a^{\rm eff}(\theta_1)\tilde{J}(\theta_1)\partial_{\theta_1}\left[\frac{\delta a^{\rm eff}(\theta_1)}{\delta n(\theta_2)}\partial_{\theta_1} n(\theta_1)\right] + \\ &- \int d\theta_2\, a^{\rm eff}(\theta_2)\partial_{\theta_2}\left[a^{\rm eff}(\theta_2)\partial_{\theta_2} n(\theta_2)\right]\int d\theta_1\, \frac{\delta\left[a^{\rm eff}(\theta_1)\tilde{J}(\theta_1)\right]}{\delta n(\theta_2)}\partial_{\theta_1} n(\theta_1) + \\ &- \int d\theta_3\, a^{\rm eff}(\theta_3)\partial_{\theta_3} n(\theta_3)\int d\theta_2\, \partial_{\theta_2} n(\theta_2)\int d\theta_1\, \partial_{\theta_1} n(\theta_1) \\ &\qquad\qquad \times \frac{\delta}{\delta n(\theta_3)}\left[a^{\rm eff}(\theta_2)\frac{\delta\left[a^{\rm eff}(\theta_1)\tilde{J}(\theta_1)\right]}{\delta n(\theta_2)}\right]. \end{aligned} \tag{4.15}$$

We benchmark this GHD result against numerical simulations of a paradigmatic integrable model, the XXZ spin chain, and focus on spin current response. Since spatial inversion symmetry forces spatially-averaged current response functions to vanish for any even $N$, we focus on $D^{(3)}$. We work in the easy-axis limit, and exploit the generalized Kohn formula [190, 189] combined with exact diagonalization (ED) on

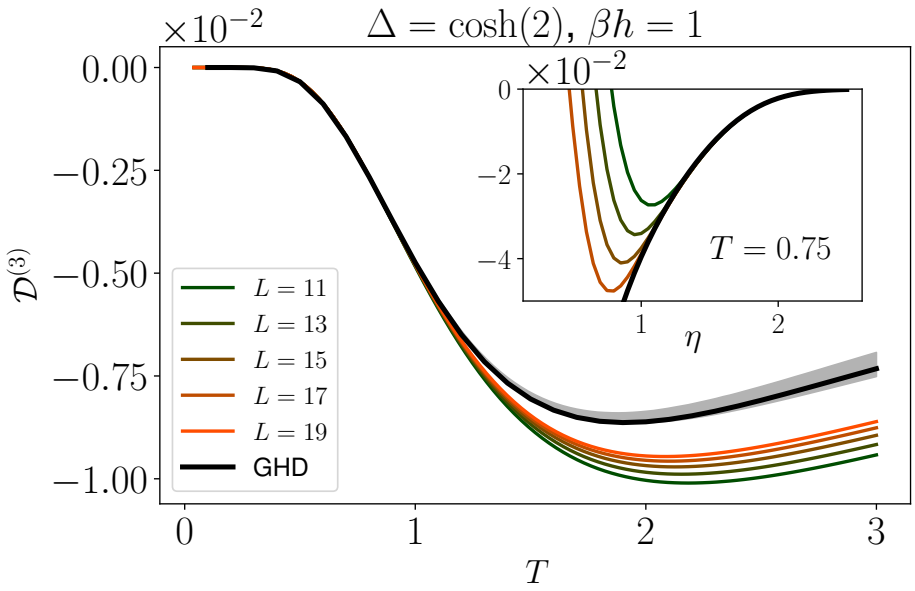


Figure 4.3: Third-order spin Drude weight $D^{(3)}$ in the easy-axis regime of the XXZ spin chain with $\beta h = 1$. Main figure: Comparison between GHD and ED results for fixed $\Delta$. The lower (upper) boundaries of the shaded region correspond to extrapolations of finite-size ED results with a degree 1 (degree 2) polynomial in $1/L$. Inset: $D^{(3)}$ as a function of $\eta = \cosh^{-1}\Delta$.

small systems. Our results are presented in Fig. 4.3; despite the difficulty of extrapolating reliably to the thermodynamic limit from the small system sizes accessible to ED, we see that the GHD results are within the range of our extrapolations at high temperature, and agree extremely well at lower temperatures. We also see good agreement as we vary the easy-axis anisotropy at fixed temperature.

Before proceeding, we note that while the formulae for $D^{(N)}$ become increasingly complex with $N$, a simple limit is always obtained for the first term of a $\beta \to 0$ expansion. In fact, every factor $\partial_\theta n$ carries a factor of $\beta$. Thus the leading-order term is always obtained by acting in Eq. (4.12) with $\frac{\delta}{\delta n(\theta_N)}$ on the factor $\partial_{\theta_{N-1}} n(\theta_{N-1})$ appearing in $D^{(N-1)}$. Integrating by parts, we then obtain

$$D^{(N)}(\beta \to 0) = -\int d\theta a^{\text{eff}}(\partial_\theta n)\partial_\theta \left[a^{\text{eff}}\partial_\theta \left[\cdots \partial_\theta \left[a^{\text{eff}} \frac{\delta \langle \hat{j}_0 \rangle}{\delta n(\theta)}\right]\right]\right] + O(\beta^2), \qquad (4.16)$$

with $\partial_\theta$ acting $N-1$ times.

## 4.6 Breakdown of perturbation theory in the XXX chain

As discussed in Chapter 3, the isotropic point of the XXX chain is extremely peculiar in linear response, with the (linear) Drude weight vanishing and spin-transport falling into the Kardar-Parisi-Zhang universality class. It is then natural to wonder what happens beyond the linear response regime.

From a technical standpoint, it is convenient to perform all calculations in the presence of a small magnetic field $h$ that breaks the $SU(2)$ symmetry, and therefore restores ballistic transport, and then take the $h \to 0$ limit to study the $SU(2)$-invariant system. To further simplify the problem we will also consider the leading order in the $\beta \to 0$ limit only. In this context a straightforward application of Eq. (4.16), then shows that as $h \to 0$, $D^{(3)}$ diverges as $h^{-2}$. This surprising result signals that perturbation theory in the electric field breaks down at the isotropic point. To understand this point further, in the Appendix 4.D we explicitly compute the spin current due to an impulse $\varphi = E\Delta t$, we find that (see Sec. 4.D)

$$J(h, \varphi) \approx h \sum_{s=1}^{1/h} s^{-4} f(h\varphi s^3), \tag{4.17}$$

for some scaling function $f$ that is approximately sinusoidal in its argument. The sum is over quasiparticle strings, which are bound states of $s$ elementary magnons. If we now take $\varphi \to 0$ at fixed $h \neq 0$, we obtain a series in powers of $\varphi$, where the first term is the linear Drude weight ($\varphi \mathcal{D}^{(1)} \sim \varphi h^2 |\log h|$), the next nonvanishing term is $\varphi^3 \mathcal{D}^{(3)} \sim \varphi^3/h^2$, and higher-order terms are even more singular in the half-filling limit. The $\varphi \to 0$ and $h \to 0$ limits strikingly fail to commute: if we instead take $h \to 0$ at fixed $\varphi$, we find that $J(h, \varphi) \sim h^2 \varphi |\log h\varphi|$. In effect, $\varphi$ can act as a *cutoff* on response: for any fixed field, sufficiently large bound states respond nonperturbatively and undergo Bloch oscillations.

## 4.7 Conclusions

In this work we have presented a general framework for computing nonlinear response within GHD, demonstrated that it is in excellent agreement with exact numerics, and illustrated how it can directly distinguish between free and interacting integrable

systems. Our results suggest a natural experimental protocol for directly measuring quasiparticle interaction effects in the Lieb-Liniger model using ultracold atomic gases. Since our proposal involves *finite-time* behavior, it can be applied to realistic experimental settings where integrability is only approximate. We have focused on regimes where the nonlinear response is perturbative, and can be expanded in powers of the field strength. In such regimes, our results for nonlinear response bear some resemblance to those for full counting statistics [50, 149, 161]. Investigating the relation between response functions to external perturbation and full-counting statistics would be an interesting direction for future work. Finally, we have also shown an example (the isotropic XXX chain) in which the response to an electric field is inherently nonperturbative. A proper description of such nonperturbative phenomena requires extending the present framework beyond Euler scale, e.g., by including diffusive corrections [42, 80, 152, 54] and other sources of irreversibility [10]. We leave this as an important direction for future work.

# Appendix

## 4.A The field vertex

In this section we derive the explicit expression for the field vertex. Specifically, we will show that the perturbation $\delta n$ in the occupation factors produced by the application of the field $E$ is given by

$$\delta n(\theta_0, x_0, t_0 + 0^+) = -a^{\text{eff}}[\boldsymbol{n}_0(x_0, t_0)](\theta)\partial_\theta n_0(\theta_0, x_0, t_0)\delta E(x_0, t_0), \tag{4.18}$$

at linear order in $\delta E_j$ and $\delta V_j$, but for a generic initial state (i.e. background occupation) $n_0(\theta; x, t)$. This will then allow us to compute non-linear responses as detailed above, by taking $n_0$ to be a non-stationary state produced by the field perturbations acting at earlier times.

The starting point is the GHD equation (4.5). Since, without loss of generality, we are restricting to the computation of the linear term in the field, we can simply evaluate the right hand side of (4.5) directly on $n_0$. We are thus left with an equation of the form

$$\partial_t n(\theta; x, t) + v^{\text{eff}}(\theta)[n(x, t)]\partial_x n(\theta; x, t) = J(\theta; x, t)[\boldsymbol{n}_0(x, t)], \tag{4.19}$$

where the source term $J$ is determined by $n_0$

$$J(\theta; x, t)[\boldsymbol{n}_0(x, t)] = -Ea^{\text{eff}}(\theta)\partial_\theta n_0(\theta). \tag{4.20}$$

We thus define a retarded Green's function

$$G(\theta, x, t; \theta_0, x_0, t_0)[\boldsymbol{n}_0] = \frac{\delta n(\theta, x, t)}{\delta J(\theta_0, x_0, t_0)}, \tag{4.21}$$

with the boundary condition $n(x, t < t_0) = n_0(x, t)$. As usual the Green's function

determines $\delta n$ by

$$\delta n(\theta, x, t_0 + 0^+) = \int d\theta_0 \int dx_0 \, G(\theta, x, t_0 + 0^+; \theta_0, x_0, t_0)[\boldsymbol{n}_0]\delta J(\theta_0, x_0, t_0)[\boldsymbol{n}_0]. \quad (4.22)$$

The rest of this subsection is devoted to showing that under the assumption (whose validity we discuss following the derivation) that $n_0(\theta, x, t)$ is smooth w.r.t. $x$, the Green's function is given by

$$G(\theta, x, t_0 + 0^+; \theta_0, x_0, t_0) = \delta(\theta - \theta_0)\delta(x - x_0), \quad (4.23)$$

whence Eq. (4.18) follows immediately.

To prove Eq. (4.23), we recognize that $G$ satisfies the equation

$$\underbrace{\partial_t G(\theta; x, t) + v^{\text{eff}}[n_0(x,t)](\theta)\partial_x G(\theta; x, t)}_{=A} + \underbrace{\int d\alpha \frac{\delta v^{\text{eff}}(\theta)}{\delta n(\alpha)}[n_0(x,t)]G(\alpha; x, t)\partial_x n_0(\theta; x, t)}_{=B} = \delta(x - x_0)\delta(t - t_0)\delta(\theta - \theta_0). \quad (4.24)$$

While solving for the full space-time dependence of $G$ is generally hard (although, see Ref. [47] for a possible approach), to determine the field vertex we only need $G(x, t_0+0^+)$, i.e. in the instant immediately after the perturbation has acted. For this purpose, we integrate both sides of the equation inside a window in rapidity and space centred at $(\theta_0, x_0)$ and with space and rapidity width $2\Delta\theta$ and $2\Delta x$ respectively. In doing so, we keep in mind that the ultimate purpose is to take the limit of $(\Delta\theta, \Delta x) \to \mathbf{0}$. The integral of the RHS of Eq. (4.24) is immediate and gives $\delta(t - t_0)$. We now separately analyze the two terms on the LHS of Eq. (4.24) labeled $A$, and $B$.

First, we can recognize that $A$ can be rewritten as

$$A = \partial_t G(\theta; x, t) + v^{\text{eff}}[n_0(x,t)](\theta)\partial_x G(\theta; x, t) = \frac{d}{dt} G(\theta; x, t)\Big|_{(\tilde{x}(\theta,t),t)}. \quad (4.25)$$

The last term represents the total derivative of $G$ evaluated along a characteristic trajectory -the space-time trajectory along which $n_0(\theta)$ is constant- with $\frac{d}{dt}\tilde{x}(\theta, t) =$

$v^{\text{eff}}(\theta)$. This means that, if $B$ can be neglected, as we will show later, we must have

$$\int_{\theta_0-\Delta\theta}^{\theta_0+\Delta\theta} d\theta \int_{x_0-\Delta x}^{x_0+\Delta x} dx \frac{d}{dt} G(\theta; x, t)\Big|_{(\tilde{x}(\theta,t),t)} + O(\Delta\theta) = \delta(t - t_0). \tag{4.26}$$

Taking the limit $(\Delta\theta, \Delta x) \to \mathbf{0}$, this readily implies Eq. (4.23).

Finally, we show that the solution Eq. (4.23) is consistent with the assumption that the integral of $B$ is of order $\Delta\theta$. Assuming that $n_0$ is smooth and that the dependence of $v^{\text{eff}}$ on $n$ is also smooth, we have

$$\begin{aligned}
&\int_{\theta_0-\Delta\theta}^{\theta_0+\Delta\theta} d\theta \int_{x_0-\Delta x}^{x_0+\Delta x} dx\, B \\
&\quad = 2\Delta\theta \int d\alpha \frac{\delta v^{\text{eff}}(\theta_0)}{\delta n(\alpha)} [n_0(x_0, t_0)] \partial_x n_0(\theta_0; x_0, t_0) \int_{x_0-\Delta x}^{x_0+\Delta x} dx\, G(\alpha, x, t) = O(\Delta\theta),
\end{aligned} \tag{4.27}$$

thus completing the proof of Eq. (4.23).

We close this subsection by commenting on the smoothness assumption of $n_0$ w.r.t. $x$ that we have used to show that the integral of $B$ is $O(\Delta\theta)$ and could thus be neglected. If $n_0(x)$ is not differentiable, then Eq. (4.23) is not the solution of Eq. (4.24); extra terms would appear in Eq. (4.23), depending on the specific nature of the discontinuity/singularity in $n_0$. However, if we start from a homogeneous state, such singularities can only appear if (i) the time-evolution is evaluated *strictly* at the Euler scale and (ii) there is a time when the perturbing potential is not smooth. However, (i) and (ii) are ultimately inconsistent with each other. In fact if (ii) applies, the gradient expansion that underlies a hydrodynamic treatment is ultimately unjustified. [This is for example clear from the derivation of Eq. (4.5) in Ref. [52], which requires higher spatial derivatives of $V_j(x)$ to be suppressed. While this is ensured by the Euler scaling limit if $V_j(x)$ is smooth, this assumption breaks down if $V_j(x)$ has discontinuities.] On the other hand, we are ultimately interested in determining the response to localized perturbations in order to define $\chi^{(N)}(\{x_j, t_y\})$. We can resolve this tension by *defining* $\chi^{(N)}(\{x_j, t_y\})$ as the response to smooth fields whose amplitude is localized around position $x_j$. This can be achieved e.g. by considering Gaussian perturbations of spatial width $\eta$ (see e.g. Eq. (4.42)). In this way, the Euler-scale treatment is justified, $n(x)$ will be a smooth function of spacetime, and Eq. (4.23) will hold. Finally, we can take the limit $\eta \to 0$ at the end of the calculation. This will ultimately amount to regulating the calculation by introducing a Gaussian

broadening of the propagator $D_\theta = \delta_\eta(x - v_\theta^{\text{eff}} t)$ with $\delta_\eta$ denoting a Gaussian of with $\eta$ , and then recovering Euler-scale results by taking the regulator to zero.

## 4.B The scattering vertex

In this section we will show show that adding the scattering vertex to the diagrammatic formulation properly accounts for the functional derivatives of the propagator, i.e. quantities of the form

$$\Gamma^{(p)} = \frac{\delta^p n(\alpha; x_p, t_p)}{\delta n(\theta_{p-1}; x_{p-1}, t_{p-1}) \cdots \delta n(\theta_0; x_0, t_0)} = \frac{\delta^p n(\alpha; x_p, t_p)}{\delta n_{p-1} \cdots \delta n_0}, \tag{4.28}$$

where we have introduced a shorthand notation $n_i = n(\theta_i; x_i, t_i)$. In particular, we claim that $\Gamma^{(p)}$ can be obtained by summing all diagrams containing propagator lines and a single scattering vertex only, under the condition that the number of incoming lines is $p$ and there is only one outgoing line (or equivalently that the diagram is connected).

To compute $\Gamma^{(2)}$ we take the functional derivative of Eq. (2.54) w.r.t. $n(x_0, t_0)$ and $n(x_1, t_1)$, with $V_j \equiv 0$ and evaluate it on top of a homogeneous background, obtaining

$$\left(\partial_t + v^{\text{eff}}(\alpha)\partial_x\right) \frac{\delta n(\alpha; y, \tau)}{\delta n_1 \delta n_0} = -\left( \int d\theta' \, \frac{\delta v^{\text{eff}}(\alpha)}{\delta n(\theta')} \frac{\delta n(\theta'; y, \tau)}{\delta n_1} \partial_y \frac{\delta n(\alpha; y, \tau)}{\delta n_0} + (0 \leftrightarrow 1) \right). \tag{4.29}$$

Note that, since we have now fixed $\boldsymbol{n}$ to be the uniforrm thermal background, we have dropped terms proportional to $\partial_x n$. On the RHS, we recognize the structure of a scattering vertex with two incoming legs, and the two $D$ propagators connected to it. The LHS of this equation consists of the required quantity $\Gamma^{(2)}$ acted upon by a linear partial differential operator [since $n$ is now fixed to be the thermal background] whose Green function is given by $D(\theta, \alpha, z_p, z_s)$ with $z_s = (y, \tau)$, corresponding to a $\delta n$-line exiting the scattering vertex. Inverting the PDO using its Green's function, we see that $\Gamma^{(2)}$ is indeed given by the sum of the two possible diagrams of the required form.

We will now proceed to prove the general statement by induction on $p$, with the (trivial) base case $\Gamma^{(1)} = D$. To prove the inductive step, we proceed in the same way as our computation of $\Gamma^{(2)}$ above. We begin with the GHD equation (2.54) and take

its the functional derivatives w.r.t. the set $\{n_0, \dots, n_{p-1}\}$

$$\partial_{t_p}\Gamma^{(n)}(\alpha; x_p, t_p) + \frac{\delta^n \left[v^{\text{eff}}(\alpha)\partial_x n(\alpha; x_p, t_p)\right]}{\delta n_{p-1}\cdots\delta p_0} = 0, \tag{4.30}$$

where we have left implicit the arguments $\{\theta_j, x_j, t_j\}$ of $\Gamma^{(p)}$. Upon evaluating the above equation on a static background $n$, this can be immediately recast as an equation for $\Gamma^{(p)}$

$$\begin{aligned}&\left(\partial_t + v^{\text{eff}}(\alpha)\partial_x\right)\Gamma^{(p)}(\alpha; x_p, t_p) = \\ &= -\sum_{I\in P}\frac{\delta^{(k)}v^{\text{eff}}(\alpha)}{\delta n(\bar\theta_1)\cdots\delta n(\bar\theta_k)}\frac{\delta^{\#I_1}n(\bar\theta_1; x_p, t_p)}{\prod_{j\in I_1}\delta n_j}\cdots\frac{\delta^{\#I_k}n(\bar\theta_k; x_p, t_p)}{\prod_{j\in I_k}\delta n_j}\partial_x\frac{\delta^{\#R_I}n(\alpha; x_p, t_p)}{\prod_{j\in R_I}\delta n_j}.\end{aligned} \tag{4.31}$$

In the above expression $P$ is a collection of sets $I = \{I_1, \cdots, I_k\}$ with the following properties: (i) each $I_j$ is a non-empty subset of $\{0, \cdots, p-1\}$, (ii) the $I_j$ are pairwise disjoint, (iii) $R_I = \{0, \cdots, p-1\}\backslash\bigcup_j I_j$ is a non-empty set. This reflects the fact that we are computing $\Gamma^{(p)}$ on top of a homogeneous state, i.e. $\partial_x n = 0$.

The solution of Eq. (4.31) can be found as for the $p = 2$ case above. The LHS is a partial differential operator with a known Green's function acting on the quantity of interest. Therefore, denoting the 'source' term on the RHS by $J(\alpha; y, \tau) = \sum_{I\in P} J_I(\alpha; y, \tau)$, we find that

$$\begin{aligned}\Gamma^p(\alpha; x_p, t_p) &= \int d\theta \int dy \int d\tau\, D(\alpha, \theta, z_p, (y, \tau))J(\alpha; y, \tau) = \\ &= \int d\theta \int dy \int d\tau\, D(\alpha, \theta, z_p, (y, \tau))\sum_I J_I(\alpha; x', t') = \sum_I \Gamma^p_I(\alpha; x_p, t_p).\end{aligned} \tag{4.32}$$

We recognize in Eq. (4.32) the structure of the scattering vertex reported in Table 4.1, situated in position $(y, \tau)$, and with $k$ legs entering the vertex from the left and one — corresponding to $R$ — from the right. Each of the incoming legs $\frac{\delta^{\#I_m}n(\bar\theta_m; y,\tau)}{\prod_{j\in I_m}\delta n_j} = \Gamma^{(\#I_m)}$. We then note that $\#I_m < n\ \forall m$ and $\#R_I < n$, so that the inductive hypothesis guarantees that $\forall m$ there is a set of diagrams $D_{I_k}$ whose sum gives $\Gamma^{(\#I_k)}$. Then, summing over the set of diagrams $D_{I_1}\times\cdots\times D_{I_k}\times D_{R_I}$ combined with the scattering vertex in $(y, \tau)$, we obtain $\Gamma^{(p)}_I$. Summing over $I \in P$, we then have that $\Gamma^{(n)}$ is given by a sum of connected diagrams composed of propagators and scattering vertices.

So far we have shown that $\Gamma^{(p)}$ is a sum of connected diagrams of propagators and scattering vertices. To complete the proof of our statement we need to show

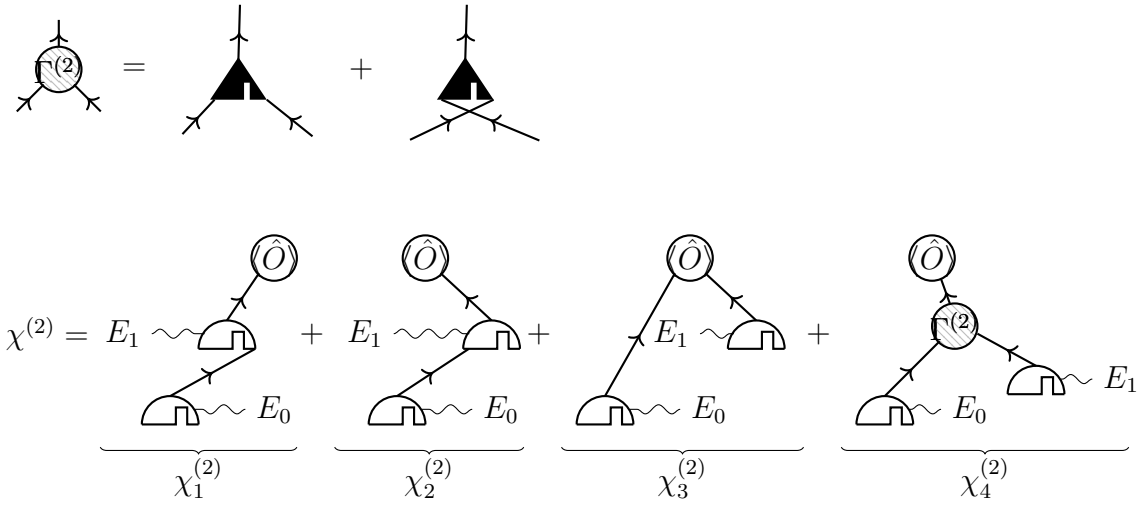


Figure 4.C.1: Diagrams contributing to $\Gamma^{(2)}$ and $\chi^{(2)}$.

that each diagram $D$ of this type contributes to $\Gamma^{(p)}$ with a prefactor 1. To do this, we start by identifying in $D$ the last scattering vertex time-wise (which coincides with the vertex from which the last line emerges). Defining $k+1$ to be the number of incoming legs, the diagram in question can only contribute to $\Gamma^{(p)}_I$ for $\#I = k$. To determine the specific partition $I$, we remove the last scattering vertex. Due to the tree-like structure of the diagram, this operation splits the diagram into $k+1$ disconnected pieces $D_j$ $(0 \leq j \leq k-1)$ - connected to the left side of the scattering vertex - and $D_R$ - connected to the right side. This automatically induces a partition $\tilde{I} = I \cup \{R\}$ on the legs associated to $\delta n_i$ $(0 < j < p-1)$, depending on the $D_j$ to which they belong. We claim that $D$ is a diagram contributing to $\Gamma^{(n)}_I$. In fact, by the inductive hypothesis, each $D_j$ (and $D_R$) will be a diagram contributing to $\frac{\delta^{\#I_j} n(\bar{\theta}_j;x',t')}{\prod_{i\in I_j}\delta n_i}$. Therefore, putting back the last scattering vertex, we recognize that $D$ is a term contributing to $\Gamma^{(p)}_I$. Finally, note that the choices of $I$ and $R$ were forced by the structure of the diagram, so that the same diagram could not contribute to a $\Gamma_{I'}$ with $I' \neq I$. Thus the prefactor of $D$ is just given by the products of the prefactors of $D_j$ and $D_R$, which are 1 by the inductive hypothesis, thus completing the proof of our statement.

## 4.C Explicit expressions for the diagrams contributing to $\chi^{(2)}$

The four diagrams reported in Fig. 4.C.1, respectively give the following explicit expressions contributing to $\chi^{(2)}_{\hat{O}}(x_0, 0; x_1, \tau_0; x_2, \tau_1 + \tau_0)$. Before reporting their full expression we exemplify how we can use the evaluation scheme described in Sec. 4.3 to write the expression corresponding to a given diagram.

$\chi^{(2)}_1$ We start from the measurement node, which gives us a factor $\frac{\delta\langle\hat{O}\rangle}{\delta n(\theta)}$. The uppermost element in the remaining diagram is a propagator $D_\theta(x_2 - x_1, \tau_1)$. Removing the propagator, we find a field node without any leg entering from the left, which yields $a^{\text{eff}}(\theta)$. Next, according to the rules previously outlined, we need to multiply the result thus far with the derivative w.r.t. $\theta$ of the subdiagram that enters the marked leg of the field node. Proceeding similarly to before, we thus find $\partial_\theta \left( D_\theta(x_1 - x_0, \tau_0) a^{\text{eff}}(\theta) \partial_\theta n \right)$. Putting everything together we obtain

$$\chi^{(2)}_1 = \int d\theta \left[ \frac{\delta\langle\hat{O}\rangle}{\delta n(\theta)} \right] \delta\left(x_2 - x_1 - v^{\text{eff}}(\theta)\tau_1\right) a^{\text{eff}}(\theta) \times \partial_\theta \left\{ \delta\left(x_1 - x_0 - v^{\text{eff}}(\theta)\tau_0\right) a^{\text{eff}}(\theta) \partial_\theta n, \right\} \quad (4.33)$$

$\chi^{(2)}_2$ The evaluation of $\chi^{(2)}_2$ proceeds similarly to that of $\chi^{(2)}_1$, up to the uppermost field node (excluded). This first part yields $\frac{\delta\langle\hat{O}\rangle}{\delta n(\theta_2)} D_{\theta_2}(x_2 - x_1, \tau_1)$. The field node now has one leg connected to the left side, corresponding to a factor $\frac{\delta a^{\text{eff}}(\theta_2)}{\delta n(\theta_1)} \partial_{\theta_2} n(\theta_2)$ — note that the rapidity of legs entering a node from the left and the outgoing rapidity from that node need to be labelled by distinct variables. This has to be multiplied by the subdiagram connected to the incoming leg, which, as before, gives us $D_{\theta_1}(x_1 - x_0, \tau_0) a^{\text{eff}}(\theta_1) \partial_{\theta_1} n(\theta_1)$. Multiplying everything gives

$$\chi^{(2)}_2 = \int d\theta_1 \left[ a^{\text{eff}}(\theta_1) \partial_\theta n(\theta_1) \right] \delta\left(x_1 - x_0 - v^{\text{eff}}(\theta_1)\tau_0\right) \times \times \int d\theta_2 \left[ \frac{\delta a^{\text{eff}}(\theta_2)}{\delta n(\theta_1)} \partial_\theta n(\theta_2) \right] \left[ \frac{\delta\langle\hat{O}\rangle}{\delta n(\theta_2)} \right] \delta\left(x_2 - x_1 - v^{\text{eff}}(\theta_2)\tau_1\right), \quad (4.34)$$

$\chi^{(2)}_3$ The measurement vertex now has two incoming legs, whose rapidity we can label by $\theta_1$ and $\theta_2$. This vertex then gives $\frac{\delta^2\langle\hat{O}\rangle}{\delta n(\theta_1)\delta n(\theta_2)}$. This has to be multiplied by the two disconnected diagrams obtained by removing the measurement vertex.

These are $D_{\theta_2}(x_2-x_1,\tau_1)a^{\text{eff}}(\theta_2)\partial_{\theta_2}n(\theta_2)$ and $D_{\theta_1}(x_2-x_0,\tau_1+\tau_0)a^{\text{eff}}(\theta_1)\partial_{\theta_1}n(\theta_1)$. Explicitly, this yields

$$\chi_3^{(2)} = \int d\theta_1 \int d\theta_2 \left[a^{\text{eff}}(\theta_1)\partial_\theta n(\theta_1)\right]\left[a^{\text{eff}}(\theta_2)\partial_\theta n(\theta_2)\right]\left[\frac{\delta^2\langle\hat{O}\rangle}{\delta n(\theta_1)\delta n(\theta_2)}\right] \times \delta\left(x_2 - x_1 - v^{\text{eff}}(\theta_2)\tau_1\right)\delta\left[x_2 - x_0 - v^{\text{eff}}(\theta_1)(\tau_1+\tau_0)\right], \quad (4.35)$$

$\chi_4^{(2)}$ There are two diagrams corresponding to $\chi_4^{(2)}$, which can be obtained by replacing the graphical representation of $\chi_4^{(2)}$ in Fig. 4.C.1 with the two terms corresponding with $\Gamma^{(2)}$ in Fig. 4.C.1. For concreteness we focus on the first one here and report the complete expression for the sum later. We call the space-time location of the scattering vertex $(y, s+\tau_0)$. The measurement vertex gives as usual $\frac{\delta\langle\hat{O}\rangle}{\delta n(\theta_2)}$. The remaining diagram terminates with a propagator - associated to $D_{\theta_2}(x_2-y,\tau_1-s)$. The topmost object is then the scattering vertex. This corresponds to $\frac{\delta v^{\text{eff}}(\theta_2)}{\delta n(\theta_1)}$. Removing the scattering vertex splits the diagram in two connected sub-diagrams. For the specific diagram we are considering, the left-most one gives $D_{\theta_1}(y-x_0,s+\tau_0)a^{\text{eff}}(\theta_1)\partial_{\theta_1}n(\theta_1)$. The rightmost part can be evaluated similarly, however we must remember to take its derivative w.r.t. $y$, since it enters the marked/rightmost leg of the scattering vertex: $\partial_y D_{\theta_2}(y-x_1,s)a^{\text{eff}}(\theta_2)\partial_{\theta_2}n(\theta_1)$. Summing with the other diagram in $\chi_4^{(2)}$ then gives

$$\begin{aligned}\chi_4^{(2)} = &-\int d\theta_1 \int d\theta_2 \int dy \int_0^{\tau_1} ds \\ &\times \left[a^{\text{eff}}(\theta_1)\partial_\theta n(\theta_1)\right]\left[a^{\text{eff}}(\theta_2)\partial_\theta n(\theta_2)\right]\left[\frac{\delta v^{\text{eff}}(\theta_2)}{\delta n(\theta_1)}\right]\left[\frac{\delta\langle\hat{O}\rangle}{\delta n(\theta_2)}\right]\times \\ &\times \delta\left(y - x_0 - v^{\text{eff}}(\theta_1)(s+\tau_0)\right)\delta'\left(y - x_1 - v^{\text{eff}}(\theta_2)s\right) \\ &\times \delta\left(x_2 - y - v^{\text{eff}}(\theta_2)(\tau_1 - s)\right) \\ &-\int d\theta_1 \int d\theta_2 \int dy \int_0^{\tau_1} ds \\ &\times \left[a^{\text{eff}}(\theta_1)\partial_\theta n(\theta_1)\right]\left[a^{\text{eff}}(\theta_2)\partial_\theta n(\theta_2)\right]\left[\frac{\delta v^{\text{eff}}(\theta_1)}{\delta n(\theta_2)}\right]\left[\frac{\delta\langle\hat{O}\rangle}{\delta n(\theta_1)}\right] \\ &\times \delta\left(y - x_1 - v^{\text{eff}}(\theta_2)s\right)\delta'\left(y - x_0 - v^{\text{eff}}(\theta_1)(s+\tau_0)\right) \\ &\times \delta\left(x_2 - y - v^{\text{eff}}(\theta_1)(\tau_1 - s)\right). \end{aligned} \quad (4.36)$$

The functional derivatives reported above can be readily computed using the iden-

tity

$$\frac{\delta f^{\rm dr}(\theta)}{\delta n(\theta_1)} = K^{\rm dr}(\theta,\theta_1) f^{\rm dr}(\theta_1), \tag{4.37}$$

where $f$ is an arbitrary function of $\theta$. The field and scattering vertices can be computed b combining this identity with the definitions

$$a^{\rm eff} = \frac{q_0^{\rm dr}}{(\partial_\theta k)^{\rm dr}} \tag{4.38}$$

$$v^{\rm eff} = \frac{(\partial_\theta e)^{\rm dr}}{(\partial_\theta k)^{\rm dr}}. \tag{4.39}$$

Finally, the expression for the measurement vertex can be found in the case where $\hat{O}$ is a charge or current density, in which case the vertex with one incoming line is given by [51, 96]

$$\frac{\delta\langle\hat{q}_i\rangle}{\delta n(\theta_1)} = \frac{1}{2\pi}\left(k'\right)^{\rm dr}(\theta_1) q_i^{\rm dr}(\theta_1), \tag{4.40}$$

$$\frac{\delta\langle\hat{j}_i\rangle}{\delta n(\theta_1)} = \frac{1}{2\pi}\left(e'\right)^{\rm dr}(\theta_1) q_i^{\rm dr}(\theta_1). \tag{4.41}$$

From these, measurement vertices with more incoming lines can be derived using Eq. (4.37).

Fig. 4.2 has been obtained by numerically evaluating the expressions above and regularizing the Dirac-$\delta$ function as

$$\delta(x) \mapsto \delta_\eta(x) = \frac{1}{\sqrt{2\pi}\eta}\exp\left(-\frac{x^2}{2\eta^2}\right). \tag{4.42}$$

For $\chi_4^{(2)}$ the integrals over $s$ and $y$ were first analytically evaluated through Mathematica and the simplified analytical expression was used to speed up the numerical computation.

## 4.D Finite-field scaling in the XXX model

In this section we study the finite-field behavior of the XXX chain and obtain the scaling form reported in Eq. (4.17).

### 4.D.1 Infinite-temperature expansion of the TBA equations

Before proceeding to study the GHD equations, we summarise here the results from Ref. [98]. Recall that the excitations of interest are quasiparticle "strings", which are bound states of $s$ elementary magnons. Throughout, we will assume that the length of the string $s$ is much smaller than $1/\mu = 1/(\beta h)$.

The occupation factors can be expanded in the $\beta \to \infty$ limit as

$$n_s = n_s^{(0)} + \beta n_s^{(1)} + O(\beta^2) \tag{4.43}$$

where

$$n_0 \sim 1/s^2 \tag{4.44}$$

asymptotically at large $s$. To obtain a response we need to have some rapidity-dependence in $n$, so we must consider at least $n^{(1)}$. Expanding the Yang-Yang equation, one can see that

$$n^{(1)} = -n^{(0)} \left(1 - n^{(0)}\right) e^{\mathrm{dr}}. \tag{4.45}$$

This can be combined with the results

$$e^{\mathrm{dr}} = (k')^{\mathrm{dr}} = \frac{s+1}{2}\left(\frac{K_s}{s} - \frac{K_{s+1}}{s+2}\right) \tag{4.46}$$

$$m^{\mathrm{dr}} \sim \frac{1}{3}\mu s^2, \tag{4.47}$$

with

$$K_s(\theta) = \frac{s}{2\pi}\frac{1}{\theta^2 + \frac{s^2}{4}} \tag{4.48}$$

Finally, recall that at infinite temperature $\partial_\theta$ and dressing commute.

### 4.D.2 Solution of the GHD equation

The equation we set out to solve is the inhomogeneous GHD equation (2), restricted to the case where $E$ and $n$ are uniform. Then, we have (see also Ref. [10])

$$\partial_t n_s - E a_s^{\mathrm{eff}} \partial_\theta n_s = 0. \tag{4.49}$$

This equation can be solved through the method of characteristics (see e.g. Ref. [10]). Introducing the vector potential

$$\varphi = -\int dt\, E(t), \tag{4.50}$$

and using $\varphi$ to parametrize time we have

$$n_s(\theta,\varphi) = n_s(\theta_B(\varphi,\theta,s),0), \tag{4.51}$$

along the trajectory defined by

$$\frac{d\theta_B}{d\varphi} = -a_s^{\text{eff}}, \tag{4.52}$$

$$\theta_B(0,\theta,s) = \theta. \tag{4.53}$$

Finally the $\varphi$-dependence of $\langle\hat{j}_0\rangle$ is given by

$$\langle\hat{j}_0\rangle = \sum_s j_s = \sum_s m_s^{\text{dr}} \int \frac{d\theta}{2\pi} n_s^{(1)}(\theta_B(\varphi,\theta))(e')_s^{\text{dr}}(\theta). \tag{4.54}$$

We now proceed to show that at large $s$, but $\mu s \ll 1$, the expectation value of the current obeys the following asymptotic relation

$$j_s(\varphi) \sim \mu s^{-4} f(\mu s^3 \varphi), \tag{4.55}$$

for some function $f$. We consider the set of equations (4.52), (4.53), and (4.54), and perform the rescaling

$$\lambda = \theta s^{-1}, \tag{4.56}$$

$$\lambda_B = \theta_B s^{-1}, \tag{4.57}$$

$$\phi = \mu\varphi s^3. \tag{4.58}$$

Plugging this into (4.52), we have

$$\frac{d\lambda_B}{d\phi} = \frac{m_s^{\text{dr}}}{\mu s^2} \frac{1}{s^2 (k')_s^{\text{dr}}(s\lambda_B)}. \tag{4.59}$$

It is now easy to check that both ratios on the RHS of this equation tend to a well defined limit for large $s$ (while holding $\lambda_B = \mathcal{O}(1)$ fixed). Thus we see that $\lambda_B(\phi)$ will be $s$-independent.

We can now apply the same rescaling to Eq. (4.54), where we get

$$j_s(\phi) = -\underbrace{\beta n_s^{(0)}\left(1-n_s^{(0)}\right) m_s^{\text{dr}}}_{=\mu\mathcal{O}(1)} \int \frac{s d\lambda}{2\pi} \underbrace{e_s^{\text{dr}}(s, s\lambda_B(\phi))}_{s^{-2}\mathcal{O}(1)} \underbrace{(e')^{\text{dr}}(s,s\lambda)}_{s^{-3}\mathcal{O}(1)}, \tag{4.60}$$

Regrouping all the $s$-dependencies and denoting the remaining $\mathcal{O}(1)$ function by $G$, we have

$$j_s(\varphi) \sim \mu s^{-4} \int d\lambda G(\lambda, \varphi) \sim \mu s^{-4} f\left(\mu s^3 \varphi\right), \tag{4.61}$$

for some function $f$. Finally, note that $f$ must be odd and periodic with some period $\zeta$. The first observation follows from parity, under which both $\phi$ and $\hat{j}$ are odd. The periodicity, instead follows from the following result. For any $s$ there is a value of $\phi$ for which $\theta_B(\phi, \theta, s) = \theta \, \forall \theta$, thus $j_s(\phi)$ must be periodic, and consequently so must $f$.

To show this last statement, we note that Eq. (4.52) is separable. Denoting the primitive of $(k')_s^{\mathrm{dr}}$ by $I_s(\theta)$, we have

$$I_s(\theta_B(\varphi, \theta, s)) = -\varphi m_s^{\mathrm{dr}} + I_s(\theta), \tag{4.62}$$

until the time $\theta_B$ reaches $+\infty$. At that point, recalling the periodic boundary condition in rapidity space (see e.g. Ref. [10]), we can imagine that $\theta_B$ is transported to $-\infty$. Thereafter the evolution is described by

$$I_s(\theta_B(\varphi, \theta, s)) = -\varphi m_s^{\mathrm{dr}} + I_s(\theta) + \left(I_s(+\infty) - I_s(-\infty)\right). \tag{4.63}$$

From this last equation we can immediately notice that for

$$\varphi = \frac{I_s(+\infty) - I_s(-\infty)}{m_s^{\mathrm{dr}}}, \tag{4.64}$$

$\theta_B(\phi, \theta, s) = \theta \, \forall \theta$, as claimed.

# Chapter 5

# Long-time divergences of nonlinear response and quasiparticle scattering

While in the previous chapter we discussed nonlinear transport in integrable models starting from generic stationary states, here we are interested in understanding nonlinear response functions for more general operators that can also create and annihilate quasiparticles.

To simplify the problem, we focus on a simple model: the transverse field Ising model

$$\hat{H} = -J \sum_{j=0}^{L-1} \left( \hat{\sigma}_j^z \hat{\sigma}_{j+1}^z + h \hat{\sigma}_j^x \right) \tag{5.1}$$

and restrict ourselves to zero-temperature states. We would like to consider perturbations that can create or annihilate a single quasiparticle. While there are no such local operators in the ferromagnetic phase, in the paramagnetic phase of the model, i.e. when $h > 1$, the $z$ component of the spin can create or annihilate odd numbers of quasiparticles.

We will then consider momentum-resolved perturbations

$$\hat{A}(q) = \sum_j e^{iqj} \hat{\sigma}_j^z \tag{5.2}$$

and study zero-temperature connected four-point functions [1] time-ordered on the

[1] Only even-order correlators are non-zero for $\hat{\sigma}^z$, since it can create or annihilate only an odd number of QP. Equivalently, one can see that odd-order correlators vanish because $\hat{\sigma}^z$ is odd under $\mathbb{Z}_2$ symmetry

Keldysh contour

$$C_4(\boldsymbol{q};\boldsymbol{t}) = \frac{1}{L}\left\langle \Omega \,\middle|\, \hat{A}(q_4,t_4)\hat{A}(q_3,t_3)\hat{A}(q_2,t_2)\hat{A}(q_1,t_1) \,\middle|\, \Omega \right\rangle_C \tag{5.3}$$

where $|\Omega\rangle$ is the ground state of the system. Note that momentum conservation constrains $\sum_j q_j = 0$. Our main result will be to show that in the long-time limit $C_4$ diverges and, more precisely, $C_4(\boldsymbol{q};\lambda\boldsymbol{t}) \propto \lambda$, i.e. it diverges proportionally to the overall timescale if the momenta are pairwise equal and opposite (i.e. either $q_1 = -q_3$ and $q_2 = -q_4$, or $q_1 = -q_4$ and $q_2 = -q_3$). Furthermore, we will show that this divergence can be interpreted through a simple semiclassical picture inspired by Ref. [171].

Our interest in $C_4$ stems from its relation to third-order response functions of the form

$$\chi^{(3)} = \frac{i}{L}\left\langle \Omega \,\middle|\, \left[\left[\left[\hat{A}(q_4',t_4'),\hat{A}(q_3',t_3')\right],\hat{A}(q_2',t_2')\right],\hat{A}(q_1',t_1')\right] \,\middle|\, \Omega \right\rangle \tag{5.4}$$

with $t_4' > t_3' > t_2' > t_1'$. Indeed, by expanding the commutators above we can immediately obtain

$$\chi^{(3)} = -\Im\left[C_4(t_1',t_2',t_3',t_4') - C_4(t_2',t_3',t_4',t_1') - C_4(t_1',t_3',t_4',t_2') + C_4(t_3',t_4',t_2',t_1')\right], \tag{5.5}$$

where, to simplify the notation we did not indicate the momentum arguments of $C_4$, which are permuted in the same fashion of the time argument. Note that only the connected component of the correlation function contribute to $\chi^{(3)}$ as disconnected components would cancel from the sum. Our result on the long-time divergence of $C_4$ immediately translates into a long-time divergence of $\chi^{(3)}$, since, as it will be easy to verify, the divergences in the four term in Eq. (5.5) do not cancel among each other.

The rest of the chapter is structured as follows. In Sec. 5.1 we introduce the model and explain the technique that we will use for the calculations. In Sec. 5.2 we give the main results and explain how they can interpreted using a semiclassical picture. Finally, the main aspects of the calculation are reported in the sections from 5.3 to 5.5.

## 5.1 The Ising model

Since we expect the boundary conditions not to alter the results in the thermodynamic limit, we choose periodic boundary conditions for the spin problem, i.e. $\hat{\sigma}_0^\alpha = \hat{\sigma}_L^\alpha$ for

$\alpha = x, y, z$. The Hamiltonian (5.1) can be diagonalized through a Jordan-Wigner transformation (see e.g. Appendix B of Ref. [27] or Ref. [143]), which maps the spin operators to fermionic operators $\hat{c}_j$, in terms of which

$$\hat{\sigma}_j^x = 1 - 2\hat{c}_j^\dagger \hat{c}_j \tag{5.6}$$

$$\hat{\sigma}_j^z = \left( \prod_{j=0}^{j-1} 1 - 2\hat{c}_l^\dagger \hat{c}_l \right) \left( \hat{c}_j^\dagger + \hat{c}_j \right). \tag{5.7}$$

When expressed in terms of the fermionic operators, the Hamiltonian becomes quadratic and can be readily diagonalized by going to Fourier space.

Before that, however, we note that the Hamiltonian conserves the parity of fermions $\hat{P} = \exp(i\pi \sum_j \hat{c}_j^\dagger \hat{c}_j)$, therefore the Hilbert space of the model splits into two independent sectors: the sector with an odd number of fermions, usually called the Ramond (R) sector, and the one with an even number of fermions, often called the Neveu-Schwarz (NS) sector. The periodic boundary conditions for the spin translates into different boundary conditions for the fermion problem depending on the fermion parity. In the Ramond sector, the fermion have periodic boundary conditions, i.e. the possible momenta are taken from the set

$$\mathrm{R} = \frac{2\pi}{L}\{0, \ldots, L-1\}, \tag{5.8}$$

instead, in the Neveu-Schwarz the fermion have anti-periodic boundary conditions and the set of momenta is

$$\mathrm{NS} = \frac{2\pi}{L}\left( \{0, \ldots, L-1\} + \frac{1}{2} \right). \tag{5.9}$$

Finally, once in Fourier space, the Hamiltonian can be finally diagonalized in terms of a Bogoliubov transformation (see e.g. Appendix B of Ref. [27]). The eigenstates can then be labeled by their QP number and their momenta. For odd number of QPs, the state lies in the Ramond sector

$$|k_1, \ldots, k_{2m+1}\rangle_{\mathrm{R}}\,,\ k_j \in \mathrm{R}. \tag{5.10}$$

Conversely, for even number of QPs, the state lies in the Neveu-Schwartz sector

$$|p_1, \ldots, p_{2n}\rangle_{\mathrm{NS}}\,,\ p_j \in \mathrm{NS}. \tag{5.11}$$

In both cases the energy of the state is simply given by the sum of the one-QP energies

$$\epsilon(k) = 2J\sqrt{1 + h^2 - 2h\cos(k)}. \tag{5.12}$$

Note that, in spite of the free-fermion nature of the model, the computation of $C_4$ cannot be easily tackled using free-fermion techniques (e.g. Wick theorem). In fact, note that the $\hat{A}$ operator maps to a highly nonlocal object in the fermionic basis. [2] Our approach is then to use a form-factor expansion, i.e. to expand the four-point function $\tilde{C}_4$ (including disconnected parts) in terms of eigenstates of $\hat{H}$

$$\tilde{C}_4 = \sum_{n^a\, n^b\, n^c} \tilde{C}_4^{n^a,n^b,n^c} \tag{5.13}$$

$$\tilde{C}_4^{n^a,n^b,n^c} = \sum_{\boldsymbol{k^a},\boldsymbol{p^b},\boldsymbol{k^c}} \text{Ff Kin Mom} \tag{5.14}$$

*with*Ff, Kin, and Mom encoding for the form-factor amplitude, the kinematics of the time-evolution, and the momentum conservation condition respectively.

$$\text{Ff} = \frac{1}{n^a! n^b! n^c!} \langle\Omega|\hat{\sigma}_0^z|\boldsymbol{k^c}\rangle_{\text{R}} \langle\boldsymbol{k^c}|\hat{\sigma}_0^z|\boldsymbol{p^b}\rangle_{\text{NS}} \langle\boldsymbol{p^b}|\hat{\sigma}_0^z|\boldsymbol{k^a}\rangle_{\text{R}} \langle\boldsymbol{k^a}|\hat{\sigma}_0^z|\Omega\rangle \tag{5.15}$$

$$\text{Kin} = \exp\left[-it_{21}\sum_j \epsilon(k_j^a) - it_{32}\sum_j \epsilon(p_j^b) - it_{43}\sum_j \epsilon(k_j^c)\right] \tag{5.16}$$

$$\text{Mom} = L^3 \delta_{q_1,\sum_j k_j^a} \delta_{q_1+q_2,\sum_j p_j^b} \delta_{-q_4,\sum_j k_j^c} \tag{5.17}$$

Here $n^a$, $n^b$, and $n^c$ denote the number of QPs in the intermediate states. More explicitly, $\boldsymbol{k^a}$ and $\boldsymbol{k^c}$ are vectors of respectively $n^a$ and $n^c$ momenta, each of which is in R; similarly $\boldsymbol{p^b}$ is a vector of $n^b$ momenta, each of which is in NS. We have also introduced a shorthand for time differences $t_{ij} = t_i - t_j$.

Note that the operator $\hat{\sigma}_0^z$ changes the fermion parity and couples the R only to the

[2] This is unlike the case of four-point functions of the $\hat{\sigma}^x$, which was presented in Ref. [187].

NS sector and vice versa. Finally the form factors of $\hat{\sigma}_0^z$ are given by [23, 24, 186, 100]

$$
\begin{aligned}
{}_{NS}\langle p_1,\dots,p_{2n}|\sigma^z|k_1,\dots,k_{2m+1}\rangle_R &= i^{n+m}(4J^2h)^{(2m+1-2n)^2/4}|1-h^2|^{1/8} \\
&\times \prod_{j=1}^{2n}\left(\frac{1}{L\epsilon(p_j)}\right)^{1/2}\prod_{l=1}^{2m+1}\left(\frac{1}{L\epsilon(k_l)}\right)^{1/2} \\
&\times \prod_{j<j'}^{2n}\frac{2\sin\frac{p_j-p_{j'}}{2}}{\epsilon(p_j)+\epsilon(p_{j'})}\prod_{l<l'}^{2m+1}\frac{2\sin\frac{k_l-k_{l'}}{2}}{\epsilon(k_l)+\epsilon(k_{l'})}\prod_{j=1}^{2n}\prod_{l=1}^{2m+1}\frac{\epsilon(p_j)+\epsilon(k_l)}{2\sin\frac{p_j-k_l}{2}}
\end{aligned}
\tag{5.18}
$$

up to exponentially small correction in the number of sites $L$. For future convenience we will also introduce a special notation to denote form factors between the ground state $|\Omega\rangle$ and a state in the Ramond sector

$$
F(\boldsymbol{k}) = \langle\Omega|\hat{\sigma}_0^z|k_1,\dots,k_n\rangle_{\mathrm{R}}\,. \tag{5.19}
$$

The same approach was previously used to compute three and four-point functions in integrable Quantum Field Theories (QFTs) in Refs. [3, 4], including the Ising QFT, which can be obtained as the continuum limit of the transverse-field Ising model. However, Refs. [3, 4] computed only the first contribution ($\tilde{C}_4^{1,2,1}$) and furthermore restricted themselves to the case where all momenta $q_j$ are zeros. Under the combination of these two restrictions the long-time divergence porportional to the overall timescale is not apparent and the results of the authors can be shown to lead a weaker long-time divergence proportional to the square root of the overall timescale.

Our approach differs in that we will not restrict ourselves a priori to states with a given particle number, but rather focus on the long-time limit, use a power-counting argument to identify which terms can yield long-time divergences, and finally we will try to evaluate their leading behavior in the long-time limit. Of crucial importance to our analysis will be the annihilation-pole structure of the form factors: for $k_i - p_j \to 0$ [3]

$$
{}_{NS}\langle p_1,\dots,p_{2n}|\sigma_0^z|k_1,\dots,k_{2m+1}\rangle_R \propto \frac{1}{k_i-p_j}. \tag{5.20}
$$

This will allows us to identify singular contributions, which will in turn dominate the long-time behavior.

Before proceeding, however, we summarize our results and explain how they can be understood from a simple semiclassical picture.

[3] Note that since $p_j \in$ NS and $k_i \in$ R, the form factor is finite for any finite $L$, as expected.

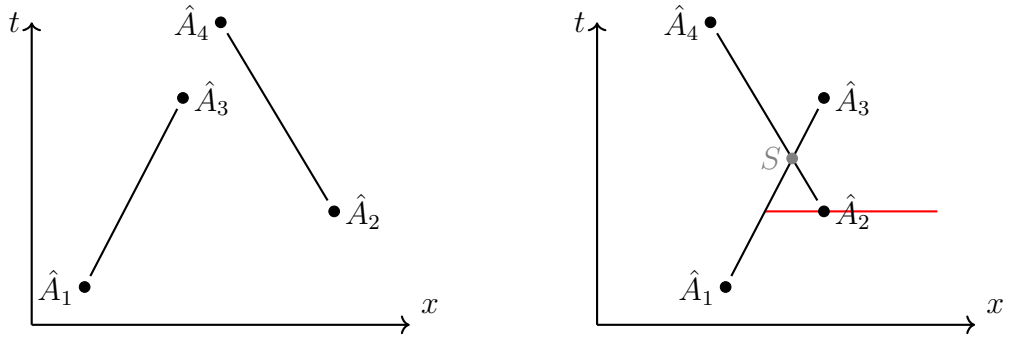


Figure 5.1: Cartoon of the type of processes which give rise to the leading contribution to $C_4$ in the case of distinct times and $q_4 = -q_2$ and $q_3 = -q_1$. In the figure $\hat{A}_j$ denotes the operator $\hat{A}(q_j, t_j)$, whose effect is to either create or annihilate a QP at the space-time coordinates $(x_j, t_j)$. For simplicity, the cartoon is drawn for $t_1 < t_2 < t_3 < t_4$, altough this assumption is not necessary for the result to apply. The QP trajectories are denoted by black straight lines, corresponding to the ballistic motion of the QP. (leftmost panel) If the trajectories of the two QPs do not cross, the amplitude of the process factorizes into a product of two two-point functions. (rightmost panel) If the trajectories cross, the amplitude of the process acquires an extra phase $S = -1$ and does not cancel once the disconnected contribution are subtracted. A red line denotes the possible positions of $x_2$ for which scattering would take place. The length of the red segment is $|v(q_1) - v(q_2)||t_{32}|$.

## 5.2 Summary of results

### 5.2.1 Distinct times

We will consider two different cases, depending on how the long-time limit is taken. Here, we start by studying the case where all $t_j$ are distinct, the times are then rescaled by a factor $\lambda$, and then the limit $\lambda \to \infty$ is taken, so that all time differences become large.

As we mentioned above, long-time divergences arise when $q_4 = -q_2$ and $q_3 = -q_1$, or $q_3 = -q_2$ and $q_4 = -q_1$. In the first case we will have that

$$C_4(q_1, q_2, -q_1, -q_2; \boldsymbol{t}) = -2|F(q_1)|^2|F(q_2)|^2 e^{-i\epsilon(q_1)t_{31}} e^{-i\epsilon(q_2)t_{42}} |v(q_1) - v(q_2)||t_{32}| + O\left(\|\boldsymbol{t}\|^0\right). \tag{5.21}$$

[Equivalently, upon rescaling all times by $\lambda$, the first term will be proportional to $\lambda$ and the corrections are $O(\lambda^0)$.] In the second case, a similar result holds

$$C_4(q_1, q_2, -q_2, -q_1; \boldsymbol{t}) = -2|F(q_1)|^2|F(q_2)|^2 e^{-i\epsilon(q_1)t_{41}} e^{-i\epsilon(q_2)t_{32}} |v(q_1) - v(q_2)||t_{32}| + O\left(\|\boldsymbol{t}\|^0\right). \tag{5.22}$$

The results above have a clear semiclassical interpretation, where we assume that quasiparticles have well-defined position and momentum. To explain the semiclassical picture we focus on the first case $C_4(q_1, q_2, -q_1, -q_2; \boldsymbol{t})$. The operator $\hat{A}(q_1, t_1)$ can create a QP with momentum $q_1$ at an arbitrary position $x_1$, which we will need to integrate upon. This QP travel ballistically with velocity $v(q_1)$ until it gets annihilated in position $x_3 = x_1 + t_{31}v(q_1)$ by $\hat{A}(-q_1, t_3)$. Similarly, the operator $\hat{A}(q_2, t_2)$ can create a QP with momentum $q_2$ in an arbitrary position $x_2$. This QP would then travel ballistically, until it get annihilated by $\hat{A}(-q_2, t_4)$ in position $x_4 = x_2 + v(q_1)t_{42}$. If the trajectories of the two QPs always remain well separated from each other, as in Fig. 5.1(leftmost panel) then the amplitude of the whole process can be written as $|F(q_1)|^2|F(q_2)|^2 e^{-i\epsilon(q_1)t_{31}} e^{-i\epsilon(q_2)t_{42}}$. Note that the amplitude factorizes into the product two two-point functions $\langle \hat{A}(-q_1, t_1)\hat{A}(q_1, t_1)\rangle \langle \hat{A}(-q_2, t_4)\hat{A}(q_2, t_2)\rangle$, therefore this contribution must be subtracted.

The discussion above needs to be modified slightly if the two QPs' trajectories cross (Fig. 5.1(rightmost panel)). In this case the amplitude of the process get multiplied by the scattering matrix $S$ — which in the Ising model simply encodes for the fermionic nature of the QPs, and therefore $S = -1$. Once the disconnected components are subtracted we would have a contribution of $(S-1)|F(q_1)|^2|F(q_2)|^2 e^{-i\epsilon(q_1)t_{31}} e^{-i\epsilon(q_2)t_{42}}$ for each position $x_1$ and $x_2$ such that the two QPs' trajectories cross. Finally, we need to integrate over all positions $x_1$ and $x_2$ that give rise to a scattering process. Once $x_1$ is fixed, in order for the scattering process to take place, $x_2$ can be within a segment of length $|v(q_1) - v(q_2)||t_{32}|$. Multiplying the amplitude above by the length of this segment, we can recover the result in Eq. (5.21).

Finally, we comment on the stability of the long-time divergence to perturbations of the momenta. For example, in the first case, even if the conditions $\{q_4 = -q_2, q_3 = -q_1\}$ are not perfectly satisfied, then we will show that the result in Eq. (5.21) still hold up to a cutoff timescale $t_{cut}$ given by

$$t_{cut} \sim [(\delta q)|v(q_1) - v(q_2)||t_{32}|]^{-1} \tag{5.23}$$

where $\delta q = q_4 + q_2$, which by momentum conservation is also equal to $\delta q = q_3 + q_1$. The same discussion applies also in the second case if the conditions $\{q_4 = -q_2, q_3 = -q_1\}$ are not exactly satisfied. In this case, $\delta q = q_4 + q_1 = q_3 + q_2$.

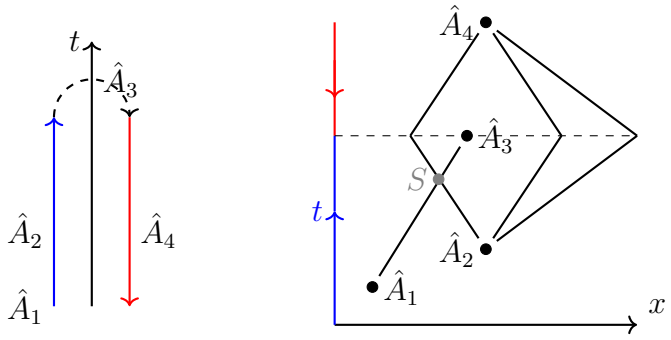


Figure 5.2: (Left cartoon) $C_{NR}$ is a correlator where the state is evolved forward in time from $t_1 = 0$ to $t_3 = \tau_1 + \tau_2$, to finally be evolved backward to time $t_4 = \tau_1$ again. (Right cartoon) Types of processes giving rise to the leading contribution in the $\tau_1, \tau_2 \to \infty$ limit (see also caption of Fig. 5.1). The time axis is divided into two parts: a blue part where time runs forward, and a red part where, time runs backward. For graphical convenience the two parts are divided by a dashed line, corresponding to the time $\tau_1 + \tau_2$. Here the second operator $\hat{A}_2$ can create a shower of $m$ QPs ($m = 3$ in the figure), which spread ballistically up to time $\tau_1 + \tau_2$ and can scatter against the QP exchanged between $\hat{A}_1$ and $\hat{A}_3$. When the QPs encounter the dashed line, they are evolved backward, i.e. the slope of their trajectory is reflected w.r.t. the $y$-axis of the figure. Therefore, the $m$ QPs refocus at the same position and can be annihilated by $\hat{A}_4$.

### 5.2.2 Two equal times

While the distinct-times case above is quite simple, it is also less relevant for some experiments. In fact, common setups to measure nonlinear response can only measure $\chi^{(3)}$ when two times are close. For example, pump-probe spectroscopy (see e.g. Ref. [92]) can approximately measure only $\chi^{(3)}(0, 0, \tau_1, \tau_1 + \tau_2)$, i.e. the response function where the first two times coincide. Similarly, Two-Dimensional Coherent Spectroscopy can approximately measure $\chi^{(3)}(0, 0, \tau_1, \tau_1 + \tau_2)$ and $\chi^{(3)}(0, \tau_1, \tau_1, \tau_1 + \tau_2)$. Therefore, we also consider a second case, where we take two times to coincide and only afterwards rescale the times by the factor $\lambda$ and take the $\lambda \to \infty$ limit, thus sending to $\infty$ all other time differences, except one that remains zero.

In this case, we find that the long-time behavior of $C_4$ is different in two cases depending on which times are chosen to equal.

**Non-rephasing correlator** The first one, which we will refer to as "non-rephasing correlator" [4] is given by

$$C_{NR}(q_1,q_2)=\frac{1}{L}\left\langle\Omega\left|\,\hat{A}(-q_2,\tau_1)\hat{A}(-q_1,\tau_1+\tau_2)\hat{A}(q_2,\tau_1)\hat{A}(q_1,0)\,\right|\Omega\right\rangle_C \tag{5.24}$$

with $\tau_1,\tau_2>0$. $C_{NR}$ appears in the expansion of $\chi^{(3)}(0,\tau_1,\tau_1,\tau_1+\tau_2;q_1,q_2,-q_2,-q_1)$ — in this paragraph we are explicitly indicating the momenta of the various $\hat{A}$ operators as arguments of $\chi^{(3)}$ and $C_4$.

$$\begin{aligned}&\chi^{(3)}(0,\tau_1,\tau_1,\tau_1+\tau_2;q_1,q_2,-q_2,-q_1)=\\&-\Im\left[C_4(0,\tau_1,\tau_1,\tau_1+\tau_2;q_1,q_2,-q_2,-q_1)-C_{NR}(q_1,q_2)\right.\\&\left.-C_{NR}(q_1,-q_2)+C_4(0,\tau_1+\tau_2,\tau_1,\tau_1;q_1,-q_1,q_2,-q_2)\right].\end{aligned} \tag{5.25}$$

Here the terms denoted as $C_4$ do not divergence in the long-time limit.

Note that $C_{NR}$ is a correlator time-ordered on the Keldysh contour, as illustrated in the leftmost panel of Fig. 5.2. Through a form-factor expansion we will show that

$$C_{NR}=e^{-i\epsilon(q_1)(\tau_1+\tau_2)}\alpha_{NR}(q_1,q_2)\tau_2+O(\tau_1^0,\tau_2^0) \tag{5.26}$$

$$\alpha_{NR}=-2|F(q_1)|^2\sum_m\frac{1}{m!}\int\frac{d^m\boldsymbol{k}}{(2\pi)^{m-1}}\delta(q_2-\sum_{j=1}^m k_j)|F(\boldsymbol{k})|^2 v_{NR}(q_1,\boldsymbol{k}) \tag{5.27}$$

where $v_{NR}(q_1,\boldsymbol{k})$ has the dimension of a velocity and can be computed as follows. Consider the set of velocities $\{v(q_1),v(k_1),\ldots,v(k_m)\}$, by permuting its elements we can define an ordered set of velocities $(\tilde{v}_1,\ldots,\tilde{v}_{m+1})$ such that $\tilde{v}_1<\tilde{v}_2<\cdots<\tilde{v}_{m+1}$. Then

$$v_{NR}(q_1,\boldsymbol{k})=\sum_{j=1}^{m+1}(-1)^j\tilde{v}_j. \tag{5.28}$$

The result above has again a natural semiclassical interpretation, as illustrated in the rightmost panel of Fig. 5.2. Here the operators $\hat{A}(q_1,0)$ (denoted as $\hat{A}_1$ in Fig. 5.2) and $\hat{A}(-q_1,\tau_1+\tau_2)$ (denoted as $\hat{A}_3$ in Fig. 5.2) respectively create and annihilate a QP in position $x_1$ and $x_3$. The remaining pair of operators ($\hat{A}(q_2,\tau_1)\equiv\hat{A}_2$ and $\hat{A}(-q_2,\tau_1)\equiv\hat{A}_4$ in Fig. 5.2) will then exchange a shower of $m$ QPs. Note that this is possible since the operators act at the same time, therefore, given that they start at the same position $x_2$, even if they have different velocities, they will all refocus at

[4] The name "non-rephasing" is commonly used in nonlinear optics to denote signals which oscillate in time as $e^{-i\omega(\tau_1+\tau_2)}$ for some $\omega$. As we will discuss later, the divergent part of $C_{NR}$ has this frequency modulation with $\omega=\epsilon(q_1)$.

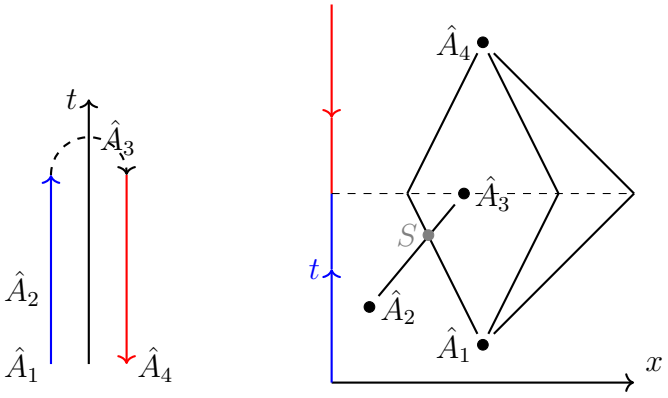


Figure 5.3: (Left cartoon) $C_{PP}$ is a correlator where the state is evolved forward in time from $t_1 = 0$ to $t_3 = \tau_1 + \tau_2$, to finally be evolved backward to time $t_4 = 0$ again. (Right cartoon) Types of processes giving rise to the leading contribution in the $\tau_1, \tau_2 \to \infty$ limit (see also the caption of Fig. 5.1). The time axis is divided into two parts: a blue part where time runs forward, and a red part where, time runs backward. For graphical convenience the two parts are divided by a dashed line, corresponding to the time $\tau_1 + \tau_2$. Here the first operator $\hat{A}_1$ can create a shower of $n$ QPs ($n = 3$ in the figure), which spread ballistically up to time $\tau_1 + \tau_2$ and can scatter against the QP exchanged between $\hat{A}_2$ and $\hat{A}_3$. When evolved backward in time, the $n$ QPs refocus at the same position and can be annihilated by $\hat{A}_4$. When the QPs encounter the dashed line, they are evolved backward, i.e. the slope of their trajectory is reflected w.r.t. the $y$-axis of the figure. Therefore, the $n$ QPs refocus at the same position and can be annihilated by $\hat{A}_4$.

$x_2$ and can therefore be annihilated by a single operator, namely $\hat{A}_4 = \hat{A}(-q_2, \tau_1)$. Finally, depending on the position of $x_1$ and $x_2$ the amplitude of the process gets multiplied by $(-1)^{\#\text{scattering events}}$. For a given $x_1$ and $x_2$, if there is an even number of scattering processes, then the amplitude factorizes into the product of two-point functions and cancels from $C_{NR}$. Instead, if the number of scattering processes is odd, once the disconnected component is subtracted, the amplitude gets multiplied by a factor $S - 1 = -2$. Finally, we can recognize that the factor $v_{NR}\tau_2$ in Eq. (5.28) is the total length of the region of $x_1$ positions which yields an odd number of scattering events for a fixed position $x_2$.

**Pump-probe correlator** The second case where we find a different long-time divergence is the pump-probe correlator $C_{PP}$

$$C_{PP}(q_1, q_2) = \frac{1}{L} \left\langle \Omega \middle| \hat{A}(-q_1, 0)\hat{A}(-q_2, \tau_1 + \tau_2)\hat{A}(q_2, \tau_1)\hat{A}(q_1, 0) \middle| \Omega \right\rangle_C . \tag{5.29}$$

$C_{PP}$ appears in the expansion of $\chi^{(3)}(0,0,\tau_1,\tau_1+\tau_2;q_1,-q_1,q_2,-q_2)$ — in this paragraph we are explicitly indicating the momenta of the various $\hat{A}$ operators as arguments of $\chi^{(3)}$ and $C_4$.

$$\begin{aligned}&\chi^{(3)}(0,0,\tau_1,\tau_1+\tau_2;q_1,-q_1,q_2,-q_2)=\\&-\Im\left[C_4(0,0,\tau_1,\tau_1+\tau_2;q_1,-q_1,q_2,-q_2)-C_{PP}(q_1,q_2)\right.\\&\left.-C_{PP}(-q_1,q_2)+C_4(\tau_1,\tau_1+\tau_2,0,0;q_2,-q_2,-q_1,q_1)\right].\end{aligned}\tag{5.30}$$

Here the terms denoted as $C_4$ do not divergence in the long-time limit. Similarly to $C_{NR}$, also $C_{PP}$ is time-ordered on the Keldysh contour, as shown in Fig. 5.3.

In analogy with $C_{NR}$, one might expect that a similar semiclassical picture holds (see Fig. 5.3). Here $\hat{A}(q_1,0)$ creates a shower of $n$ QPs, which are then annihilated by $\hat{A}(-q_1,0)$. Since they are at different times, $\hat{A}(q_2,\tau_1)$ and $\hat{A}(-q_2,\tau_1+\tau_2)$ will only exchange a single QP. In this case, the length of the region for which an odd number of scattering processes takes place is given by $v_{PP}(\tau_1+\tau_2)$, where $v_{PP}$ has the dimension of a velocity and can be computed as follows from the momentum $q_2$ and the momenta $k_1,\dots,k_n$ of the $n$QPs created by $\hat{A}(q_1,0)$. Consider the set of positions

$$\begin{aligned}\{&v(k_1)\tau_1,\dots,v(k_n)\tau_1,v(k_1)(\tau_1+\tau_2)-v(q_2)\tau_2,\\&\dots,v(k_n)(\tau_1+\tau_2)-v(q_2)\tau_2\}\end{aligned}\tag{5.31}$$

and define the permuted set of coordinates $(\tilde{y}_1,\dots,\tilde{y}_{2n})$ such that $\tilde{y}_1<\tilde{y}_2<\cdots<\tilde{y}_{2n}$. In terms of these we have

$$v_{PP}=\frac{1}{\tau_1+\tau_2}\sum_{j=1}^{2n}(-1)^j\tilde{y}_j.\tag{5.32}$$

From the previous discussion, we conjecture that following results hold for this correlator

$$C_{PP}=(\tau_1+\tau_2)e^{-i\epsilon(q_2)\tau_2}\mathcal{C}_{PP}\left(\frac{\tau_2}{\tau_1+\tau_2};q_1,q_2\right)+O(\tau_1^0,\tau_2^0)\tag{5.33}$$

$$\mathcal{C}_{PP}=-2|F(q_2)|^2\sum_n\frac{1}{n!}\int\frac{d^n\boldsymbol{k}}{(2\pi)^{n-1}}\delta(q_1-\sum_{j=1}^n k_j)|F(\boldsymbol{k})|^2 v_{PP}(\frac{\tau_2}{\tau_1+\tau_2},q_2,\boldsymbol{k}).\tag{5.34}$$

Through the form-factor expansion, we will manage to isolate the divergent terms from $C_4$ and check that the terms in the series up to $n=3$ are correct.

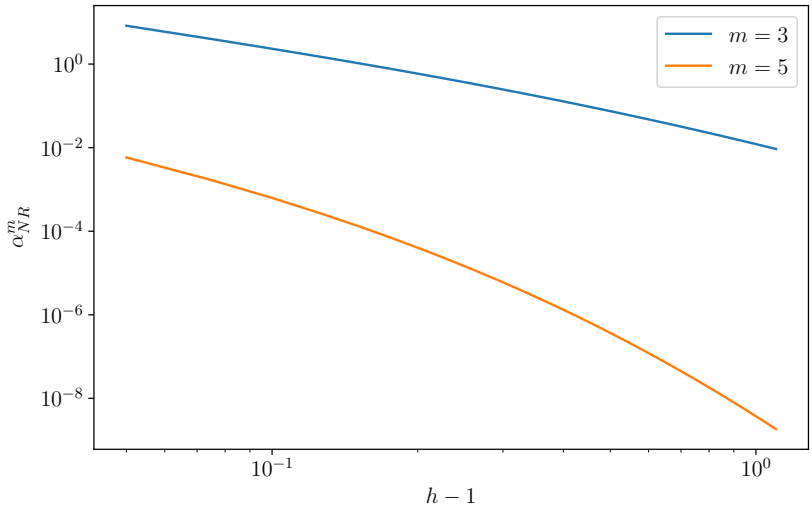


Figure 5.4: $m$-particle contributions to $\alpha_{NR} = \sum_m \alpha^m_{NR}$ in Eq. (5.27). The figure reports the $m = 3$ and $m = 5$ contributions as a function of $h$ for $q_1 = q_2 = 0$. (Note that only odd $m$ contribute and for $q_1 = q_2 = 0$, the $m = 1$ contribution vanishes.)

While the results reported in Eq. (5.27) and Eq. (5.34) seem quite involved, they can be numerically evaluated for the first few values of $n$, which we expect to give the leading contributions when the system is sufficiently deep within the paramagnetic phase. We report the contribution of $m = 3$ and $n = 5$ to $\alpha_{NR}$ as a function of $h$ for $q_1 = q_2 = 0$ in Fig. 5.4. Again, these expressions can be computed numerically. We plot $\mathcal{C}_{PP}$ as a function of $\tau_1/(\tau_1 + \tau_2)$ for $q_1 = q_2 = 0$ and different values of the field in Fig. 5.5.

## 5.3 Divergences and subtraction scheme

### 5.3.1 Identifying long-time divergences through power counting

We want to study possible divergences in the long-time behaviour of $\tilde{C}_4^{n^a,n^b,n^c}$. For the analysis in this paragraph it is convenient to work in terms of frequencies rather than times directly. The idea is that long-time divergences transform to singularities in frequency space, which are easier to identify. We thus define

$$\hat{C}_4^{n^a,n^b,n^c}(\boldsymbol{\omega}) = \int_{-\infty}^{+\infty} \left( \prod_{j=1}^{3} dt_{j+1,j}\, e^{i\omega_j t_{j+1,j}} \right) C_4^{n^a,n^b,n^c} \tag{5.35}$$

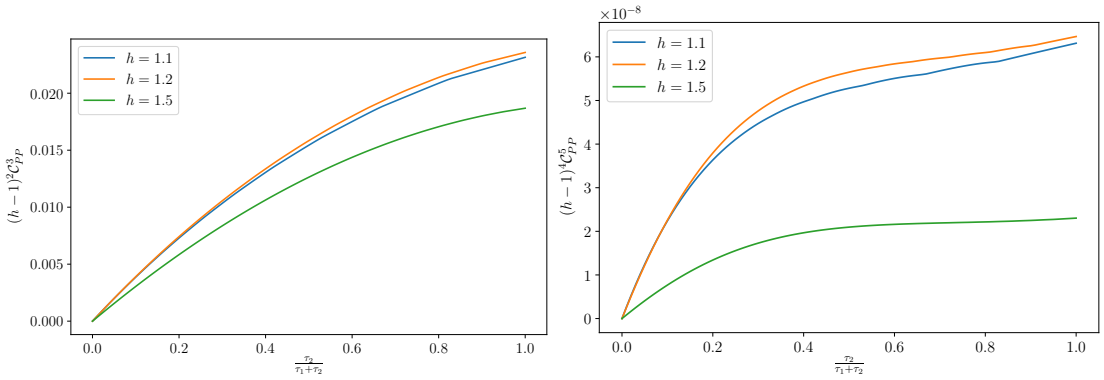


Figure 5.5: $n$-particle contribution to the scaling function $\mathcal{C}_{PP} = \sum_n \mathcal{C}^n_{PP}$. The left panel reports the $n = 3$ contribution as a function of $\frac{\tau_2}{\tau_1+\tau_2}$ for various values of the magnetic field $h$. The different curves have been rescaled by $(h-1)^2$ to show all of them on the same plot. Similarly, the right panel reports the $n = 5$ contribution rescaled by $(h-1)^4$. In both plots $q_1 = q_2 = 0$. (The $n = 1$ contribution is exactly zero in this case.)

with $\boldsymbol{\omega} = (\omega_1, \omega_2, \omega_3)$. $\hat{C}_4^{n^a,n^b,n^c}$ has a form-factor expansion similar to the one of $\tilde{C}_4^{n^a,n^b,n^c}$

$$\hat{C}_4^{n^a,n^b,n^c} = \frac{1}{n^a!n^b!n^c!} \sum_{\boldsymbol{k^a},\boldsymbol{p^b},\boldsymbol{k^c}} \text{Ff } \widehat{\text{Kin}} \text{ Mom} \tag{5.36}$$

$$\begin{aligned}\widehat{\text{Kin}} = (2\pi)^3 \delta \left( \omega_1 - \sum_j \epsilon(k_j^a) \right) \\ \times \delta \left( \omega_2 - \sum_j \epsilon(p_j^b) \right) \delta \left( \omega_3 - \sum_j \epsilon(k_j^c) \right) .\end{aligned} \tag{5.37}$$

We thus see that singularities at a given point $\boldsymbol{\omega}$ can arise through a combination of two mechanisms. (i) When the condition in Mom is enforced, the sum of $\widehat{\text{Kin}}$ is divergent, viz. the density of states is singular at $\boldsymbol{\omega}$, once the total momenta $q_{1,2,3}$ are fixed. (ii) There is a momentum region contributing to the neighbourhood of $\boldsymbol{\omega}$, such that the sum over momenta of Ff Mom diverges as $L \to \infty$. As we will see, such a divergence of Ff Mom can be produced by annihilation poles.

Regarding (i), in 1D the density of states is divergent at the onset of 2QP continuum only. Thus (i) can produce divergences only for $(n^a, n^b, n^c) = (1, 2, 1)$ when $q_1 \simeq q_2 \simeq -q_3$; this case has been already studied in Ref. [3, 4] and has been shown to produce a $\sqrt{t_{32}}$ divergence. Therefore, in the following we focus our attention on divergences of Ff Mom produced by annihilation poles.

We start by considering a generic set of momenta, far away from annihilation

poles. In the limit of large $L$, then $\mathrm{Ff}\,\mathrm{Mom} = O(L^{-n^a-n^b-n^c+3})$. Focusing on a region in momentum space of $O(1)$ volume, this will contain $O(L^{n^a+n^b+n^c-3})$ points that contribute to the sum. Thus, as expected, the powers of $L$ cancel and a generic momentum region gives an $O(1)$ contribution to $\tilde{C}_4$.

Next we want to understand how this is modified if the momentum region encompasses one annihilation pole. E.g. suppose that $k_1^a - p_1^b = O(1/L)$, while other momenta are otherwise generic and far from annihilation poles. In this case Ff will increase by a factor $L$, however the condition $k_1^a - p_1^b = O(1/L)$ heuristically reduces the number of points in the momentum region under consideration by a factor $L$. Therefore, also this momentum region would give an overall $O(1)$ condition. Generalizing the argument above, we see that imposing proximity to $m$ annihilation poles will increase the magnitude of Ff by $O(L^m)$, but the number of points that satisfy the proximity condition to the $m$ annihilation poles are reduced by a factor $O(L^{-m})$ w.r.t. a generic region. In summary, if we are considering a momentum region proximate to any number of poles, this region will not produce divergences in $\tilde{C}_4$ if the proximity to every annihilation pole must be independently enforced.

This argument can be evaded only if, after imposing the proximity to $m$ annihilation poles — thus reducing the number of points to $O(L^{-m})$— the momentum-conservation conditions in Mom force the proximity to other $m_e$ annihilation poles. In this case the overall contribution to $\tilde{C}_4$ would be $O(L^{m_e})$.

It is then immediate to see that for $m_e$ to be greater than zero, all momenta $k_j^a$ and $k_j^c$ must be approximately fixed by the proximity to a pole. In particular, there are only two possible cases in which $m_e > 0$. (i) $(n^c, n^b, n^a) = (m, n+m, n)$, $q_3 \simeq -q_1$, and, up to permutations, $\boldsymbol{p^b}$ can be split into two set of momenta $\boldsymbol{p^b} = (\boldsymbol{p^c}, \boldsymbol{p^a})$ with $\boldsymbol{p^c} \simeq \boldsymbol{k^c}$ and $\boldsymbol{p^a} \simeq \boldsymbol{k^a}$. (ii) $(n^c, n^b, n^a) = (n, n+m, n)$, $q_3 \simeq -q_2$, and, up to permutations, $\boldsymbol{p^b}$ can be split into two set of momenta $\boldsymbol{p^b} = (\boldsymbol{p^{b,1}}, \boldsymbol{p^{b,2}})$ with $\boldsymbol{k^c} \simeq \boldsymbol{p^{b,1}} \simeq \boldsymbol{k^a}$. In both cases $m_e = 1$, thus the overall contribution would be a singularity $O(L)$.

Cases (i) and (ii) should be supplemented with the extra case (iii): $n^b = 0$ and $q_2 = -q_1$, which immediately yields an $O(L)$ contribution due to the automatic enforcement of the $\sum_j p_j^b = 0$ in Mom.

### 5.3.2 Disconnected components

Note that in all three cases, the possibility of a long-time divergence arises from momentum regions proximate to disconnected contributions. In fact, this could have

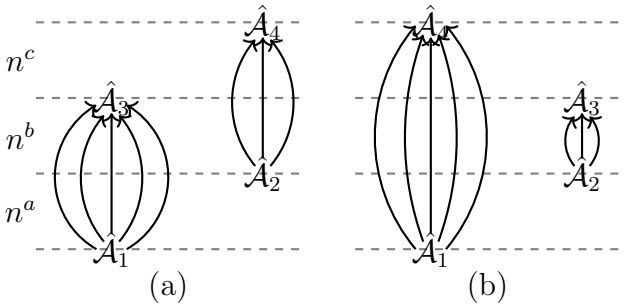


Figure 5.1: Disconnected contributions appear when $(n^a, n^b, n^c)$ are either of the form (i) $(m, n+m, n)$ (as in panel (a) where $n = 5$, $m = 3$), (ii) $(n, n+m, n)$ (as in panel (b) where $n = 5$, $m = 3$), or (iii) $(m, 0, n)$.

been expected independently from the power-counting argument. A disconnected contribution to $C_4$ is schematically of the form $L^{-1}\langle\hat{A}\hat{A}\rangle\langle\hat{A}\hat{A}\rangle$. Given that $\hat{A}$ are extensive operators, the disconnected contributions are proportional to $L$, i.e. they are extensive. This factor of $L$ appears in the form-factor expansion of $\tilde{C}_4$ through the annihilation poles in Ff.

However, $C_4$, the connected component of the four-point function, cannot be extensive. Indeed, once the disconnected components are subtracted from $\tilde{C}_4$, the extensive part must cancel. The connected four-point function is given by

$$\begin{aligned} C_4 = \tilde{C}_4 \\ &- L^{-1} \langle\Omega|A(q_4,t_4)A(q_3,t_3)|\Omega\rangle \langle\Omega|A(q_2,t_2)A(q_1,t_1)|\Omega\rangle \\ &- L^{-1} \langle\Omega|A(q_4,t_4)A(q_2,t_2)|\Omega\rangle \langle\Omega|A(q_3,t_3)A(q_1,t_1)|\Omega\rangle \\ &- L^{-1} \langle\Omega|A(q_3,t_3)A(q_2,t_2)|\Omega\rangle \langle\Omega|A(q_4,t_4)A(q_1,t_1)|\Omega\rangle \,. \end{aligned} \tag{5.38}$$

Note that the all disconnected contributions that must be subtracted are $O(L)$ if the momenta are appropriately matched.

Thinking about the intermediate number of particles that contribute to the disconnected part (see Fig. 5.1), we propose the following scheme to eliminate $O(L)$

divergences at the level of every $\tilde{C}_4^{n^a,n^b,n^c}$:

$$\begin{aligned} C_4^{m,n+m,n} &= \tilde{C}_4^{m,n+m,n} \\ &\quad - L\delta_{q_3,-q_1} C_2^n(q_1,t_{31}) C_2^m(q_2,t_{42}) \qquad (5.39) \\ C_4^{n,n+m,n} &= \tilde{C}_4^{m,n+m,n} \\ &\quad - L\delta_{q_4,-q_1} C_2^n(q_1,t_{41}) C_2^m(q_2,t_{32}) \qquad (5.40) \\ C_4^{1,2,1} &= \tilde{C}_4^{1,2,1} \\ &\quad - L\delta_{q_3,-q_1} C_2^1(q_1,t_{31}) C_2^1(q_2,t_{42}) \\ &\quad - L\delta_{q_4,-q_1} C_2^1(q_1,t_{41}) C_2^1(q_2,t_{32}) \qquad (5.41) \\ C_4^{m,0,n} &= 0. \qquad (5.42) \end{aligned}$$

Here $C_2^n$ denotes the $n-$QP contribution to the two-point function

$$C_2^n(q,t) = \frac{1}{n!} \sum_{\boldsymbol{k}\in \mathrm{R}^n} \delta_{q,\sum_{j=1}^n k_j} |F(\boldsymbol{k})|^2 e^{-it\sum_j \epsilon(k_j)}. \qquad (5.43)$$

Note that all terms in the expression above are smooth w.r.t. $\boldsymbol{k}$, therefore the sum over $\boldsymbol{k}$ can be replaced by an integral in the thermodynamic limit:

$$C_2^n(q,t) = \frac{1}{n!} \int \frac{d^n\boldsymbol{k}}{(2\pi)^{n-1}} \delta\left(q - \sum_{j=1}^n k_j\right) |F(\boldsymbol{k})|^2 e^{-it\sum_j \epsilon(k_j)}. \qquad (5.44)$$

After the subtraction we expect that every $C_4^{n^a,n^b,n^c}$ will be finite at any finite time. However, the region proximate to the disconnected component in $\tilde{C}_4^{n^a,n^b,n^c}$ and the actual disconnected component $LC_2^nC_2^m$ have different frequency dependence, therefore the subtraction can produced singularities in frequency space. Equivalently, in real time, this amounts to the possibility of divergences in the long-time limit.

In the following we check for the Ising model that the scheme we just proposed eliminates extensive terms. Furthermore, after the appropriate subtractions, we will find that the leading term in the long-time limit are the ones summarized in Sec. 5.2.

## 5.4 Distinct times

### 5.4.1 $C_4^{1,2,1}$, $q_3 \simeq -q_1$

Following the previous discussion, we consider $\tilde{C}_4^{1,2,1}$ for $q_3 \simeq -q_1$ and expand the contribution due to kinematic poles After imposing the momentum constraints we are left with only one unconstrained momentum $p := p_1^b$

$$\begin{aligned}\tilde{C}_4^{1,2,1} \simeq C_2^1(q_1, t_{31}) C_2^1(-q_4, t_{42}) e^{i(\epsilon(q_1)+\epsilon(-q_4))t_{32}} \\ \times \frac{1}{L} \sum_{p \in \mathrm{NS}} \frac{e^{-it_{32}(\epsilon(p)+\epsilon(q_1+q_2-p))}}{\frac{p-q_1}{2}\frac{p+q_3}{2}}\end{aligned} \tag{5.45}$$

where $C_2^1(q,t)$ is the 1-particle contribution to the two point function, which, can be written more explicitly as $C_2^1(q,t) = |F(q)|^2 e^{-it\epsilon(q)}$.

If $q_1 = -q_3$ exactly, we can use Eq. (5.80) to extract the leading behaviour in the $L \to \infty$ and large times limit. After subtracting the disconnected component we then have

$$C_4^{1,2,1} = -2C_2^1(q_1, t_{31}) C_2^1(q_2, t_{42}) |t_{32}||v(q_1) - v(q_2)| + O(\|\boldsymbol{t}\|^0), \tag{5.46}$$

as anticipated in Sec. 5.2. If $q_1 \neq -q_3$, we can instead use Eq. (5.83) to extract the leading behavior in the $L \to \infty$ and $\delta q = q_3 + q_1 \to 0$ limit, thus obtaining

$$\begin{aligned}C_4^{1,2,1} \simeq -2C_2^1(q_1, t_{31}) C_2^1(q_2, t_{42}) \mathrm{sign}\left(t_{32}(v(q_2) - v(q_1))\right) \\ \times \frac{1 - e^{-it_{32}[\epsilon(-q_3)+\epsilon(-q_4)-\epsilon(q_1)-\epsilon(q_2)]}}{i(q_1+q_3)} \\ + O(\|\boldsymbol{t}\|^0).\end{aligned} \tag{5.47}$$

For time $t_{32}$ short enough, and in particular for $|t_{32}| \lesssim t_{br}$ as defined in Eq. (5.23), the exponential can be Taylor expanded to first order and the result in Eq. (5.46) is approximately recovered.

### 5.4.2 $C_4^{1,2,1}$, $q_4 \simeq -q_1$

Proceeding in a similar fashion, we can extract the asymptotic behavior for $q_4 \simeq -q_1$. In this case we would have

$$\begin{aligned}\tilde{C}_4^{1,2,1} \simeq\ & C_2^1(q_1,t_{41})C_2^1(q_2,t_{32})e^{-i(\epsilon(-q_4)-\epsilon(q_1))t_{43}}e^{+i(\epsilon(q_1)+\epsilon(q_2))t_{32}} \\ & \times \frac{1}{L}\sum_{p\in \mathrm{NS}} \frac{e^{-it_{32}(\epsilon(p)+\epsilon(q_1+q_2-p))}}{\frac{p-q_1}{2}\frac{p-q_4}{2}}.\end{aligned} \tag{5.48}$$

Thus, for $q_1+q_4=0$, employing Eq. (5.80), we get

$$C_4^{1,2,1} = -2C_2^1(q_1,t_{41})C_2^1(q_2,t_{32})|t_{32}||v(q_1)-v(q_2)| + O(\|\boldsymbol{t}\|^0), \tag{5.49}$$

confirming the result reported in Sec. 5.2. Instead for $q_4 \neq -q_1$, but in the limit $q_4+q_1 \to 0$

$$\begin{aligned}C_4^{1,2,1} \simeq\ & -2C_2^1(q_1,t_{41})C_2^1(q_2,t_{32})e^{-i(\epsilon(-q_4)-\epsilon(q_1))t_{43}}\mathrm{sign}\left(t_{32}(v(q_2)-v(q_1))\right) \\ & \times \frac{1-e^{-it_{32}[\epsilon(-q_3)+\epsilon(-q_4)-\epsilon(q_1)-\epsilon(q_2)]}}{i(q_1+q_4)}.\end{aligned} \tag{5.50}$$

Again, for $|t_{32}| \lesssim t_{br}$, the exponential can be Taylor expanded to first order and the result in Eq. (5.49) is approximately recovered.

### 5.4.3 Contributions from more-QP states

Next, we consider divergent contributions from more-QP states, i.e. $(m, n+m, n)$ and $(n, n+m, n)$. We will show in the subsequent sections that, once the disconnected part is canceled, they can be bounded by the product of two-point functions times a term proportional to the overall timescale. More specifically

$$C_4^{m,n+m,n} = C_2^n(q_1,t_{31})C_2^m(q_2,t_{42})O(|t_{32}|) \tag{5.51}$$

$$C_4^{n,n+m,n} = C_2^n(q_1,t_{41})C_2^m(q_2,t_{32})O(|t_{32}|+|t_{21}|). \tag{5.52}$$

The form-factor expansion of $C_2^n(q,t)$ contains an integral over $n-1$ momenta. In the limit of large $t$, the integral can thus be bounded through a stationary phase approximation, that yields $C_2^n(q,t) = O(t^{-(n-1)/2})$. We can therefore bound the

overall contributions as

$$C_4^{m,n+m,n} = O\left(\frac{|t_{32}|}{|t_{31}|^{(n-1)/2}|t_{42}|^{(m-1)/2}}\right) \tag{5.53}$$

$$C_4^{n,n+m,n} = O\left(\frac{|t_{32}|+|t_{21}|}{|t_{41}|^{(n-1)/2}|t_{32}|^{(m-1)/2}}\right). \tag{5.54}$$

Thus, when all times are taken to be distinct and they are rescaled by $\lambda$, in the $\lambda \to \infty$ limit the leading contribution is given by $C_4^{1,2,1}$, which, as discussed in the previous subsections, gives the results presented in Sec. 5.2.

## 5.5 Two equal times

When we analyzed the structure of the form-factor expansion in the Ising model we noticed that proximity to any disconnected contribution can produce divergences in the long-time limit. In the limit where all $|t_{ij}| \to \infty$ we recognized that the leading behavior was given by $C_4^{1,2,1}$. In principle, there are two other families of terms that could give rise to further divergences in the long-time limit: $C_4^{m,n+m,n}$ for $q_3 \simeq -q_1$, and $C_4^{n,n+m,n}$ for $q_3 \simeq -q_2$.

We now focus on these two families of terms and extract their leading long-time behaviour from the form-factor expansion. The main conclusions we expect from this analysis are the following. (i) In the case of distinct times, we want to show that the bounds anticipated in Eqs. (5.52) and (5.51) hold. (ii) The sum of terms of the form $C_4^{m,1+m,1}$ gives the leading contribution to $C_{NR}$ and allows us to recover the results in Eqs. (5.26) (5.27), and (5.28) (iii) The sum of terms of the form $C_4^{n,1+n,n}$ gives the leading contribution to $C_{PP}$ and allows us to recover Eqs. (5.33) (5.34), and possibly give us a way to systematically pursue a proof that Eq. (5.28).

We set up the form-factor calculation for generic times and later restrict ourselves to $C_{NR}$ and $C_{PP}$. Additionally, it will be useful to split the two limits of $C_4$: near $q_3 = -q_1$ or near $q_3 = -q_2$. We denote the limit of $C_4$ in these two cases as $C_{NR'}$ and $C_{PP'}$ respectively — they have the same form of $C_{NR}$ and $C_{PP}$, but for arbitrary times. Finally, in the technical calculations it will be useful to add an extra regulator

$\gamma$ and define

$$C_{NR',\gamma} = \sum_{q_1' \in \mathrm{R}} \frac{1}{L^2} \frac{2\gamma}{\gamma^2 + (q_1 - q_1')^2} \times \langle \Omega | A(-q_2', t_4) A(-q_1', t_3) A(q_2, t_2) A(q_1, t_1) | \Omega \rangle \tag{5.55}$$

$$C_{PP',\gamma} = \sum_{q_1' \in \mathrm{R}} \frac{1}{L^2} \frac{2\gamma}{\gamma^2 + (q_1 - q_1')^2} \times \langle \Omega | A(-q_1', t_4) A(-q_2', t_3) A(q_2, t_2) A(q_1, t_1) | \Omega \rangle \,, \tag{5.56}$$

where $q_2'$ is fixed by momentum conservation to $q_2' = q_1 + q_2 - q_1'$. The idea is that instead of constraining the momenta to a precise value, we average over the values of $q_1'$ within a window of length $\gamma$ inside the region giving rise to divergent contributions. We will perform the form-factor calculation in the limit where $L \gg \gamma^{-1} \gg t_{ij}$ and finally take the limit $\lim_{\gamma \to 0} \lim_{L \to \infty}$. Note that the normalization of the Lorentzian distribution is chosen such that

$$\lim_{L \to \infty} \sum_{q \in \mathrm{R}} \frac{1}{L} \frac{2\gamma}{\gamma^2 + (q - q')^2} = 1 \tag{5.57}$$

which implies that

$$\lim_{\gamma \to 0} \lim_{L \to \infty} \sum_{q \in \mathrm{R}} \frac{1}{L} \frac{2\gamma}{\gamma^2 + (q - q')^2} A(q') = A(q). \tag{5.58}$$

Therefore

$$C_{NR'} = \lim_{\gamma \to 0} \lim_{L \to \infty} C_{NR',\gamma} \tag{5.59}$$

$$C_{PP'} = \lim_{\gamma \to 0} \lim_{L \to \infty} C_{PP',\gamma}. \tag{5.60}$$

Finally, while the times of $C_{NR',\gamma}$ and $C_{PP',\gamma}$ are arbitrary, we can study the non-rephasing and pump-probe correlator through the substitution

$$C_{NR} = \lim_{\gamma \to 0} \lim_{L \to \infty} C_{NR',\gamma} \Big|_{\substack{t_{42}=0 \\ t_{32}=\tau_2 \\ t_{21}=\tau_1}} \tag{5.61}$$

$$C_{PP} = \lim_{\gamma \to 0} \lim_{L \to \infty} C_{PP',\gamma} \Big|_{\substack{t_{41}=0 \\ t_{32}=\tau_2 \\ t_{21}=\tau_1}}. \tag{5.62}$$

[Note that since all the timescales are kept finite while taking the limits $L \to \infty$ and

$\gamma \to 0$, the time substitution can be made at any point. In particular, we will take the limits first and then replace the times $t_j$ in terms of $\tau_{1,2}$.]

### 5.5.1 Non-rephasing and $C^{m,n+m,n}$

As emerged from the discussion in Sec. 5.3, long-time divergences originates when the momenta of the various QP in the form-factor expansion are proximate to the momenta of a disconnected process. Specifically, for $C_{NR'}$, this can happen in terms of the form $C^{m,n+m,n}$. The disconnected component of the four point-function takes contributions from the momenta where, up to internal permutations of $\boldsymbol{p}^b$, $\boldsymbol{p^b} \equiv (\boldsymbol{p^c}, \boldsymbol{p^a})$ with $\boldsymbol{p^c} \simeq \boldsymbol{k^c}$ and $\boldsymbol{p^a} \simeq \boldsymbol{k^a}$. Expanding the form-factor product Ff around this case, we obtain

$$\begin{aligned} \mathrm{Ff} \simeq{}& (-1)^{(n+m)/2} \left|F(\boldsymbol{k^a})\right|^2 \left|F(\boldsymbol{k^c})\right|^2 \\ &\times L^{-(n+m)} \left(\prod_{j=1}^{n} \frac{2}{p_j^a - k_j^a}\right) \left(\prod_{j=1}^{m} \frac{2}{p_j^c - k_j^c}\right). \end{aligned} \tag{5.63}$$

with $F(\boldsymbol{k})$ denoting the finite-volume form factors. Consequently, the singular contributions to the four-point function $C_{NR',\gamma}$ can be expanded as

$$C_{NR',\gamma} \simeq \sum_{n,m} C^{m,n+m,n}_{NR',\gamma} \tag{5.64}$$

$$\begin{aligned} C^{m,n+m,n}_{NR',\gamma} \simeq{}& \sum_{\boldsymbol{k^a}\in \mathrm{R}} L\delta_{q_1,\sum_j k_j^a} \left|F(\boldsymbol{k^a})\right|^2 e^{-i\sum_j \epsilon(k_j^a)t_{31}} \\ &\times \sum_{\boldsymbol{k^c}\in \mathrm{R}} L\delta_{q_2,\sum_j k_j^c} \left|F(\boldsymbol{k^c})\right|^2 e^{-i\sum_j \epsilon(k_j^c)t_{42}} H_{NR}(t_{32}; \boldsymbol{k^a}, \boldsymbol{k^c}) \end{aligned} \tag{5.65}$$

$$H_{NR}(t; \boldsymbol{k^a}, \boldsymbol{k^c}) = \tilde{H}_{NR}(t; \boldsymbol{k^a}, \boldsymbol{k^c}) - \frac{2}{\gamma} \tag{5.66}$$

$$\begin{aligned} \tilde{H}_{NR}(t; \boldsymbol{k^a}, \boldsymbol{k^c}) ={}& (-1)^{(n+m)/2} L^{-(n+m)} \sum_{\boldsymbol{p^a},\boldsymbol{p^c}\in \mathrm{NS}} \left(\prod_{j=1}^{n} \frac{2}{p_j^a - k_j^a}\right) \left(\prod_{j=1}^{m} \frac{2}{p_j^c - k_j^c}\right) \\ &\times \frac{2\gamma}{\gamma^2 + \left(\sum_{j=1}^{n}(p_j^a - k_j^a) + \sum_{j=1}^{n}(p_j^a - k_j^a)\right)^2} \\ &\times \exp\left[-it\left(\sum_{j=1}^{n}(\epsilon(p_j^a) - \epsilon(k_j^a)) + \sum_{j=1}^{n}(\epsilon(p_j^c) - \epsilon(k_j^c))\right)\right]. \end{aligned} \tag{5.67}$$

The second equation is a direct application of the subtraction scheme in Eq. (5.39), where the disconnected contribution is now weighted by $2/\gamma$, as a consequence of

the $\gamma$-regularization. Finally, we anticipate that in the first equation the dependence on $\boldsymbol{k}^{\boldsymbol{a}}$ and $\boldsymbol{k}^{\boldsymbol{c}}$ is regular, therefore the sums over momenta can be approximated by integrals in the $L \to \infty$ limit.

Next, we need to compute $H_{NR}$. Before proceeding, it is however useful to redefine $H_{NR}(t; \boldsymbol{k}^{\boldsymbol{a}}, \boldsymbol{k}^{\boldsymbol{c}})$ as $H_{NR}(t; \boldsymbol{k})$ with $\boldsymbol{k} = (\boldsymbol{k}^{\boldsymbol{a}}, \boldsymbol{k}^{\boldsymbol{c}})$. This manipulation is useful since $H_{NR}(t; \boldsymbol{k})$ is invariant under the permutation of the elements in $\boldsymbol{k}$. We show in Appendix 5.B that, if the vectors $\boldsymbol{k} = (k_1, \ldots, k_{n+m})$ are reordered in such a way that $v(k_1) < \cdots < v(k_{n+m})$, then

$$\lim_{\gamma \to 0} \lim_{L \to \infty} H_{NR}(t, \boldsymbol{k}) = -2t \sum_{j=1}^{n+m} (-1)^j v(k_j) + O(1). \tag{5.68}$$

From this result, we can easily obtain everything we set out to achieve. (i) Since the velocities are bounded we have

$$\lim_{\gamma \to 0} \lim_{L \to \infty} H_{NR} = O(|t_{32}|) \tag{5.69}$$

Plugging this into the expression for $C^{m,n+m,n}_{NR',\gamma}$ above we immediately obtain the bound in Eq. (5.51). (ii) Furthermore, when considering $C_{NR}$, from the same bound we find that

$$C^{m,n+m,n}_{NR',\gamma \to 0}\Big|_{\substack{t_{21}=\tau_1 \\ t_{32}=\tau_2 \\ t_{42}=\tau_0}} = C_2^m(q_2, 0) C_2^n(q_1, \tau_1 + \tau_2) O(\tau_2). \tag{5.70}$$

From this it follows that the contributions with $n > 1$ are subleading w.r.t. the ones with $n = 1$. To show this we can evaluate $C_2^n(q_1, \tau_1 + \tau_2)$ within the stationary-phase approximation to obtain that $C_2^n(q_1, \tau_1 + \tau_2) = O((\tau_1 + \tau_2)^{(n-1)/2})$, thus reaching the conclusion that contributions terms with $n > 1$ are subleading in the large-$\tau_1, \tau_2$ limit. Furthermore, we can immediately note that, when $n = 1$

$$\lim_{\gamma \to 0} \lim_{L \to \infty} H_{NR}\Big|_{\substack{t_{21}=\tau_1 \\ t_{32}=\tau_2 \\ t_{42}=\tau_0}} = v_{NR} \tau_2 \tag{5.71}$$

with $v_{NR}$ defined in Eq. (5.28). From this it follows that, by summing the $n = 1$ terms in the form factor expansion, we can recover the expressions in Eqs. (5.26), (5.27), and (5.28).

### 5.5.2 Pump-probe and $C^{n,n+m,n}$

The discussion for the pump-probe signal follows closely the one for the non-rephasing one. From the power-counting argument in Sec. 5.3, we expect long-time divergences to arise in proximity of disconnected contributions. For terms of the form $C^{n,n+m,n}$ this takes place if the momenta of the first and third state approximately coincide, i.e. up to permutations $\boldsymbol{k^c} \simeq \boldsymbol{k^a}$, and a subset of the momenta of the second state approximately coincides with $\boldsymbol{k^a}$, i.e. $\boldsymbol{p^b} \equiv (\boldsymbol{p^{b,1}}, \boldsymbol{p^{b,2}})$ with $\boldsymbol{p^{b,1}} \simeq \boldsymbol{k^c} \simeq \boldsymbol{k^a}$. In this case, we can expand the product of form factors as

$$\begin{aligned}\mathrm{Ff} &\simeq |F(\boldsymbol{k^a})|^2 \left|F(\boldsymbol{p^{b,2}})\right|^2 \\ &\quad \times L^{-(n+m)} \left(\prod_{j=1}^{n} \frac{2}{p_j^{b,1} - k_j^a}\right) \left(\prod_{j=1}^{m} \frac{2}{p_j^{b,1} - k_j^c}\right). \end{aligned} \tag{5.72}$$

Consequently, the four-point function $C_{PP',\gamma}$ can be expanded as

$$C_{PP',\gamma} \simeq \sum_{n,m} C^{n,n+m,n}_{PP',\gamma} \tag{5.73}$$

$$\begin{aligned} C^{n,n+m,n}_{PP',\gamma} &\simeq \sum_{\boldsymbol{k^c} \in \mathrm{R}} L\delta_{q_1, \sum_j k_j^c} \left|F(\boldsymbol{k^c})\right|^2 e^{-i\sum_j \epsilon(k_j^c) t_{41}} \\ &\quad \times \sum_{\tilde{\boldsymbol{p}}^{\boldsymbol{b,2}}} L\delta_{q_2, \sum_j \tilde{p}_j^{b,2}} \left|F(\tilde{\boldsymbol{p}}^{\boldsymbol{b,2}})\right|^2 e^{-i\sum_j \epsilon(\tilde{p}_j^{2,b}) t_{32}} H_{PP}(\boldsymbol{t}; \boldsymbol{k^c}, \tilde{p}_1^{b,2}) \end{aligned} \tag{5.74}$$

$$H_{PP}(\boldsymbol{t}; \boldsymbol{k^c}, \tilde{p}_1^{b,2}) = \tilde{H}_{PP}(\boldsymbol{t}; \boldsymbol{k^c}, \tilde{p}_1^{b,2}) - \frac{2}{\gamma} \tag{5.75}$$

$$\begin{aligned} \tilde{H}_{PP}(\boldsymbol{t}; \boldsymbol{k^c}, \tilde{p}_1^{b,2}) &= L^{-(n+m)} \sum_{\substack{\boldsymbol{p^{b,1}} \in \mathrm{NS} \\ \boldsymbol{k^a} \in \mathrm{R}}} \left(\prod_{j=1}^{n} \frac{2}{p_j^{b,1} - k_j^a}\right) \left(\prod_{j=1}^{m} \frac{2}{p_j^{b,1} - k_j^c}\right) \\ &\quad \times \frac{2\gamma}{\gamma^2 + \left(\sum_j k_j^a - k_j^c\right)^2} \\ &\quad \times \exp\left[-it_{32} \sum_{j=1}^{n} (\epsilon(p_j^{b,1}) - \epsilon(k_j^c)) - it_{21} \sum_{j=1}^{n} (\epsilon(k_j^a) - \epsilon(k_j^c))\right] \\ &\quad \times \exp\left[-it_{32} \left(\epsilon\left(\tilde{p}_1^{b,2} + q_1 - \sum_{j=1}^{n} p_j^{b,1}\right) - \epsilon(\tilde{p}_1^{b,2})\right)\right]. \end{aligned} \tag{5.76}$$

The idea of this rewriting is as follows. In the first line we expressed the four-point functions in terms of product of two-point functions and the function $H_{PP}$. Note that to do so, we had to modify the set of momenta $\boldsymbol{p^{b,2}}$ into a new set $\tilde{\boldsymbol{p^{b,2}}}$ in such a way

that they satisfied the momentum conservation condition $q_2 = \sum_j \tilde{p}_j^{b,2}$, as opposed to $q_1 + q_2 = \sum_{j=1}^m p_j^{b,2} + \sum_{j=1}^n p_j^{b,1}$. We chose to do so by taking $\tilde{p}_j^{b,2} = p_j^{b,2}$ for $j \geq 2$ and $\tilde{p}_j^{b,2} = q_2 - \sum_{j=2}^m p_j^{b,2}$. This substitution means that $\tilde{H}_{PP}$ should include the correction to the phase $\exp(-it_{32}\epsilon(p_1^{b,2}))\exp(+it_{32}\epsilon(\tilde{p}_1^{b,2}))$, which indeed appears in the last line of Eq. (5.75). Similarly, we should also have included a factor of the form $F(\boldsymbol{p}^{\boldsymbol{b,2}})/F(\tilde{\boldsymbol{p}}^{\boldsymbol{b,2}})$ in $\tilde{H}_{PP}$, however, this factor can be neglected since it is smooth, i.e. its derivatives are $O(1)$ in the limit $\lim_{t\to\infty}\lim_{\gamma\to 0}\lim_{L\to\infty}$.

To confirm Eq. (5.52), we need to prove that for any fixed $m$ and $n$,

$$\lim_{\gamma\to 0}\lim_{L\to\infty} H_{PP} = O(|t_{32}| + |t_{21}|). \tag{5.77}$$

This property is derived in Appendix 5.C. Furthermore, from the bound on $H_{PP}$ we also have that

$$C^{n,n+m,n}_{PP',\gamma\to 0}\Big|_{\substack{t_{41}=0\\ t_{32}=\tau_2\\ t_{21}=\tau_1}} = C_2^m(q_2,\tau_2)C_2^n(q_1,0)O(\tau_2+\tau_1), \tag{5.78}$$

implying that contributions with $m > 1$ are subleading in $C_{PP}$.

Finally, to confirm the validity of Eqs. (5.33), (5.34), and (5.32) we would need to show that for $m = 1$,

$$\lim_{\gamma\to 0}\lim_{L\to\infty} H_{PP} = v_{PP}(\tau_1+\tau_2) + O(\tau_1^0,\tau_2^0). \tag{5.79}$$

This statement is more complex to derive explicitly for any $n$. In Appendix 5.C we write recursion relations that allow to compute $\lim_{\gamma\to 0}\lim_{L\to\infty} H_{PP}$ for arbitrary $n$. Using these relations we checked explicitly that property Eq. (5.79) holds for $n = 1, 2, 3$. Although we have not been able to prove it for arbitrary $n$, we conjecture that Eq. (5.79) is valid nonetheless, in agreement with the semiclassical picture put forward in Sec. 5.2.

## 5.6 Conclusions

In this chapter we studied Keldysh-ordered momentum-resolved four-point functions of the order parameter in the paramagnetic phase of the Ising model. We found that in the long-time limit these correlator diverge proportionally to the overall time-scale. The divergence is due to processes that would give rise to a product of two-point functions, except for some scattering process among the QPs. We have furthermore

given an explicit way to compute the long-time divergence in terms of the form factors on top of the ground state (which, unlike form factors among general states, are regular functions).

We have focused on two different ways to take the long-time limit. In the first and simplest case all time differences are taken to $\infty$. In this case the leading processes are the ones where each operator creates or annihilates a single QP. Furthermore, motivated by experiments, like pump-probe and two-dimensional coherent spectroscopy, we considered a long-time limit where two times are kept equal, while all other time differences are taken to $\infty$. In this case we identified two correlators: the non-rephasing correlator and the pump-probe correlator, whose long-time limit involves $n$-particle processes. These divergences could in principle be observed in state-of-the-art optical experiments, like the ones performed in Ref. [140, 33].

This initial investigation opens many potentially interesting directions for future studies concerning the divergence of four-point functions. In the Ising model, the divergence can be easily understood through a semiclassical picture. The key elements of the picture are stable ballisticaly-propagating quasiparticles, which can scatter among each other, and that one-QP excitations can be created by $\hat{A}$. It would then appear that the free-fermion nature of the quasiparticles is not fundamental for the long-time divergence, although it greatly simplifies the form-factor calculations. It would be interesting to understand if the same picture is then valid in other circumstances, like integrable QFTs, or even more generally to clean non-integrable models with stable QP excitations on top of their ground state.

A further direction concerns the effect of considering a finite-temperature state initially. In this case, we expect that the linear growth would be cut-off by an exponential suppression at long times. A possible approach to understand the low-temperature physics in this case is to expand the method of Ref. [171] to compute four-point functions. A more ambitious goal would be to perform a calculation based on GHD by generalizing the approach of Ref. [184]., which could potentially be exact at any temperature.

Finally, a more speculative direction concerns whether it is possible to have similar long-time divergences in higher dimension, either through scattering processes, or, in models with anyonic excitations, through linking of QPs' trajectories.

# Appendix

## 5.A Summation formulas for $\tilde{C}_4^{1,2,1}$

**Lemma 1:**
We assume $k \in \mathrm{R}$ and that $L \gg v_M t \gg \xi$ with $v_M$ maximum QP velocity, then, in the limit $L, t \to \infty$

$$\frac{1}{L}\sum_{p\in \mathrm{NS}} 4\frac{e^{-it(\epsilon(p)+\epsilon(q-p))}}{(k-p)^2} = \left[L - 2|t|\,|v(k)-v(q-k)|\right] e^{-it(\epsilon(k)+\epsilon(q-k))} + O(1), \quad (5.80)$$

To show that this is the case, we draw inspiration from Ref. [27] and consider the contour integrals

$$I_\pm = \oint \frac{dz}{2\pi} \frac{e^{-it(\epsilon(z)+\epsilon(q-z))}}{(z-k)^2\left(e^{\pm izL}+1\right)} \quad (5.81)$$

where the contour runs over a region such as the one represented in Fig. 5.A.1. The If $t(v(k)-v(q-k)) > 0$, then we can choose the contour such that $I_- = O(1)$. In fact, when $\Im z > 0$ the factor $\left(e^{\pm izL}+1\right)$ at the denominator becomes exponentially large in $L\Im z$. Similarly, in the region where $\Im z < 0$, but small enough such that $t\Re\left(\epsilon'(z)-\epsilon'(q-z)\right)) > 0$ on all the contour, the integrand becomes exponentially suppressed in $t(v(k)-v(k-q))\Im z$. Consequently the integrand can always be bounded by $(z-k)^{-2}$, whose integral along the contour is a finite number, independently of $L$ and $t$. Similarly, if $t(v(k)-v(q-k)) < 0$, we can choose the contour in such a way that $I_+ = O(1)$. Finally, we can compute $I_\pm$ through standard contour integration techniques obtaining

$$I_\pm = \mp\frac{1}{L}\sum_{p\in \mathrm{NS}\bigcap \square} 4\frac{e^{-it(\epsilon(p)+\epsilon(q-p))}}{(k-p)^2} + e^{-it(\epsilon(k)+\epsilon(q-k))}\left[\pm L + 2t\left(v(k)-v(q-k)\right)\right], \quad (5.82)$$

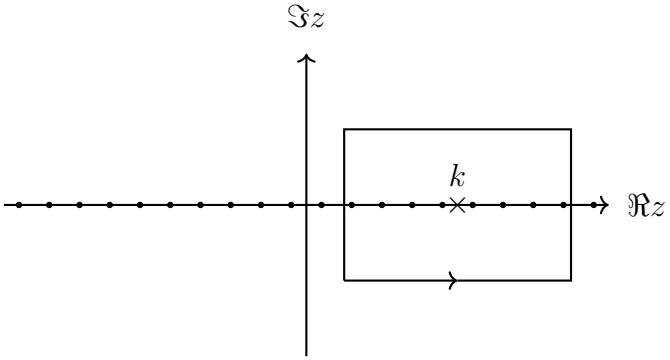


Figure 5.A.1: Contour of integration used in the proof of Lemma 1. The dots denote the set NS, where the integrand of $I_\pm$ has poles. The vertical boundaries of the integration contour are chosen close enough to $k$ such that $\mathrm{sign}(v(z))$ and $\mathrm{sign}(v(q-z))$ are constant within the rectangle.

where $\mathrm{NS}\bigcap\square$ denotes the subset NS contained inside the integration contour. Noticing that the sum over the complement of $\mathrm{NS}\bigcap\square$ is regular, this immediately yields Eq. (5.80).

**Lemma 2:** Similarly, we can show that, if $k_1, k_2 \in \mathrm{R}$, then, as $L, t \to \infty$ and $k_1 - k_2 \to 0$

$$\frac{1}{L}\sum_{p\in\mathrm{NS}} 4\frac{e^{-it(\epsilon(p)+\epsilon(q-p))}}{(p-k_1)(p-k_2)} = -2i\mathrm{sign}(t)\mathrm{sign}(v(k_1)-v(q-k_1)) \times \frac{e^{-i(\epsilon(k_1)+\epsilon(q-k_1))t} - e^{-i(\epsilon(k_2+\epsilon(q-k_2))t}}{k_1-k_2} + O(1) \tag{5.83}$$

# 5.B Computation of $H_{NR}$

In this appendix, we use summation formulas similar to the ones derived in Appendix 5.A to compute the long-time limit of $H_{NR}$ and ultimately prove Eq. (5.68). We begin by introducing a summation operator $\hat{\Sigma}_{NR}(k)$ with $k \in \mathrm{R}$, acting on functions $f(r;\dots)$ as

$$\hat{\Sigma}_{NR}(k)f(r;\dots) = \frac{1}{L}\sum_{p\in\mathrm{NS}} \frac{2}{p-k} e^{-it(\epsilon(p)-\epsilon(k))} f(r+p-k). \tag{5.84}$$

By further defining the initial function

$$A_{NR}(r) = \frac{2\gamma}{r^2+\gamma^2}, \tag{5.85}$$

$\tilde{H}_{NR}$ can be rewritten as

$$\tilde{H}_{NR}(t;\boldsymbol{k}) = \left[\hat{\Sigma}_{NR}(k_N)\hat{\Sigma}_{NR}(k_{N-1})\cdots\hat{\Sigma}_{NR}(k_1)A(r)\right]\Big|_{r=0}. \tag{5.86}$$

By introducing an extra function $B_{NR}$,

$$B_{NR}(r;k_0,\xi) = e^{-it(\epsilon(k_0-r-i\xi\gamma)-\epsilon(k_0))}\frac{2}{r+i\xi\gamma} \quad \xi=\pm 1, \tag{5.87}$$

we can define a close set of recursion relations for $\hat{\Sigma}_{NR}$:

$$\hat{\Sigma}_{NR}(k)A_{NR}(r) = -i\text{sign}(tv(k))A_{NR}(r) - 2B_{NR}(r;k,\text{sign}(v(k))) + O(1) \tag{5.88}$$

$$\begin{aligned}\hat{\Sigma}_{NR}(k)B_{NR}(r;k_0,\xi) = &-i\text{sign}(t)\text{sign}(v(k)-v(k_0))B_{NR}(r;k_0,\xi)\\ &+2i\text{sign}(t)\text{sign}(v(k)-v(k_0))\delta_{\xi,\text{sign}(t)\text{sign}(v_k-v_{k_0})}B_{NR}(r;k,\xi)\\ &+O(1)\end{aligned} \tag{5.89}$$

to leading order in $\gamma^{-1}$ and $t$. The proof of these identities is very similar to the proof of Lemma 1 and 2. An important difference is that there are extra poles at $z = k - r \pm i\gamma$. The residue in one of these two poles can always be neglected for $L \gg \gamma^{-1}$, as it is exponentially suppressed by the factor $(1+e^{\pm iLz})^{-1}$. Finally, we assumed $r$ to be small enough such that $\text{sign}\, v(k) = \text{sign}\, v(k-r)$.

Using the two identities before we can now perform explicitly compute $\tilde{H}_{NR}$. The final result we will obtain will be expressed in terms of $A_{NR}$ and $B_{NR}$ functions evaluated at $r = 0$

$$A_{NR}(0) = \frac{2}{\gamma} \tag{5.90}$$

$$B_{NR}(0,k,\xi) = -i\xi\frac{2}{\gamma} + 2itv(k) + O(1). \tag{5.91}$$

To derive the last expression, we used that $\gamma^{-1} \gg t$ and thus Taylor-expanded the exponential in $B_{NR}$ in powers of $\gamma t$.

To explicitly compute $\tilde{H}_{NR}$, we reorder the momenta such that $tv(k_1) < \cdots < tv(k_l) < 0 < tv(k_N) < tv(k_{N-1}) < \cdots < tv(k_{l+1})$ (with $N$ even). Note that in this way the second term in Eq. (5.89) is always zero. After $N$ steps, all summation will

be removed and the following expression is obtained

$$\begin{aligned}\tilde{H}_{NR}(t;\boldsymbol{k}) = (-1)^{N/2}(+i)^{l}(-i)^{N-l}A(0) \\ + (-1)^{N/2}\sum_{j=1}^{l}(+i)^{j-1}(-1)(-i)^{N-j}B_{NR}(0;k_j,-1) \\ + (-1)^{N/2}\sum_{j=1}^{N-l}(-i)^{j-1}(-1)(+i)^{N-j}B_{NR}(0;k_{l+j},+1)\end{aligned} \tag{5.92}$$

To show the explicit form in Eq. (5.68) we reorder the momenta in order of increasing velocities. We thus define a new index $j'$ as follows: $j' = j$ for $j \leq l$, $j' = N - j + 1$ for $j \geq l + 1$, and consequently we define the ordered momenta $\tilde{k}_{j'} = k_j$. Note that the momenta satisfy the ordering $tv(\tilde{k}_1) < \cdots < tv(\tilde{k}_N)$. In this way, and with some basic algebra, we can rewrite the previous expression as

$$\tilde{H}_{NR}(t;\boldsymbol{k}) = (-1)^{l}\frac{2}{\gamma} + i\sum_{j'=1}^{N}(-1)^{j'}B_{NR}(0,\tilde{k}_{j'},\mathrm{sign}(l-j'+1/2)) \tag{5.93}$$

Finally, plugging in the expression for $B_{NR}(0;k,\xi)$, we obtain

$$\tilde{H}_{NR}(t;\boldsymbol{k}) = \frac{2}{\gamma} - 2t\sum_{j'=1}^{N}(-1)^{j'}v(\tilde{k}_{j'}). \tag{5.94}$$

We note that the term $2/\gamma$ is exactly the disconnected part that get subtracted in $H_{NR}$, thus leaving us with Eq. (5.68).

## 5.C Computation of $H_{PP}$

To compute $H_{PP}$ we take similar steps to the ones that we used to compute $H_{NR}$. We begin by defining a $\hat{\Sigma}_{PP}$ operator as

$$\begin{aligned}\hat{\Sigma}_{PP}(k)[f(Q,r;\dots)] = \frac{1}{L^2}\sum_{\substack{p\in\mathrm{NS}\\ h\in\mathrm{R}}}\frac{2}{p-h}\frac{2}{p-k}e^{-it_{21}\epsilon(h)-it_{32}\epsilon(p)}e^{it_{31}\epsilon(k)} \\ \times f(Q+p-k,r+h-k;\dots),\end{aligned} \tag{5.95}$$

with the dots denoting possible extra arguments of $f$. By further defining the initial function

$$A_{PP}(Q,r) = e^{-it_{32}\epsilon(P-Q)}\frac{2\gamma}{\gamma^2+r^2}, \tag{5.96}$$

$H_{PP}$ can be written as

$$\tilde{H}_{PP}(\boldsymbol{t};\boldsymbol{k},P) = e^{+it_{32}\epsilon(P)}\left[\hat{\Sigma}_{PP}(k_N)\hat{\Sigma}_{PP}(k_{N-1})\cdots\hat{\Sigma}_{PP}(k_1)A_{PP}(Q,r)\right]\Big|_{Q=0,r=0}. \tag{5.97}$$

To define a closed set of recursion relations, we introduce the two extra functions

$$B_{PP}(Q,r;k,\xi) = 2i\frac{e^{-it_{31}\epsilon(k-r-i\xi\gamma)}e^{+it_{31}\epsilon(k)}e^{-it_{32}\epsilon(P-Q+r+i\xi\gamma)}}{r+i\xi\gamma} \tag{5.98}$$

$$C_{PP}(Q,r;k,\xi) = 2i\frac{e^{-it_{32}\epsilon(P-Q)}e^{-it_{21}\epsilon(k-r-i\xi\gamma)+it_{21}\epsilon(k)}}{r+i\xi\gamma} \tag{5.99}$$

with $\xi = \pm 1$.

Assuming $r$ to be small enough such that $\operatorname{sign} v(k-r) = \operatorname{sign} v(k)$ and $\operatorname{sign} v(P-Q+r) = \operatorname{sign} v(P-Q))$, we can now compute the following recusion relations.

$$\begin{aligned}
&\hat{\Sigma}_{PP}(k)A_{PP}(Q,r)\\
&\quad= \operatorname{sign}(t_{21}v(k))\operatorname{sign}\left(v(k)t_{31}-v(P)t_{32}\right)A_{PP}(Q,r)\\
&\qquad+\operatorname{sign}(t_{32}(v(k)-v(P)))B_{PP}(Q,r;\operatorname{sign}\left(v(k)t_{31}-v(P)t_{32}\right))\\
&\qquad-\operatorname{sign}(t_{32}(v(k)-v(P)))C_{PP}(Q,r;k,\operatorname{sign}(t_{21}v(k)))\\
&\qquad+O(1)
\end{aligned} \tag{5.100}$$

$$\begin{aligned}
&\hat{\Sigma}_{PP}(k)B_{PP}(Q,r;k_0,\xi)\\
&\quad= \operatorname{sign}(t_{21}v(k)-t_{31}v(k_0)+t_{32}v(P))\operatorname{sign}(t_{32}(v(k)-v(k_0)))B_{PP}(Q,r;k_0,\xi)\\
&\qquad+2\xi\operatorname{sign}(t_{32}(v(k)-v(P)))\delta_{\xi,\operatorname{sign}(t_{31}(v(k)-v(k_0))}B_{PP}(Q,r;k,\xi)\\
&\qquad-2\xi\operatorname{sign}(t_{32}(v(k)-v(P)))\delta_{\xi,\operatorname{sign}(t_{21}v(k)-t_{31}v(k_0)+t_{32}v(P))}C_{PP}(Q,r;k,\xi)\\
&\qquad+O(1)
\end{aligned} \tag{5.101}$$

$$\begin{aligned}
&\hat{\Sigma}_{PP}(k)C_{PP}(Q,r;k_0,\xi) =\\
&\quad= \operatorname{sign}(t_{21}(v(k)-v(k_0)))\operatorname{sign}(t_{32}v(k)-t_{21}v(k_0)-t_{32}v(P))C_{PP}(Q,r;k_0,\xi)\\
&\qquad+2\xi\operatorname{sign}(t_{32}(v(k)-v(P)))\delta_{\xi,\operatorname{sign}(t_{31}v(k)-t_{21}v(k_0)-t_{32}v(P))}B_{PP}(Q,r;k,\xi)\\
&\qquad-2\xi\operatorname{sign}(t_{32}(v(k)-v(P)))\delta_{\xi,\operatorname{sign}(t_{21}(v(k)-v(k_0)))}C_{PP}(Q,r;k,\xi)\\
&\qquad+O(1).
\end{aligned} \tag{5.102}$$

All of these can be derived by performing the sum over $h \in \mathrm{R}$ first and then the sum over $p \in \mathrm{NS}$. In both sums the leading term can be extracted using a complex integration techniques identical to the ones used for the non-rephasing signal. By repeatedly applying the recursion relations above, one could in principle express $\tilde{H}_{PP}$ in terms of various sign functions, depending on the velocities, and $A$, $B$, and $C$ functions evaluated at $r = Q = 0$:

$$e^{+it_{32}\epsilon(P)} A_{PP}(0,0) = \frac{2}{\gamma} \tag{5.103}$$

$$e^{+it_{32}\epsilon(P)} B_{PP}(0,0;,k,\xi) = \xi\frac{2}{\gamma} - 2\left[t_{31}v(k) - t_{32}v(P)\right] \tag{5.104}$$

$$e^{+it_{32}\epsilon(P)} C_{PP}(0,0;,k,\xi) = \xi\frac{2}{\gamma} - 2t_{21}v(k). \tag{5.105}$$

As anticipated in the main text, we would like to now show the following properties of $\tilde{H}_{PP}$. (i) $\tilde{H}_{PP} - 2/\gamma$ is finite in the $\gamma \to 0$ limit and the cancellation scheme we proposed is correct. (ii) The remaining part can be bounded as $O(|t_{32}|+|t_{31}|)$ for every $n$. To prove (i), we can inspect the three recursion relations and, by analyzing all possible cases of the sign-functions, we can show the following. If the initial function on the LHS(either $A_{PP}$, $B_{PP}$, or $C_{PP}$), once evaluated at $Q, r = 0$ gives a leading term of $\zeta 2/\gamma$, with $\zeta = \pm 1$, then also the sum of the various terms in the RHS, once evaluated at $Q, r = 0$, will yield the same leading contribution of $\zeta 2/\gamma$. Since the starting point of the recursion is $A_{PP}$, whose leading term is $2/\gamma$, by induction, we immediately know that the leading term of $\tilde{H}_{PP}$ is again $2/\gamma$. Thus the cancellation scheme we proposed works and $H_{PP}$ is finite

Once we know that (i) holds, (ii) is trivial. In fact, given the form of the recursion relation, we know that $H_{PP}$ will be a linear combination of objects of the type $[t_{31}v(k_j) - t_{32}v(P)]$ and $t_{21}v(k_j)$ with finite integer coefficients. Note that, since the maximum velocity is bounded, all the terms are bounded by $4v_{\mathrm{MAX}}(|t_{32}| + |t_{21}|)$. Therefore, $H_{PP}(\boldsymbol{t}; \boldsymbol{k}, P)$ is bounded by some $\boldsymbol{k}$- and $P$-independent constant times $|t_{32}| + |t_{21}|$.

Finally, we focus on the case where $t_{32} = \tau_2 > 0$, $t_{21} = \tau_1 > 0$. We conjecture that by repeated application of the recursion relation one obtains the following formula for $\tilde{H}_{PP}$

$$\tilde{H}_{PP}(\tau_1, \tau_2; \boldsymbol{k}, P) = \frac{2}{\gamma} - 2\sum_{j=1}^{2n}(-1)^j \tilde{y}_j \tag{5.106}$$

where the $\tilde{y}_j$ are drawn from the set

$$Y = \{v(k_1)\tau_1, \ldots, v(k_n)\tau_1, v(k_1)(\tau_1+\tau_2)-v(P)\tau_2, \ldots, v(k_n)(\tau_1+\tau_2)-v(P)\tau_2\} \quad (5.107)$$

in increasing order, viz. $\tilde{y}_1 < \tilde{y}_2 < \cdots < \tilde{y}_{2n}$. If the conjecture were true, this would imply that the semiclassical picture presented in Sec. 5.2 is indeed correct. We are currently unable to prove this conjecture for general $n$, however, we can verify it explicitly for $n = 1, 2, 3$.

# Chapter 6

# Summary and outlook

We now proceed to summarize the results presented in this thesis and related open questions that might be worth investigating in the future.

Throughout the thesis we focused on dynamical response and correlation functions in many-body systems and computed them in some integrable models.

In Chapter 3, motivated by experimental advances in the field of cold atoms, we considered the one-dimensional Hubbard model. Here, within the framework of GHD, we studied the Drude weights of the model in various regimes controlled by the temperature. Possibly one of the most interesting parts of the study is the presence of spin and charge superdiffusion when the filling and magnetization endow the system with non-abelian symmetries (either $SU(2)$ or $SO(4)$). In this case, dynamical two-point functions are conjectured to exhibit KPZ scaling, a feature that is possibly common to all integrable models with non-abelian symmetries [97, 196].

In the rest of the thesis we focused on dynamical nonlinear response and multi-point functions. Compared to linear response and two-point functions, these quantities are less understood. In this context, therefore, potentially much could be learned by their characterization in exactly-solvable models.

In Chapter 4 we developed a framework to compute nonlinear response to external fields coupling to charge densities. Our framework is based on GHD and therefore we expect it to provide asymptotically exact results at the Euler scale. We have exemplified our technique by computing second-order response functions in the Lieb-Liniger gas, highlighting that the nonlinear response functions are much more sensitive to interactions than their linear-response counterpart. Furthermore, we described the computation of nonlinear generalization of the Drude weights and benchmarked the correctness of our formulas against exact diagonalization in the XXZ chain.

Given that the topic of nonlinear response functions in GHD has not been widely studied yet, there are many natural questions related to this work. A more common setting in which multi-point correlators in GHD have been studied is that of ballistic large deviation theory [149, 149, 161], which is instead concerned with characterizing the full counting statistics of the charge imbalance across some bipartition of the system. While nonlinear response to an external perturbation and large-deviation theory seem potentially unrelated, in classical systems nonlinear response can be computed from large-deviation functions [70]. It would be interesting to understand to what extent this connection remains valid within GHD.

Another interesting line of inquiry concerns nonlinear response functions when linear response shows KPZ scaling, like at the isotropic point of the XXX chain. In this case, we showed that nonlinear Drude weights diverge. While we expect this result to hold in the Euler scaling limit, where the external field is infinitesimal and applied for an infinite time, it would be interesting to understand the finite-time corrections to these results to gain insight into how the long-time divergence comes about. This could potentially be achieved by studying the GHD equations in the presence of inhomogeneous fields and diffusive corrections [54] while treating the field perturbatively at a fixed order. It would also be interesting to understand whether the divergence of the nonlinear Drude weights can be related to the divergence of the cumulants of the large-deviation function [121, 81].

Finally, in Chapter 5 we studied multi-point functions of operators that can also create and annihilate QPs — a problem which cannot be straightforwardly addressed within GHD. To simplify the problem we considered one of the simplest integrable models: the transverse-field Ising model. Here we showed that when the perturbation couples to an operator which can create or annihilate single QPs excitations, four-point functions grow linearly in time. We explained this long-time divergence in terms of a simple semiclassical picture including ballistic propagation of QPs and scattering processes.

This study also opens a few natural questions. The semiclassical picture seems in fact to be applicable beyond the Ising model. The most natural extension is the context of integrable QFTs, which is another natural setting where the ground state coincides with the quasiparticle vacuum. Here, also the form-factor calculation might be quite similar to the one for the Ising model, given that form factors of integrable QFTs have a similar annihilation pole structure.

Furthermore, the semiclassical picture does not seem to rely on integrability, but only on the fact that isolated quasiparticles on top of the ground state are stable. It

would then be interesting to find a non-integrable system where four-point functions can be computed in a controlled fashion and see whether the long-time divergences are present also in that context.

More broadly, there are still many settings where nonlinear response functions have not been computed and their qualitative behavior is unknown. Understanding the possible phenomenology of nonlinear response functions in as many contexts as possible is a challenge for the future, which might hopefully help improve the experimental applicability of nonlinear response measurements in probing and characterizing exotic phases of matter.

# References


[1] P. W. Anderson. More is different. *Science*, 177(4047):393–396, August 1972.

[2] Rhys Anderson, Fudong Wang, Peihang Xu, Vijin Venu, Stefan Trotzky, Frédéric Chevy, and Joseph H. Thywissen. Conductivity spectrum of ultracold atoms in an optical lattice. *Phys. Rev. Lett.*, 122:153602, Apr 2019.

[3] H. M. Babujian, M. Karowski, and A. M. Tsvelik. Probing strong correlations with light scattering: Example of the quantum ising model. *Phys. Rev. B*, 94:155156, Oct 2016.

[4] H.M. Babujian, M. Karowski, and A.M. Tsvelik. Multipoint green's functions in 1+1 dimensional integrable quantum field theories. *Nuclear Physics B*, 917:122–153, 2017.

[5] W. S. Bakr, A. Peng, M. E. Tai, R. Ma, J. Simon, J. I. Gillen, S. Fölling, L. Pollet, and M. Greiner. Probing the superfluid–to–mott insulator transition at the single-atom level. *Science*, 329(5991):547–550, 2010.

[6] Waseem S. Bakr, Jonathon I. Gillen, Amy Peng, Simon Fölling, and Markus Greiner. A quantum gas microscope for detecting single atoms in a hubbard-regime optical lattice. *Nature*, 462(7269):74–77, November 2009.

[7] Leon Balents and Matthew P. A. Fisher. Correlation effects in carbon nanotubes. *Phys. Rev. B*, 55:R11973–R11976, May 1997.

[8] A.-L. Barabsi and H. E. Stanley. *Fractal Concepts in Surface Growth*. Cambridge University Press, 1995.

[9] Alvise Bastianello, Vincenzo Alba, and Jean-Sébastien Caux. Generalized hydrodynamics with space-time inhomogeneous interactions. *Phys. Rev. Lett.*, 123:130602, Sep 2019.

[10] Alvise Bastianello and Andrea De Luca. Integrability-protected adiabatic reversibility in quantum spin chains. *Phys. Rev. Lett.*, 122:240606, Jun 2019.

[11] Alvise Bastianello, Andrea De Luca, Benjamin Doyon, and Jacopo De Nardis. Thermalization of a trapped one-dimensional bose gas via diffusion. *Phys. Rev. Lett.*, 125:240604, Dec 2020.

[12] Gerardo Beni and Cornelius F. Coll. Thermoelectric power in half-filled bands. *Phys. Rev. B*, 11:573–576, Jan 1975.

[13] B. Bertini, F. Heidrich-Meisner, C. Karrasch, T. Prosen, R. Steinigeweg, and M. Znidaric. Finite-temperature transport in one-dimensional quantum lattice models. *arXiv e-prints*, page arXiv:2003.03334, March 2020.

[14] Bruno Bertini, Mario Collura, Jacopo De Nardis, and Maurizio Fagotti. Transport in out-of-equilibrium $xxz$ chains: Exact profiles of charges and currents. *Phys. Rev. Lett.*, 117:207201, Nov 2016.

[15] Bruno Bertini and Lorenzo Piroli. Low-temperature transport in out-of-equilibrium XXZ chains. *Journal of Statistical Mechanics: Theory and Experiment*, 2018(3):033104, mar 2018.

[16] Bruno Bertini, Lorenzo Piroli, and Pasquale Calabrese. Universal broadening of the light cone in low-temperature transport. *Phys. Rev. Lett.*, 120:176801, Apr 2018.

[17] Immanuel Bloch. Ultracold quantum gases in optical lattices. *Nature Physics*, 1(1):23–30, October 2005.

[18] Martin Boll, Timon A. Hilker, Guillaume Salomon, Ahmed Omran, Jacopo Nespolo, Lode Pollet, Immanuel Bloch, and Christian Gross. Spin- and density-resolved microscopy of antiferromagnetic correlations in fermi-hubbard chains. *Science*, 353(6305):1257–1260, 2016.

[19] Márton Borsi, Balázs Pozsgay, and Levente Pristyák. Current operators in bethe ansatz and generalized hydrodynamics: An exact quantum-classical correspondence. *Phys. Rev. X*, 10:011054, Mar 2020.

[20] Márton Borsi, Balázs Pozsgay, and Levente Pristyák. Current operators in integrable models: a review. *Journal of Statistical Mechanics: Theory and Experiment*, 2021(9):094001, sep 2021.

[21] C. Broholm, R. J. Cava, S. A. Kivelson, D. G. Nocera, M. R. Norman, and T. Senthil. Quantum spin liquids. *Science*, 367(6475), 2020.

[22] Peter T. Brown, Debayan Mitra, Elmer Guardado-Sanchez, Peter Schauß, Stanimir S. Kondov, Ehsan Khatami, Thereza Paiva, Nandini Trivedi, David A. Huse, and Waseem S. Bakr. Spin-imbalance in a 2d fermi-hubbard system. *Science*, 357(6358):1385–1388, 2017.

[23] A. I. Bugrii. *Theoretical and Mathematical Physics*, 127(1):528–548, 2001.

[24] A.I. Bugrij and O. Lisovyy. Spin matrix elements in 2d ising model on the finite lattice. *Physics Letters A*, 319(3):390–394, 2003.

[25] Vir B. Bulchandani. Kardar-parisi-zhang universality from soft gauge modes. *Phys. Rev. B*, 101:041411, Jan 2020.

[26] Vir B Bulchandani, Sarang Gopalakrishnan, and Enej Ilievski. Superdiffusion in spin chains. *Journal of Statistical Mechanics: Theory and Experiment*, 2021(8):084001, aug 2021.

[27] Pasquale Calabrese, Fabian H L Essler, and Maurizio Fagotti. Quantum quench in the transverse field ising chain: I. time evolution of order parameter correlators. *Journal of Statistical Mechanics: Theory and Experiment*, 2012(07):P07016, jul 2012.

[28] X. Cao, V.B. Bulchandani, and J.E. Moore. Incomplete Thermalization from Trap-Induced Integrability Breaking: Lessons from Classical Hard Rods. *Physical Review Letters*, 120(16):164101, Apr 2018.

[29] J.M.P. Carmelo, Shi-Jian Gu, and P.D. Sacramento. Zero finite-temperature charge stiffness within the half-filled 1d hubbard model. *Annals of Physics*, 339:484–509, 2013.

[30] J.M.P. Carmelo, S. Nemati, and T. Prosen. Absence of ballistic charge transport in the half-filled 1d hubbard model. *Nuclear Physics B*, 930:418–498, 2018.

[31] Olalla A. Castro-Alvaredo, Benjamin Doyon, and Takato Yoshimura. Emergent hydrodynamics in integrable quantum systems out of equilibrium. *Phys. Rev. X*, 6:041065, Dec 2016.

[32] Jean-Sébastien Caux, Benjamin Doyon, Jerome Dubail, Robert Konik, and Takato Yoshimura. Hydrodynamics of the interacting Bose gas in the Quantum Newton Cradle setup. *SciPost Physics*, 6(6):70, jun 2019.

[33] Dipanjan Chaudhuri, David Barbalas, Ralph Romero III, Fahad Mahmood, Jiahao Liang, John Jesudasan, Pratap Raychaudhuri, and N. P. Armitage. Anomalous high-temperature THz nonlinearity in superconductors near the metal-insulator transition. *arXiv e-prints*, page arXiv:2204.04203, April 2022.

[34] Vadim V. Cheianov and M. B. Zvonarev. Nonunitary spin-charge separation in a one-dimensional fermion gas. *Phys. Rev. Lett.*, 92:176401, Apr 2004.

[35] Lawrence W. Cheuk, Matthew A. Nichols, Melih Okan, Thomas Gersdorf, Vinay V. Ramasesh, Waseem S. Bakr, Thomas Lompe, and Martin W. Zwierlein. Quantum-gas microscope for fermionic atoms. *Phys. Rev. Lett.*, 114:193001, May 2015.

[36] Christie S. Chiu, Geoffrey Ji, Annabelle Bohrdt, Muqing Xu, Michael Knap, Eugene Demler, Fabian Grusdt, Markus Greiner, and Daniel Greif. String patterns in the doped hubbard model. *Science*, 365(6450):251–256, 2019.

[37] Wonjune Choi, Ki Hoon Lee, and Yong Baek Kim. Theory of two-dimensional nonlinear spectroscopy for the kitaev spin liquid. *Phys. Rev. Lett.*, 124:117205, Mar 2020.

[38] Kuang-chao Chou, Zhao-bin Su, Bai-lin Hao, and Lu Yu. Equilibrium and nonequilibrium formalisms made unified. *Physics Reports*, 118(1-2):1–131, 1985.

[39] Cornelius F. Coll. Excitation spectrum of the one-dimensional hubbard model. *Phys. Rev. B*, 9:2150–2158, Mar 1974.

[40] Axel Cortés Cubero, Takato Yoshimura, and Herbert Spohn. Form factors and generalized hydrodynamics for integrable systems. *Journal of Statistical Mechanics: Theory and Experiment*, 2021(11):114002, nov 2021.

[41] Jacopo De Nardis, Denis Bernard, and Benjamin Doyon. Hydrodynamic diffusion in integrable systems. *Phys. Rev. Lett.*, 121:160603, Oct 2018.

[42] Jacopo De Nardis, Denis Bernard, and Benjamin Doyon. Hydrodynamic diffusion in integrable systems. *Physical Review Letters*, 121(16), oct 2018.

[43] Jacopo De Nardis, Sarang Gopalakrishnan, Enej Ilievski, and Romain Vasseur. Superdiffusion from emergent classical solitons in quantum spin chains. *Phys. Rev. Lett.*, 125:070601, Aug 2020.

[44] Jacopo De Nardis, Sarang Gopalakrishnan, Enej Ilievski, and Romain Vasseur. Superdiffusion from Emergent Classical Solitons in Quantum Spin Chains. *Physical Review Letters*, 125(7), aug 2020.

[45] Jacopo De Nardis, Marko Medenjak, Christoph Karrasch, and Enej Ilievski. Anomalous spin diffusion in one-dimensional antiferromagnets. *Phys. Rev. Lett.*, 123:186601, Oct 2019.

[46] Jacopo De Nardis, Marko Medenjak, Christoph Karrasch, and Enej Ilievski. Universality classes of spin transport in one-dimensional isotropic magnets: the onset of logarithmic anomalies. *arXiv e-prints*, page arXiv:2001.06432, January 2020.

[47] Benjamin Doyon. Exact large-scale correlations in integrable systems out of equilibrium. *SciPost Physics*, 5(5):54, nov 2018.

[48] Benjamin Doyon. Lecture notes on generalised hydrodynamics. *SciPost Physics Lecture Notes*, aug 2019.

[49] Benjamin Doyon and Joseph Durnin. Free energy fluxes and the kubo–martin–schwinger relation. *Journal of Statistical Mechanics: Theory and Experiment*, 2021(4):043206, apr 2021.

[50] Benjamin Doyon and Jason Myers. Fluctuations in ballistic transport from euler hydrodynamics. *Annales Henri Poincaré*, 21(1):255–302, November 2019.

[51] Benjamin Doyon and Herbert Spohn. Drude Weight for the Lieb-Liniger Bose Gas. *SciPost Phys.*, 3:039, 2017.

[52] Benjamin Doyon and Takato Yoshimura. A note on generalized hydrodynamics: inhomogeneous fields and other concepts. *SciPost Phys.*, 2:014, 2017.

[53] Joseph Durnin, M. J. Bhaseen, and Benjamin Doyon. Non-Equilibrium Dynamics and Weakly Broken Integrability. *arXiv e-prints*, page arXiv:2004.11030, April 2020.

[54] Joseph Durnin, Andrea De Luca, Jacopo De Nardis, and Benjamin Doyon. Diffusive hydrodynamics of inhomogenous hamiltonians. *Journal of Physics A: Mathematical and Theoretical*, 54(49):494001, nov 2021.

[55] G. J. A. Edge, R. Anderson, D. Jervis, D. C. McKay, R. Day, S. Trotzky, and J. H. Thywissen. Imaging and addressing of individual fermionic atoms in an optical lattice. *Phys. Rev. A*, 92:063406, Dec 2015.

[56] Deniz Ertaş and Mehran Kardar. Dynamic roughening of directed lines. *Phys. Rev. Lett.*, 69:929–932, Aug 1992.

[57] D. Nasr Esfahani, L. Covaci, and F. M. Peeters. Nonlinear response to electric field in extended hubbard models. *Phys. Rev. B*, 90:205121, Nov 2014.

[58] Fabian H L Essler and Maurizio Fagotti. Quench dynamics and relaxation in isolated integrable quantum spin chains. *Journal of Statistical Mechanics: Theory and Experiment*, 2016(6):064002, June 2016.

[59] Fabian H. L. Essler, Holger Frahm, Frank Göhmann, Andreas Klümper, and Vladimir E. Korepin. *The One-Dimensional Hubbard Model*. Cambridge University Press, 2005.

[60] Tilman Esslinger. Fermi-hubbard physics with atoms in an optical lattice. *Annual Review of Condensed Matter Physics*, 1(1):129–152, 2010.

[61] Michele Fava, Sounak Biswas, Sarang Gopalakrishnan, Romain Vasseur, and S. A. Parameswaran. Hydrodynamic nonlinear response of interacting integrable systems. *Proceedings of the National Academy of Sciences*, 118(37):e2106945118, 2021.

[62] Michele Fava, Brayden Ware, Sarang Gopalakrishnan, Romain Vasseur, and S. A. Parameswaran. Spin crossovers and superdiffusion in the one-dimensional hubbard model. *Phys. Rev. B*, 102:115121, Sep 2020.

[63] Gregory A. Fiete. Colloquium: The spin-incoherent luttinger liquid. *Rev. Mod. Phys.*, 79:801–820, Jul 2007.

[64] Gregory A. Fiete, Karyn Le Hur, and Leon Balents. Transport in a spin-incoherent luttinger liquid. *Phys. Rev. B*, 72:125416, Sep 2005.

[65] Gregory A. Fiete, Karyn Le Hur, and Leon Balents. Coulomb drag between two spin-incoherent luttinger liquids. *Phys. Rev. B*, 73:165104, Apr 2006.

[66] Matthew P. A. Fisher, Peter B. Weichman, G. Grinstein, and Daniel S. Fisher. Boson localization and the superfluid-insulator transition. *Phys. Rev. B*, 40:546–570, Jul 1989.

[67] Eduardo Fradkin. *Field Theories of Condensed Matter Physics*. Cambridge University Press, 2 edition, 2013.

[68] Fabio Franchini. *An Introduction to Integrable Techniques for One-Dimensional Quantum Systems*, volume 940. 2017.

[69] Aaron J. Friedman, Sarang Gopalakrishnan, and Romain Vasseur. Diffusive hydrodynamics from integrability breaking. *Phys. Rev. B*, 101:180302, May 2020.

[70] Chloe Ya Gao and David T. Limmer. Nonlinear transport coefficients from large deviation functions. *The Journal of Chemical Physics*, 151(1):014101, July 2019.

[71] M Garst and A Rosch. Transport in a classical model of a one-dimensional mott insulator: Influence of conservation laws. *Europhysics Letters (EPL)*, 55(1):66–72, jul 2001.

[72] Florian Gebhard. *Metal-Insulator Transitions*. Springer, 1997.

[73] Antoine Georges, Gabriel Kotliar, Werner Krauth, and Marcelo J. Rozenberg. Dynamical mean-field theory of strongly correlated fermion systems and the limit of infinite dimensions. *Rev. Mod. Phys.*, 68:13–125, Jan 1996.

[74] H. A. Gersch and G. C. Knollman. Quantum cell model for bosons. *Phys. Rev.*, 129:959–967, Jan 1963.

[75] T. Giamarchi. Theoretical framework for quasi-one dimensional systems. *Chemical Reviews*, 104(11):5037–5056, 11 2004.

[76] T. Giamarchi and H. J. Schulz. Anderson localization and interactions in one-dimensional metals. *Phys. Rev. B*, 37:325–340, Jan 1988.

[77] Thierry Giamarchi. *Quantum Physics in One Dimension*. Oxford University Press, December 2003.

[78] Gabriele Giuliani and Giovanni Vignale. *Quantum Theory of the Electron Liquid*. Cambridge University Press, 2005.

[79] Sarang Gopalakrishnan, David A. Huse, Vedika Khemani, and Romain Vasseur. Hydrodynamics of operator spreading and quasiparticle diffusion in interacting integrable systems. *Phys. Rev. B*, 98:220303, Dec 2018.

[80] Sarang Gopalakrishnan, David A. Huse, Vedika Khemani, and Romain Vasseur. Hydrodynamics of operator spreading and quasiparticle diffusion in interacting integrable systems. *Physical Review B*, 98(22), dec 2018.

[81] Sarang Gopalakrishnan, Alan Morningstar, Romain Vasseur, and Vedika Khemani. Theory of anomalous full counting statistics in anisotropic spin chains, 2022.

[82] Sarang Gopalakrishnan and Romain Vasseur. Kinetic theory of spin diffusion and superdiffusion in $xxz$ spin chains. *Phys. Rev. Lett.*, 122:127202, Mar 2019.

[83] Sarang Gopalakrishnan, Romain Vasseur, and Brayden Ware. Anomalous relaxation and the high-temperature structure factor of xxz spin chains. *Proceedings of the National Academy of Sciences*, 116(33):16250–16255, 2019.

[84] Etienne Granet. Low-density limit of dynamical correlations in the lieb–liniger model. *Journal of Physics A: Mathematical and Theoretical*, 54(15):154001, March 2021.

[85] Etienne Granet, Henrik Dreyer, and Fabian H.L. Essler. Out-of-equilibrium dynamics of the XY spin chain from form factor expansion. *SciPost Phys.*, 12:19, 2022.

[86] Etienne Granet and Fabian H. L. Essler. A systematic $1/c$-expansion of form factor sums for dynamical correlations in the Lieb-Liniger model. *SciPost Phys.*, 9:82, 2020.

[87] Etienne Granet and Fabian H. L. Essler. Systematic strong coupling expansion for out-of-equilibrium dynamics in the Lieb-Liniger model. *SciPost Phys.*, 11:68, 2021.

[88] Etienne Granet, Maurizio Fagotti, and Fabian H. L. Essler. Finite temperature and quench dynamics in the Transverse Field Ising Model from form factor expansions. *SciPost Phys.*, 9:33, 2020.

[89] Markus Greiner, Olaf Mandel, Tilman Esslinger, Theodor W. Hänsch, and Immanuel Bloch. Quantum phase transition from a superfluid to a mott insulator in a gas of ultracold atoms. *Nature*, 415(6867):39–44, January 2002.

[90] Felix M. Haehl, R. Loganayagam, Prithvi Narayan, Amin A. Nizami, and Mukund Rangamani. Thermal out-of-time-order correlators, KMS relations, and spectral functions. *Journal of High Energy Physics*, 2017(12), December 2017.

[91] Elmar Haller, James Hudson, Andrew Kelly, Dylan A. Cotta, Bruno Peaudecerf, Graham D. Bruce, and Stefan Kuhr. Single-atom imaging of fermions in a quantum-gas microscope. *Nature Physics*, 11(9):738–742, July 2015.

[92] Peter Hamm. Principles of nonlinear optical spectroscopy: A practical approach or: Mukamel for dummies. *University of Zurich*, 41(5):77, 2005.

[93] Sebastian Hild, Takeshi Fukuhara, Peter Schauß, Johannes Zeiher, Michael Knap, Eugene Demler, Immanuel Bloch, and Christian Gross. Far-from-equilibrium spin transport in heisenberg quantum magnets. *Phys. Rev. Lett.*, 113(14):147205, Oct 2014.

[94] Tristan Holsten and Matthias Krüger. Thermodynamic nonlinear response relation. *Phys. Rev. E*, 103:032116, Mar 2021.

[95] J. Hubbard. Electron correlations in narrow energy bands. *Proceedings of the Royal Society of London. Series A. Mathematical and Physical Sciences*, 276(1365):238–257, November 1963.

[96] Enej Ilievski and Jacopo De Nardis. Ballistic transport in the one-dimensional hubbard model: The hydrodynamic approach. *Phys. Rev. B*, 96:081118, Aug 2017.

[97] Enej Ilievski, Jacopo De Nardis, Sarang Gopalakrishnan, Romain Vasseur, and Brayden Ware. Superuniversality of superdiffusion. *Phys. Rev. X*, 11:031023, Jul 2021.

[98] Enej Ilievski, Jacopo De Nardis, Marko Medenjak, and Tomaž Prosen. Superdiffusion in one-dimensional quantum lattice models. *Phys. Rev. Lett.*, 121:230602, Dec 2018.

[99] Enej Ilievski, Marko Medenjak, Tomaž Prosen, and Lenart Zadnik. Quasilocal charges in integrable lattice systems. *Journal of Statistical Mechanics: Theory and Experiment*, 2016(6):064008, June 2016.

[100] N Iorgov, V Shadura, and Yu Tykhyy. Spin operator matrix elements in the quantum ising chain: fermion approach. *Journal of Statistical Mechanics: Theory and Experiment*, 2011(02):P02028, feb 2011.

[101] Aníbal Iucci, Gregory A. Fiete, and Thierry Giamarchi. Fourier transform of the $2k_F$ luttinger liquid density correlation function with different spin and charge velocities. *Phys. Rev. B*, 75:205116, May 2007.

[102] D. Jaksch, C. Bruder, J. I. Cirac, C. W. Gardiner, and P. Zoller. Cold bosonic atoms in optical lattices. *Phys. Rev. Lett.*, 81:3108–3111, Oct 1998.

[103] D. Jaksch and P. Zoller. The cold atom hubbard toolbox. *Annals of Physics*, 315(1):52–79, 2005. Special Issue.

[104] P.U. Jepsen et al. Ultrafast carrier trapping in microcrystalline silicon observed in optical pump–terahertz probe measurements. *App. Phys. Lett.*, 79:1291, 2001.

[105] Denis Jérome. *Organic Conductors: From Charge Density Wave TTF-TCNQ to Superconducting (TMTSF)$_2PF_6$*, volume 104. American Chemical Society, 11 2004.

[106] Guan Xi-Wen Jiang Yu-Zhu, Chen Yang-Yang. Understanding many-body physics in one dimension from the lieb-liniger model. *Chinese Physics B*, 24(5):50311, 2015.

[107] F. Jin, R. Steinigeweg, F. Heidrich-Meisner, K. Michielsen, and H. De Raedt. Finite-temperature charge transport in the one-dimensional hubbard model. *Phys. Rev. B*, 92:205103, Nov 2015.

[108] S M João and J M Viana Parente Lopes. Basis-independent spectral methods for non-linear optical response in arbitrary tight-binding models. *Journal of Physics: Condensed Matter*, 32(12):125901, dec 2019.

[109] Jacob Jordan, Román Orús, and Guifré Vidal. Numerical study of the hard-core bose-hubbard model on an infinite square lattice. *Phys. Rev. B*, 79:174515, May 2009.

[110] Minoru Kanega, Tatsuhiko N. Ikeda, and Masahiro Sato. Linear and nonlinear optical responses in kitaev spin liquids. *Phys. Rev. Research*, 3:L032024, Jul 2021.

[111] Mehran Kardar, Giorgio Parisi, and Yi-Cheng Zhang. Dynamic scaling of growing interfaces. *Phys. Rev. Lett.*, 56:889–892, Mar 1986.

[112] C Karrasch. Hubbard-to-heisenberg crossover (and efficient computation) of drude weights at low temperatures. *New Journal of Physics*, 19(3):033027, March 2017.

[113] C. Karrasch. Nonequilibrium thermal transport and vacuum expansion in the hubbard model. *Phys. Rev. B*, 95:115148, Mar 2017.

[114] C. Karrasch, D. M. Kennes, and F. Heidrich-Meisner. Thermal conductivity of the one-dimensional fermi-hubbard model. *Phys. Rev. Lett.*, 117:116401, Sep 2016.

[115] C. Karrasch, D. M. Kennes, and J. E. Moore. Transport properties of the one-dimensional hubbard model at finite temperature. *Phys. Rev. B*, 90:155104, Oct 2014.

[116] C. Karrasch, T. Prosen, and F. Heidrich-Meisner. Proposal for measuring the finite-temperature drude weight of integrable systems. *Phys. Rev. B*, 95:060406, Feb 2017.

[117] Rebekka Koch, Alvise Bastianello, and Jean-Sébastien Caux. Adiabatic formation of bound states in the 1d Bose gas. *arXiv e-prints*, page arXiv:2010.13738, October 2020.

[118] Akira Kofuji, Yoshihiro Michishita, and Robert Peters. Effects of strong correlations on the nonlinear response in weyl-kondo semimetals. *Phys. Rev. B*, 104:085151, Aug 2021.

[119] V. E. Korepin, N. M. Bogoliubov, and A. G. Izergin. *The One-dimensional Bose Gas*, page 362. Cambridge Monographs on Mathematical Physics. Cambridge University Press, 1993.

[120] V. E. Korepin, N. M. Bogoliubov, and A. G. Izergin. *Quantum Inverse Scattering Method and Correlation Functions*. Cambridge Monographs on Mathematical Physics. Cambridge University Press, 1993.

[121] Žiga Krajnik, Enej Ilievski, and Tomaž Prosen. Absence of normal fluctuations in an integrable magnet. *Phys. Rev. Lett.*, 128:090604, Mar 2022.

[122] W Kuehn, K Reimann, M Woerner, T Elsaesser, and R Hey. Two-Dimensional Terahertz Correlation Spectra of Electronic Excitations in Semiconductor Quantum Wells. *J. Phys. Chem. B*, 115(18):5448–5455, 2011.

[123] Fabian B. Kugler, Seung-Sup B. Lee, and Jan von Delft. Multipoint correlation functions: Spectral representation and numerical evaluation. *Phys. Rev. X*, 11:041006, Oct 2021.

[124] T. D. Kühner and H. Monien. Phases of the one-dimensional bose-hubbard model. *Phys. Rev. B*, 58:R14741–R14744, Dec 1998.

[125] M. Lakshmanan, Th.W. Ruijgrok, and C.J. Thompson. On the dynamics of a continuum spin system. *Physica A: Statistical Mechanics and its Applications*, 84(3):577–590, jan 1976.

[126] J. P. F. LeBlanc, Andrey E. Antipov, Federico Becca, Ireneusz W. Bulik, Garnet Kin-Lic Chan, Chia-Min Chung, Youjin Deng, Michel Ferrero, Thomas M. Henderson, Carlos A. Jiménez-Hoyos, E. Kozik, Xuan-Wen Liu, Andrew J. Millis, N. V. Prokof'ev, Mingpu Qin, Gustavo E. Scuseria, Hao Shi, B. V. Svistunov, Luca F. Tocchio, I. S. Tupitsyn, Steven R. White, Shiwei Zhang, Bo-Xiao Zheng, Zhenyue Zhu, and Emanuel Gull. Solutions of the two-dimensional hubbard model: Benchmarks and results from a wide range of numerical algorithms. *Phys. Rev. X*, 5:041041, Dec 2015.

[127] Martin Lebrat, Pjotrs Grišins, Dominik Husmann, Samuel Häusler, Laura Corman, Thierry Giamarchi, Jean-Philippe Brantut, and Tilman Esslinger. Band and correlated insulators of cold fermions in a mesoscopic lattice. *Phys. Rev. X*, 8:011053, Mar 2018.

[128] Patrick A. Lee, Naoto Nagaosa, and Xiao-Gang Wen. Doping a mott insulator: Physics of high-temperature superconductivity. *Rev. Mod. Phys.*, 78:17–85, Jan 2006.

[129] Seung-Sup B. Lee, Fabian B. Kugler, and Jan von Delft. Computing local multipoint correlators using the numerical renormalization group. *Phys. Rev. X*, 11:041007, Oct 2021.

[130] Maciej Lewenstein, Anna Sanpera, Veronica Ahufinger, Bogdan Damski, Aditi Sen(De), and Ujjwal Sen. Ultracold atomic gases in optical lattices: mimicking condensed matter physics and beyond. *Advances in Physics*, 56(2):243–379, 2007.

[131] Zhi Li, Takami Tohyama, Toshiaki Iitaka, Haibin Su, and Haibo Zeng. Nonlinear optical response from quantum kinetic equation. *arXiv e-prints*, page arXiv:2001.07839, January 2020.

[132] Elliott H. Lieb. Exact analysis of an interacting bose gas. ii. the excitation spectrum. *Phys. Rev.*, 130:1616–1624, May 1963.

[133] Elliott H. Lieb and Werner Liniger. Exact analysis of an interacting bose gas. i. the general solution and the ground state. *Phys. Rev.*, 130:1605–1616, May 1963.

[134] Marko Ljubotina, Marko Žnidarič, and Tomaž Prosen. Kardar-parisi-zhang physics in the quantum heisenberg magnet. *Phys. Rev. Lett.*, 122:210602, May 2019.

[135] Marko Ljubotina, Marko Žnidarič, and Tomaž Prosen. Spin diffusion from an inhomogeneous quench in an integrable system. *Nature Communications*, 8(1):16117, 2017.

[136] Jian Lu, Xian Li, Harold Y. Hwang, Benjamin K. Ofori-Okai, Takayuki Kurihara, Tohru Suemoto, and Keith A. Nelson. Coherent Two-Dimensional Terahertz Magnetic Resonance Spectroscopy of Collective Spin Waves. *Phys. Rev. Lett.*, 118:207204, May 2017.

[137] Dirk-Sören Lühmann, Ole Jürgensen, and Klaus Sengstock. Multi-orbital and density-induced tunneling of bosons in optical lattices. *New Journal of Physics*, 14(3):033021, mar 2012.

[138] Stephen A Lynch, P Thornton Greenland, Alexander FG van der Meer, Benedict N Murdin, Carl R Pidgeon, Britta Redlich, Nguyen Q Vinh, and Gabriel Aeppli. First observation of a THz photon echo. In *35th International Conference on Infrared, Millimeter, and Terahertz Waves*, pages 1–2. IEEE, 2010.

[139] M. Ma, B. I. Halperin, and P. A. Lee. Strongly disordered superfluids: Quantum fluctuations and critical behavior. *Phys. Rev. B*, 34:3136–3143, Sep 1986.

[140] Fahad Mahmood, Dipanjan Chaudhuri, Sarang Gopalakrishnan, Rahul Nandkishore, and N. P. Armitage. Observation of a marginal fermi glass. *Nature Physics*, 17(5):627–631, January 2021.

[141] K. A. Matveev. Conductance of a quantum wire in the wigner-crystal regime. *Phys. Rev. Lett.*, 92:106801, Mar 2004.

[142] Anton Mazurenko, Christie S. Chiu, Geoffrey Ji, Maxwell F. Parsons, Márton Kanász-Nagy, Richard Schmidt, Fabian Grusdt, Eugene Demler, Daniel Greif, and Markus Greiner. A cold-atom fermi–hubbard antiferromagnet. *Nature*, 545(7655):462–466, May 2017.

[143] Glen Bigan Mbeng, Angelo Russomanno, and Giuseppe E. Santoro. The quantum ising chain for beginners, 2020.

[144] Márton Mestyán, Bruno Bertini, Lorenzo Piroli, and Pasquale Calabrese. Spin-charge separation effects in the low-temperature transport of one-dimensional fermi gases. *Phys. Rev. B*, 99:014305, Jan 2019.

[145] Yoshihiro Michishita and Naoto Nagaosa. Dissipation and geometry in nonlinear quantum transports of multiband electronic systems. *arXiv e-prints*, page arXiv:2204.08365, April 2022.

[146] Yoshihiro Michishita and Robert Peters. Effects of renormalization and non-hermiticity on nonlinear responses in strongly correlated electron systems. *Phys. Rev. B*, 103:195133, May 2021.

[147] Frederik Møller, Chen Li, Igor Mazets, Hans-Peter Stimming, Tianwei Zhou, Zijie Zhu, Xuzong Chen, and Jörg Schmiedmayer. Extension of the Generalized Hydrodynamics to Dimensional Crossover Regime. *arXiv e-prints*, page arXiv:2006.08577, June 2020.

[148] Shaul Mukamel. *Principles of nonlinear optical spectroscopy*. Number 6. Oxford University Press on Demand, 1999.

[149] Jason Myers, M. J. Bhaseen, Rosemary J. Harris, and Benjamin Doyon. Transport fluctuations in integrable models out of equilibrium. *SciPost Phys.*, 8:7, 2020.

[150] Rahul Nandkishore and Sarang Gopalakrishnan. Lifetimes of local excitations in disordered dipolar quantum systems. *Phys. Rev. B*, 103:134423, Apr 2021.

[151] Rahul M. Nandkishore, Wonjune Choi, and Yong Baek Kim. Spectroscopic fingerprints of gapped quantum spin liquids, both conventional and fractonic. *Phys. Rev. Research*, 3:013254, Mar 2021.

[152] Jacopo De Nardis, Denis Bernard, and Benjamin Doyon. Diffusion in generalized hydrodynamics and quasiparticle scattering. *SciPost Phys.*, 6(4):49, apr 2019.

[153] Matthew A. Nichols, Lawrence W. Cheuk, Melih Okan, Thomas R. Hartke, Enrique Mendez, T. Senthil, Ehsan Khatami, Hao Zhang, and Martin W. Zwierlein. Spin transport in a mott insulator of ultracold fermions. *Science*, 363(6425):383–387, 2019.

[154] Yuji Nozawa and Hirokazu Tsunetsugu. Generalized hydrodynamic approach to charge and energy currents in the one-dimensional hubbard model. *Phys. Rev. B*, 101:035121, Jan 2020.

[155] Ahmed Omran, Martin Boll, Timon A. Hilker, Katharina Kleinlein, Guillaume Salomon, Immanuel Bloch, and Christian Gross. Microscopic observation of pauli blocking in degenerate fermionic lattice gases. *Phys. Rev. Lett.*, 115:263001, Dec 2015.

[156] S. A. Parameswaran and S. Gopalakrishnan. Spin-catalyzed hopping conductivity in disordered strongly interacting quantum wires. *Phys. Rev. B*, 95:024201, Jan 2017.

[157] S. A. Parameswaran and S. Gopalakrishnan. Asymptotically exact theory for nonlinear spectroscopy of random quantum magnets. *Phys. Rev. Lett.*, 125:237601, Dec 2020.

[158] Daniel E. Parker, Takahiro Morimoto, Joseph Orenstein, and Joel E. Moore. Diagrammatic approach to nonlinear optical response with application to weyl semimetals. *Phys. Rev. B*, 99:045121, Jan 2019.

[159] Maxwell F. Parsons, Florian Huber, Anton Mazurenko, Christie S. Chiu, Widagdo Setiawan, Katherine Wooley-Brown, Sebastian Blatt, and Markus Greiner. Site-resolved imaging of fermionic $^6$Li in an optical lattice. *Phys. Rev. Lett.*, 114:213002, May 2015.

[160] I. Paul. Nonlinear terahertz electro-optical responses in metals. *arXiv e-prints*, page arXiv:2101.04136, January 2021.

[161] Gabriele Perfetto and Benjamin Doyon. Euler-scale dynamical fluctuations in non-equilibrium interacting integrable systems. *arXiv e-prints*, page arXiv:2012.06496, December 2020.

[162] Michael R. Peterson, Subroto Mukerjee, B. Sriram Shastry, and Jan O. Haerter. Dynamical thermal response functions for strongly correlated one-dimensional systems: Hubbard and spinless fermion $t-v$ model. *Phys. Rev. B*, 76:125110, Sep 2007.

[163] Balázs Pozsgay. Algebraic construction of current operators in integrable spin chains. *Phys. Rev. Lett.*, 125:070602, Aug 2020.

[164] Balzs Pozsgay. Current operators in integrable spin chains: lessons from long range deformations. *SciPost Phys.*, 8:16, 2020.

[165] P. Prelovšek, S. El Shawish, X. Zotos, and M. Long. Anomalous scaling of conductivity in integrable fermion systems. *Phys. Rev. B*, 70:205129, Nov 2004.

[166] Tomaž Prosen. Open $xxz$ spin chain: Nonequilibrium steady state and a strict bound on ballistic transport. *Phys. Rev. Lett.*, 106:217206, May 2011.

[167] Tomaž Prosen and Marko Žnidarič. Diffusive high-temperature transport in the one-dimensional hubbard model. *Phys. Rev. B*, 86:125118, Sep 2012.

[168] Mingpu Qin, Chia-Min Chung, Hao Shi, Ettore Vitali, Claudius Hubig, Ulrich Schollwöck, Steven R. White, and Shiwei Zhang. Absence of superconductivity in the pure two-dimensional hubbard model. *Phys. Rev. X*, 10:031016, Jul 2020.

[169] Marcos Rigol, Vanja Dunjko, Vladimir Yurovsky, and Maxim Olshanii. Relaxation in a completely integrable many-body quantum system: An ab initio study of the dynamics of the highly excited states of 1d lattice hard-core bosons. *Phys. Rev. Lett.*, 98:050405, Feb 2007.

[170] Subir Sachdev. *Quantum Phase Transitions*. Cambridge University Press, 2 edition, 2011.

[171] Subir Sachdev and AP Young. Low temperature relaxational dynamics of the ising chain in a transverse field. *Physical review letters*, 78(11):2220, 1997.

[172] Lucile Savary and Leon Balents. Quantum spin liquids: a review. *Reports on Progress in Physics*, 80(1):016502, nov 2016.

[173] Ulrich Schollwöck. The density-matrix renormalization group in the age of matrix product states. *Annals of Physics*, 326(1):96–192, 2011.

[174] Koki Shinada and Robert Peters. Nonlinear response induced by Ferromagnetism in a Noncentrosymmetric Kondo Lattice system. *arXiv e-prints*, page arXiv:2110.10496, October 2021.

[175] Inti Sodemann and Liang Fu. Quantum nonlinear hall effect induced by berry curvature dipole in time-reversal invariant materials. *Phys. Rev. Lett.*, 115:216806, Nov 2015.

[176] Herbert Spohn. Nonlinear fluctuating hydrodynamics for anharmonic chains. *Journal of Statistical Physics*, 154(5):1191–1227, February 2014.

[177] Minoru Takahashi. One-dimensional heisenberg model at finite temperature. *Progress of Theoretical Physics*, 46(2):401–415, August 1971.

[178] Minoru Takahashi. One-dimensional hubbard model at finite temperature. *Progress of Theoretical Physics*, 47(1):69–82, January 1972.

[179] Minoru Takahashi. *Thermodynamics of one-dimensional solvable models*. Cambridge university press, 2005.

[180] Minoru Takahashi and Masahiro Shiroishi. Thermodynamic bethe ansatz equations of one-dimensional hubbard model and high-temperature expansion. *Phys. Rev. B*, 65:165104, Apr 2002.

[181] Kazuaki Takasan, Masaki Oshikawa, and Haruki Watanabe. Adiabatic transport in one-dimensional systems with a single defect. *arXiv e-prints*, page arXiv:2105.11378, May 2021.

[182] Yuhi Tanikawa and Hosho Katsura. Fine structure of the nonlinear drude weights in the spin-$\frac{1}{2}$ xxz chain. *Phys. Rev. B*, 104:205116, Nov 2021.

[183] Yuhi Tanikawa, Kazuaki Takasan, and Hosho Katsura. Exact results for nonlinear drude weights in the spin-$\frac{1}{2}$ xxz chain. *Phys. Rev. B*, 103:L201120, May 2021.

[184] Giuseppe Del Vecchio Del Vecchio and Benjamin Doyon. The hydrodynamic theory of dynamical correlation functions in the XX chain. *Journal of Statistical Mechanics: Theory and Experiment*, 2022(5):053102, May 2022.

[185] Jayadev Vijayan, Pimonpan Sompet, Guillaume Salomon, Joannis Koepsell, Sarah Hirthe, Annabelle Bohrdt, Fabian Grusdt, Immanuel Bloch, and Christian Gross. Time-resolved observation of spin-charge deconfinement in fermionic hubbard chains. *Science*, 367(6474):186–189, 2020.

[186] G von Gehlen, N Iorgov, S Pakuliak, V Shadura, and Yu Tykhyy. Form-factors in the baxter–bazhanov–stroganov model II: Ising model on the finite lattice. *Journal of Physics A: Mathematical and Theoretical*, 41(9):095003, feb 2008.

[187] Yuan Wan and N. P. Armitage. Resolving continua of fractional excitations by spinon echo in thz 2d coherent spectroscopy. *Phys. Rev. Lett.*, 122:257401, Jun 2019.

[188] Enke Wang and Ulrich Heinz. Generalized fluctuation-dissipation theorem for nonlinear response functions. *Phys. Rev. D*, 66:025008, Jul 2002.

[189] Haruki Watanabe, Yankang Liu, and Masaki Oshikawa. On the general properties of non-linear optical conductivities. *Journal of Statistical Physics*, 181(6):2050–2070, October 2020.

[190] Haruki Watanabe and Masaki Oshikawa. Generalized $f$-sum rules and kohn formulas on nonlinear conductivities. *Phys. Rev. B*, 102:165137, Oct 2020.

[191] Christof Weitenberg, Manuel Endres, Jacob F. Sherson, Marc Cheneau, Peter Schauß, Takeshi Fukuhara, Immanuel Bloch, and Stefan Kuhr. Single-spin addressing in an atomic mott insulator. *Nature*, 471(7338):319–324, March 2011.

[192] Michael Woerner, Wilhelm Kuehn, Pamela Bowlan, Klaus Reimann, and Thomas Elsaesser. Ultrafast two-dimensional terahertz spectroscopy of elementary excitations in solids. *New J. Phys.*, 15(2):025039, 2013.

[193] C. N. Yang and C. P. Yang. Thermodynamics of a onedimensional system of bosons with repulsive deltafunction interaction. *Journal of Mathematical Physics*, 10(7):1115–1122, 1969.

[194] Chen Ning Yang. $\eta$ pairing and off-diagonal long-range order in a hubbard model. *Phys. Rev. Lett.*, 63:2144–2147, Nov 1989.

[195] T. L. Yang, P. Grišins, Y. T. Chang, Z. H. Zhao, C. Y. Shih, T. Giamarchi, and R. G. Hulet. Measurement of the dynamical structure factor of a 1d interacting fermi gas. *Phys. Rev. Lett.*, 121:103001, Sep 2018.

[196] Bingtian Ye, Francisco Machado, Jack Kemp, Ross B. Hutson, and Norman Y. Yao. Universal Kardar-Parisi-Zhang dynamics in integrable quantum systems. *arXiv e-prints*, page arXiv:2205.02853, May 2022.

[197] Takato Yoshimura and Herbert Spohn. Collision rate ansatz for quantum integrable systems. *SciPost Phys.*, 9:40, 2020.

[198] M. M. Zemljič and P. Prelovšek. Thermoelectric power in one-dimensional hubbard model. *Phys. Rev. B*, 71:085110, Feb 2005.

[199] X. Zotos, F. Naef, and P. Prelovsek. Transport and conservation laws. *Phys. Rev. B*, 55:11029–11032, May 1997.